ABSTRACT

In the 21ST century, the rehabilitation and renewal of aged and damaged civil concrete structures represent one of the most significant tasks around the world. Over the past decade, the rehabilitation and strengthening of structures has received much attention. Combining FRP composites with concrete which is weak in tension but strong in compression whereas FRP composites in plate form are strong in tension but will buckle under low compressive loads. The combination of these two could take advantage of the dominant properties of both materials by joining the two materials to form a structural member. The torsion in members of a structural system may be the result of primary or secondary actions. A simple member subjected to an eccentric line load along its span, cantilever, and eccentrically loaded girders are examples of primary or equilibrium torsion. In statically indeterminate structures, torsion may result from the requirements of continuity and is considered as secondary torsion. The basic difference between the shear and torsion is the formation of cracks that is, in torsion spiral cracks and in shears the cracks pattern is the same in both front and back vertical side. A limited number of mostly experimental studies were conducted to investigate torsion strengthening of RC members because mostly research has been focused on enhancing the flexural and shear behaviour, ductility, and confinement of concrete structural members. Analytical models for predicting the torsional section capacity are very few. The reason is the complexity of the torsion problem and the lack of adequate experimental results required to understand the full behaviour.

Two specimens were tested, PTR-1(Reference Beam) and PTT-1 (torsion deficient strengthened beam with CFRP Fabric). The reference beam shows three full spiral diagonal cracks and Torque Vs Twist Angle was good agreement with the past literature. The failure was crushing of concrete and yielding steel provided in tension at quarter span near to roller end.

The strengthened beam with CFRP Fabric was failed in anchorage failure, debonding of the CFRP fabric Strips, yielding of reinforcement provided in compression zone at mid span and finally crushing of the concrete. The torsional capacity of the CFRP Fabric were not fully utilised due to debonding and anchorage failure, only enhancement of torque was 58%. It also shows lower ductility than reference beams. The torsional capacity based on the strain recorded in CFRP fabric shows the good agreement with the past literature.

CONTENTS

LIST OF FIGURES

LIST OF TABLES

CHAPTER – 1

INTRODUCTION

EXPERIMENTAL STUDY OF RC BEAMS STRENGTHENED WITH CFRP FABRIC UNDER PURE TORSION

CHAPTER - 1

1.0 INTRODUCTION

In the 21ST century, the rehabilitation and renewal of aged and damaged civil concrete structures represent one of the most significant tasks around the world. Over the past decade, the rehabilitation and strengthening of structures has received much attention. The strengthening of concrete structures could be the favourable solution in many cases such as the change in the usage of the building or change in the design code provisions, as well as the deterioration of structural members of bridges and buildings. Deterioration may occur because of degradation, aging, lack of maintenance and severe earthquakes. The continuing deterioration of the world's civil concrete structures highlights the urgent need for the effective rehabilitation technique in terms of low cost and fast processing time with minimising the traffic interruption. Besides, the growing population in some developing countries requires upgrading and retrofitting the original structures because of the increasing of the traffic volume, which is beyond the original design capacity [Lau K.T (2001)].

Deficiency due to Environmental Effects

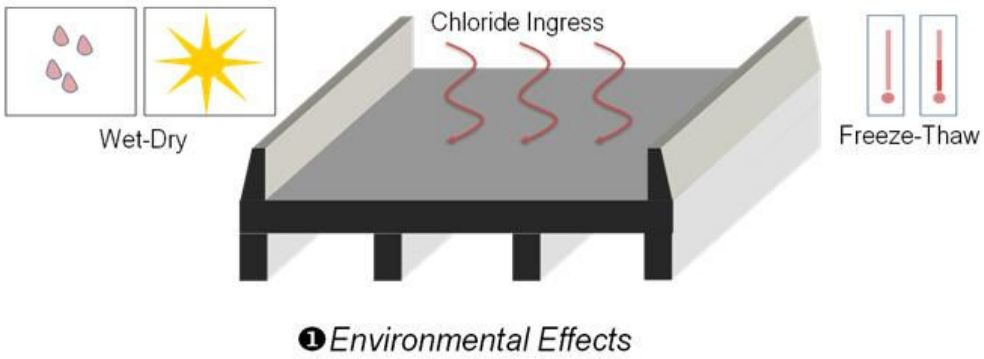

Fig. 1 Deficiency Due to Environmental Effects

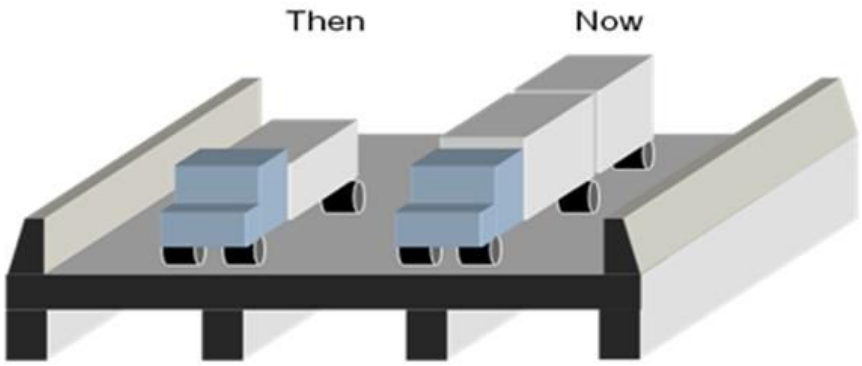

Fig. 2 Deficiency due to Updated Design Loads and Design Code Procedures

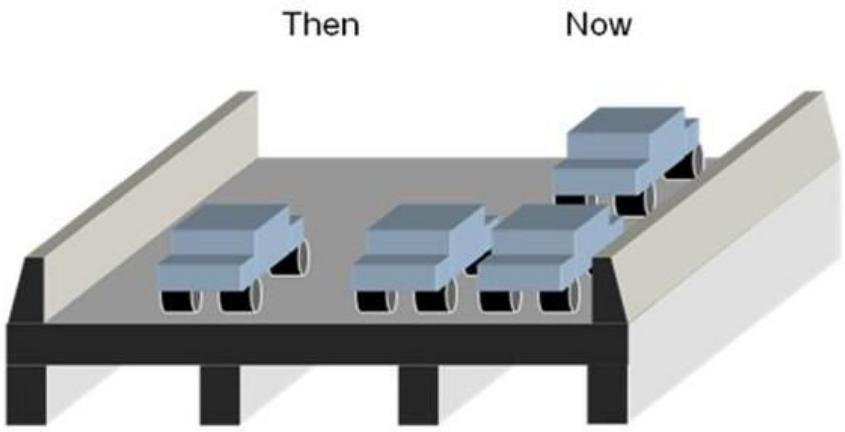

Fig. 3 Deficiency due to Increase Traffic Loads

In general, the cracks of the concrete and the corrosion of the embedded reinforced steel bars are the major forms of failure of the concrete structures because of the weak tensile properties of the concrete material. Corrosion due to chlorides and/or carbonation is the principal cause of deterioration of reinforced concrete structures.
The corrosion of steel in concrete structures requires high costs of repair and maintenance.

However, it has been increasingly used in civil infrastructures for the applications ranging from seismic retrofit and strengthening of beams and slabs, to replacement of steel rebar in the forms of rod, plate and jacket in recent years. Saadatmanesh and

Ehsani (1991) and Ritchie et al (1991) were one of the first workers to carry out experimental investigations on strengthening undamaged beams with FRP plates [Taheri F. et al (2002)]. The first research in this area was carried out in 1979. High-strength fibres were embedded into the soft matrix to form a composite with high tensile properties with compromising the fatigue and corrosion problems, which are the essential factors that the civil engineers should take into account. It is found that the average load capacity and the fatigue life of the strengthened structures were increased significantly from investigated the mechanical behaviour of the rectangular concrete beam with the external bonded fibre reinforced plastic (FRP) plate subjected to bending load. The stiffness of the strengthened beams was also increased by using the FRP bonding technique due to the reduction of internal bending moment of the beam. Besides, the time required to perform the repairing procedure was comparatively less than that taken when using the steel bonding method. However, the material cost for the carbon fibre is relative higher compared with the conventional materials [Lau K.T et al (2001)].

Gilbert Nkurunziza et al (2005) reported that many reinforced concrete structures are exposed to aggressive environments causing durability problems and are, therefore, unlikely to reach their anticipated service life.

The cost of repairs and restoration in the USA, Canada and in the majority of the European countries constitute a high percentage of the expenditure of these countries on infrastructure. In Canada, an estimate shows that more than 40% of all the bridges 40-years old or more and multi-storey parking garages are structurally deficient mainly due to corrosion caused by de-icing salts and severe climate. In the US, more than 40% of the national bridges inspected are classified as structurally or functionally defective because of the corrosion of steel and the damage from freeze-thaw cycling. In Canada, the cost of repairs of multi-storey parking garages is estimated at more than 6 billion CDN$, while it ranges between 50 and 100 billion US$ per year in the US. In Europe, the annual cost of repairs is estimated at 1.0 billion £ Sterling [Gilbert Nkurunziza et al (2005)].

Engineering of modern composite materials has had a significant impact on the technology of design and construction. The main objective of using or selecting any

material in construction is to make use of its properties efficiently for best performance and durability of the structure. The merits of a material are based on factors such as availability, structural strength, durability, and workability. Advanced composite materials, e.g. fibre-reinforced polymers (FRP), have found new applications in the rehabilitation of reinforced concrete structures. The transferring of stresses from concrete to the FRP reinforcement is central to the reinforcement effect of FRP- strengthened concrete structures. This is because these stresses are likely to cause undesirable premature and brittle failure [Boucif Guenaneche et al (2010)].

Fibre reinforced plastics (FRP) have been recognized as the strong materials, which can be used to alternate the conventional metallic materials for some structural applications, particularly in the military industry in the past thirty years. Fiber-reinforced plastics (FRPs, or advanced fibre composites) have long been successfully used by the aerospace and defence industries. These materials are currently gaining a rapid momentum in finding their way into civil engineering structural applications [Wu Hwai-Chung (2000)].

L.C. Hollaway (2010) reported that the combination of FRP and reinforced concrete can take many structural forms, as follows:

- All FRP composite bridge decks and the bridge superstructure
- An access to an existing structure for maintenance purposes and for aerodynamics of the structure – a bridge enclosure and aerodynamic fairings using FRP units.
- The rehabilitation of RC beams by the techniques of (i) external plate bonding (EPB) and (ii) Near Surface Mounted FRP rods.
- The rehabilitation of steel beams by the techniques of EPB.
- The retrofitting of RC columns by using unidirectional FRP composites.
- The FRP rebars used to reinforce concrete beams and slabs.

The constructions of a structural member enable two or more materials to take advantage of their superior properties. For instance, combining FRP composites with concrete which is weak in tension but strong in compression whereas FRP composites in plate form are strong in tension but will buckle under low compressive loads. The combination of these two could take advantage of the dominant properties of both

materials by joining the two materials to form a structural member. The structural analysis and design of the above systems generally do not present many problems; in addition, there is evidence in the literature that provides substantial reasons to believe that, if appropriately analysed, designed and fabricated FRP composites can provide longer lifetime and lower maintenance costs than equivalent structures fabricated from conventional materials. However, there are areas within the physical and in-service properties of FRP composites that are sparse particularly on the durability of composites; this property will affect the long-term behavior of the material. One of the problems with composite materials is in the general name of their component parts [L.C. Hollaway (2010)].

There is a lack of design guidelines for specific retrofitting requirements, e.g., how fiber systems should be tailored in order to provide adequate improvements in strength, ductility, or both, and to achieve cost efficiency. It is difficult, if not impossible, to optimize FRP performance from an experimental viewpoint. Therefore, a quantitative model considering both concrete and FRP properties through mechanical interaction should be developed first. A methodology of optimum selection of fiber types and architecture in relation to the target concrete is necessitated [Wu Hwai-Chung (2000)].

FRP is widely used in such structural elements in existing bridges and building structures as a strengthening material. As a result, some recommendations and guidelines for the application of reinforced concrete beams strengthened with FRP are developed in various design and practice codes [ACI 440.2R-08 (2008) and TR-55(2000)].

FRP is preferred because of the following reason (ISIS EC Module 4)

1. Light hence Easy to install
2. High Strength approximately 5 times the strength of steel in case of Carbon fibre
3. Corrosion resistant hence it enhance the durability of the retrofitted structure
4. Highly versatile so suit is any pro

1.1 Torsional Strengthening

The torsion in members of a structural system may be the result of primary or secondary actions. The case of primary torsion occurs when the external load has to be resisted by torsion. In such situations, the torsion required to maintain static equilibrium can be uniquely determined. This case may be also referred to as equilibrium torsion. It is primarily a strength problem because the structure or its components will fail if the torsion resistance cannot be provided. A simple member subjected to an eccentric line load along its span, cantilever, and eccentrically loaded girders are examples of primary or equilibrium torsion. In statically indeterminate structures, torsion may result from the requirements of continuity and is considered as secondary torsion. Disregarding continuity in statistically indeterminate reinforced concrete (RC) structures at various stages of loading could be the cause of serious damage. Early research in the torsional analysis of RC beams was based on the thin tube space truss model. It is the common method used to analyze RC beams under torsion and the basis for most of the current North American design codes. The torsion produces two orthogonal closed spiral diagonal loops. One diagonal loop is in compression and the other is in tension. The concrete resists the diagonal compression and the steel reinforcement resists the diagonal tension. Over the last four decades, the space truss model was refined and modified to include rational calculations of the equivalent thickness hollow tube analogy, the angle of inclination for the diagonal cracks, and the maximum concrete diagonal strain. Structural elements subjected to torsion experience diagonal tension which eventually leads to brittle failure. Brittle failure is an undesirable mode of failure that would compromise the ductility of the structure.

Strengthening for increased torsional capacity may be required in conventional beams and columns, as well as in bridge box girders. The principles applied to strengthening in shear are also valid in the case of torsion, with a few minor differences. As shown in Fig. 4 and 5 shows the cracks were spiral in case of torsion and mirror image of the front and back side in case of share.

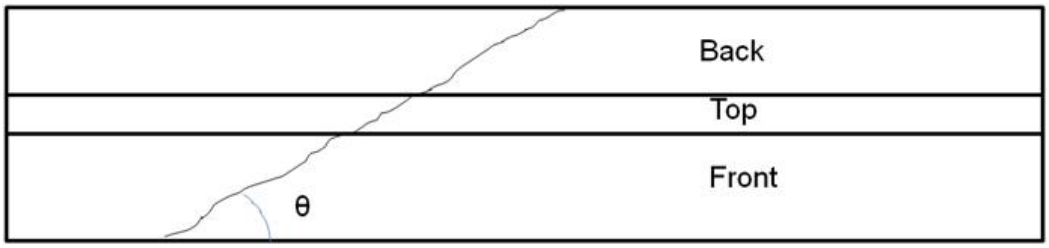

Fig. 4 Spiral Cracking Pattern Due to Torsion

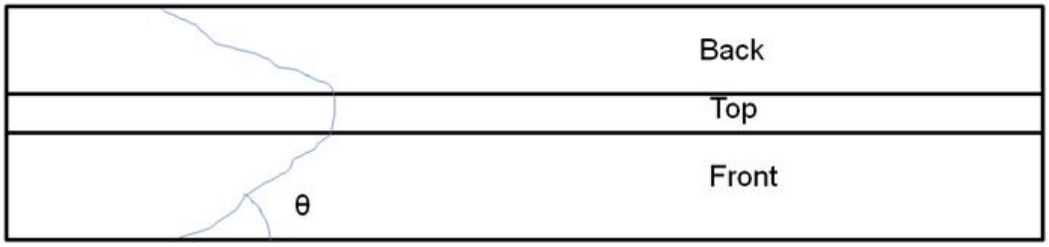

Fig. 5 Cracking Pattern Due to Shear

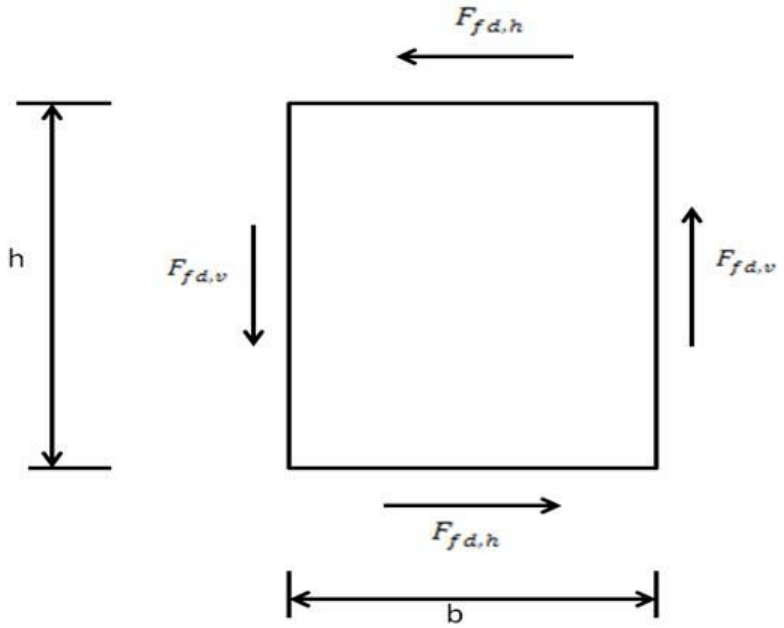

Fig. 6 Stress Distribution due to Torsion

These forces are calculated below for the case $\alpha = 90^0$ where α is fiber direction with respect to member axis and θ is diagonal crack angle with respect to member axis (approximate 45^0).

$$F_{fd,v} = \varepsilon_{fd,e} E_{fu} \frac{t_f b_f}{s_f} h \cot g\, \theta \quad (1)$$

$$F_{fd,h} = \varepsilon_{fd,e} E_{fu} \frac{t_f b_f}{s_f} b \cot g\, \theta \quad (2)$$

Hence the contribution of FRP to torsional capacity T_{fd}, is given by the following equation:

$$T_{fd} = F_{fd,v}\, b + F_{fd,h} h = 2\varepsilon_{fd,e} E_{fu} \frac{t_f b_f}{s_f} bh \cot g\, \theta \quad (3)$$

1.2 Scope of the Study

This study aims to understand the behaviour of torsion deficient RC rectangular beam specimens strengthen using carbon fabric in relation to the reference beam. It also attempts to understand the complexity of twist angle, torque and ductility of strengthened beams involved in the strengthening.

CHAPTER – 2

LITERATURE REVIEW

CHAPTER – 2

2.0 LITERATURE REVIEW

Most of the research projects investigating the use of FRP focused on enhancing the flexural and shear behaviour, ductility, and confinement of concrete structural members. A limited number of (mostly experimental) studies were conducted to investigate torsion strengthening of RC members [Ghobarah A et al (2000)]. Very few analytical models are available for predicting the section capacity [Ameli Mehran and Ronagh Hamid R (2007) and Hii Adrian K.Y., Al-Mahaidi Riadh, (2006)]. None of these models predicted the full behavior of RC beams wrapped with FRP, account for the fact that the FRP is not bonded to all beam faces, predicted the failure mode, or predicted the effective FRP strain using equations developed based on testing FRP strengthened beams in torsion. The reason is the complexity of the torsion problem and the lack of adequate experimental results required to understand the full behavior. The FIB (2001) task force report indicated that if developing a rigorous analytical model to calculate the effective FRP strain level is a possibility, it is extremely difficult. Similar to the flexure and shear strengthening, the FRP fabric is bonded to the tension surface of the RC members for torsion strengthening. In the case of torsion, all sides of the member are subjected to diagonal tension and therefore the FRP sheets should be applied to all the faces of the member cross section. However, it is not always possible to provide external reinforcement for all the surfaces of the member cross section. In cases of inaccessible sides of the cross section, additional means of strengthening has to be provided to establish the adequate mechanism required to resist the torsion. In addition, the vertical and longitudinal reinforcements (i.e., internal or external) have to interact together to provide enough force resultant to maintain equilibrium with the diagonal forces developed due to the applied torque.

Unlike shear and flexural strengthening with fiber-reinforced plastics (FRP) in which significant research advances have been made, literature on torsional strengthening is limited and inconclusive Ghobarah et al (2002) performed some torsional tests on reinforced concrete beams that were strengthened with carbon fiber reinforced polymer (CFRP) and glass fiber reinforced polymer (GFRP) in different configurations. His results showed that the strength increased considerably as well as

the ductility levels. The findings were to some extent different from the findings of Ronagh and Dux (2003) who obtained lower angles of twist at failure in contrast to the levels. Some tests on FRP strengthened beams subjected to torsion. They used GFRP in different configurations to strengthen beams. They also compared their experimental results with the analytical method introduced in FIB (2001). Users of the FIB method have so far assumed that the contribution of concrete and steel reinforcements in the ultimate torque of FRP strengthened beams can be calculated based on models applicable to unstrengthened reinforced concrete (RC) beams. This assumption may produce erroneous results. In a strengthened beam, FRP, concrete, and reinforcements interact and as such, the distribution of stresses among these elements and within the body of concrete is not similar to unstrengthened RC beams. The assumption of the applicability of unstrengthened RC beams' models to strengthened RC beams does not seem to be accurate.

Mehran Ameli and Hamid R. Ronagh (2007) were presented an analytical method to evaluate the ultimate torque of FRP strengthened reinforced concrete beams. The proposed analytical method includes the equilibrium as well as the compatibility conditions of the components so that all components interact together in resisting the external torque. The results predicted by the method were close to the experimental results. The governing failure mode predicted by the method was FRP rupture. This was found to agree with experimental observations. Implementing the effects of confinement in the proposed method for beams with fully wrapped FRP along the length brought further improvements in the analytical results compared to the experimental ones. The average torque ratios for this method showed that the proposed method is conservative for fully wrapped beams. For strip wrapping, however, the method is slightly un-conservative. Further improvements for strip wrapping may be necessary. The method was found to be more trust worthy than the FIB method. Considering the ease of computerizing the proposed method and its accuracy, it may be useful in design situations.

Meng Jing et al (2007) study the torsional behaviour; seismic behaviour and mode of failure of reinforced concrete box beam strengthened with carbon fiber reinforced sheets (CFS) under combined bending, shear and cyclic torque were investigated. The test results indicated that the externally bonded CFS can be used to enhance the

torsional capacity and deformation capacity of the beams. The strengthening effect is more obvious with the more layers of transversal U-shape wrapped CFS strips. The test results also indicated that the CFS strengthening reduce the ductility of the beams. So special attention should be paid on the amount of CFS to avoid brittle failure. The test results were used to explore the restoring force model of CFS strengthened box beam under combined actions. This model provides a good reference to the study of seismic behaviours and wind vibration behaviours of CFS strengthened box beam under cyclic torque moment.

Ronagh and Dux (2003) performed some tests on FRP strengthened beams subjected to torsion with more or less similar results. These very few studies do not lead to comfortable conclusions about the torsional behaviour of FRP strengthened reinforced concrete beams. A program of experimental research was developed by [Ameli Mehran (2007)] including a variety of strengthening configurations using two different types of FRP wraps has been performed for better understanding of this behaviour and add to the archival data on torsional strengthening. A numerical study on reinforced concrete beams with and without FRP strengthening subjected to torsion were also discussed. ANSYS finite element software has been used in order to simulate full-scale beams in both linear and nonlinear range of response up to failure and the results are compared with the experiments. Here, the focus is on the ultimate torque and corresponding twist angle, history of torque-twist, the closeness of numerical and experimental results, and the strain distribution. The results as will be shown later are in reasonable agreement with the experiments for the ultimate torques and ultimate deformations.

CFRP materials increased the strength more than GFRP. In the experimental tests, the percentage increase in the ultimate torque was from 16 to 143% for CFRP and from 18 to 110% for GFRP depending on the configuration. The torque-twist angle curves of tested beams obtained from the experiments showed an increase in the twist angle at the ultimate torque. The ductility of all torsionally strengthened beams was also increased and this increase was significant for some FRP configurations. In most cases, the values of ductility factors corresponding to CFRP or GFRP for identical configurations were similar. The behaviour of strengthened beams also demonstrated that whereas CFRP strengthened beams failed almost immediately after reaching the

peak, the GFRP post peak response took some time to occur. This suggests that GFRP may be a better choice for earthquake strengthening scenarios by providing better energy absorption. Experimental observations showed that the pattern of concrete cracks in the strengthened beams have a wider spread along the length compared to individual cracks formed in beams without strengthening. This spread was distributed more uniformly in fully wrapped beams. The numerical results also exhibited that cracks mostly occurred at around an angle of 45° from the longitudinal axis thus confirming the experiments. It is also seen that crushing signs at ultimate for strengthened beams are more distributed compared to unstrengthened beams again confirming the experiments. Numerical solution in most cases is in reasonable agreement with the corresponding experimental data in terms of the ultimate torque and the ultimate angle of twist. Whereas numerical torque twist angle curves deviate from the experimental observations after the cracking of concrete, they catch up with the experimental results again at around the ultimate torque. As this trend was observed in all beams, the numerical model presented here can be used with confidence when ultimate values are sought.

2.1 Constitutive stress–strain laws of the materials [Constantin E. Chalioris (2007)]

The concrete struts' strength is greatly reduced by the diagonal cracking caused by tension in the perpendicular direction (concrete softening).

$$\sigma_d = \zeta f_c \left[2\frac{\varepsilon_d}{\zeta \varepsilon_o} - \left(\frac{\varepsilon_d}{\zeta \varepsilon_o}\right)^2 \right] \quad for\ \varepsilon_d \leq \zeta \varepsilon_o \tag{4}$$

$$\sigma_d = \zeta f_c \left[2\frac{\varepsilon_d}{\zeta \varepsilon_o} - \left(\frac{\varepsilon_d}{\zeta \varepsilon_o}\right)^2 \right] \quad for\ \varepsilon_d \leq \zeta \varepsilon_o \tag{5}$$

where f_c is the concrete cylinder compressive strength; $\varepsilon_o = -0.002$ (concrete strain corresponding to peak strength); and ζ is the softening coefficient taken as

$$\zeta = \frac{0.9}{\sqrt{1+400\varepsilon_r}} \tag{6}$$

In the cases of totally wrapped beams with FRP, the external confinement of concrete due to FRP is taken into account in the present study. For this reason, a special compressive stress versus strain curve for softened and FRP-confined concrete is formulated. The proposed stress–strain relationship is defined as a parabolic equation until the point of ultimate stress and after that point the curve is linearly reduced until the point of ultimate strain $\zeta\varepsilon_{cu}$. The Fig. 7 (a) shows the stress-strain relationship of Plain, Softened and softened and FRP-confinement concrete.

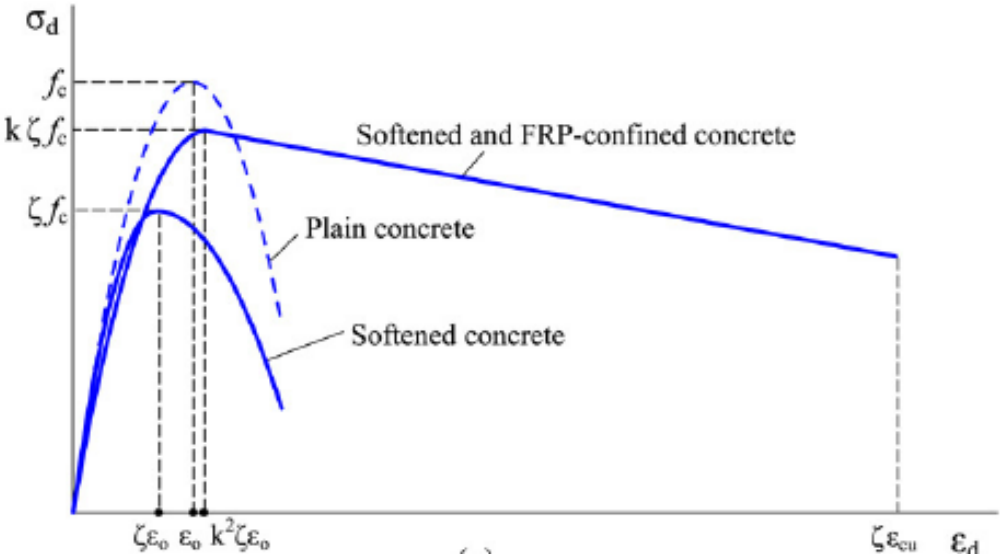

(a)

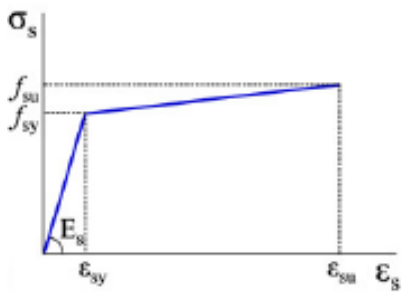

(b)

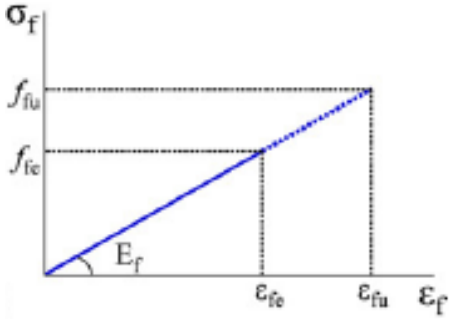

(c)

Fig. 7 Constitutive stress–strain laws for the materials: (a) concrete; (b) steel; (c) FRP

The following confinement parameters of an empirical model for FRP-confined concrete which recently has been proposed by Vinzileou and Panagiotidou (2007) have been considered.

$$\varepsilon_{cu} = 0.003k^2 \quad (7)$$

$$k = 1 + 2.8 * 0.5\alpha_n\omega_n \quad (8)$$

Where α_n is the in-section coefficient confinement calculated by the cross-section dimensions b and h:

$$\alpha_n = 1 - \frac{b^2+h^2}{3A_c} \quad (9)$$

And ω_n denotes the volumetric mechanical ratio for external FRP-confinement taken as

$$\omega_n = \frac{\text{volume of FRP material}}{\text{volume of the confined concrete core}} \frac{f_{fu}}{f_c} \quad (10)$$

Where f_{fu} is the ultimate tensile strength of the FRP. For the steel reinforcement and the FRP materials the idealized stress–strain relationships shown in Fig. 7 (b) and (c) are used, respectively. Especially for the FRP, the maximum developed tensile strain of the fibres, or else the effective strain in the principal material direction f_c, is estimated using the following analytical approaches, depending on the material (carbon or glass) of the FRP. For the case of carbon FRP, the model of Triantafillou and Antonopoulos (2000) which fib Bulletin 14 (2001) has adopted is considered:
For wrapping and rupture failure:

$$\varepsilon_{fe} = 0.17 \left(\frac{f_{cm}^{2/3}}{E_{fu}\rho_f}\right)^{0.3} \varepsilon_{fu} \quad (11)$$

For U-jacketing and rupture or peeling-off failure:
ε_{fe} is minimum of the following:

$$\varepsilon_{fe} = 0.17 \left(\frac{f_{cm}^{2/3}}{E_{fu}\rho_f} \right)^{0.30} \varepsilon_{fu} \quad (12)$$

$$\varepsilon_{fe} = 0.65 \left(\frac{f_{cm}^{2/3}}{E_{fu}\rho_f} \right)^{0.56} x\ 10^{-3} \quad (13)$$

$$\rho_f = \frac{2t_f w_f}{bs_f} \quad (14)$$

Where ε_{fu} is the ultimate is strain in the FRP and ρ_f is FRP reinforcement ratio with respect to concrete

2.2 Ultimate and Cracking Moment in RC Beams under Pure Torsion

2.2.1 Cracking Moment in RC Beams under Pure Torsion [Metin Husem et al (2009)]

Following are the some theory for calculating the cracking moment under pure torsion for reinforced concrete beams [Metin Husem et al (2009]
Elastic Theory [Timoshenko & Goodier 1969; Popov 1990]

$$T_c = \alpha\ (x^2 y)\left(\sqrt[6]{f_c'}\right) \quad (15)$$

Plastic Theory [Nilson 1985; Popov 1990]

$$T_c = \ (0.5 - \frac{x}{6y})\ (x^2 y)(\sqrt[6]{f_c'}) \quad (16)$$

Space Truss Analogy [ACI 318-99 1999]

$$T_c = \sqrt[4]{f_c' \frac{A_c^2}{P_c}} \quad (17)$$

TS 500 2000 [Turkish Standards Institutions]

$$T_c = (1.35)\left(\sqrt[0.35]{f_c'}\right)\left(\frac{b^2 h}{3}\right) \quad (18)$$

Skew B. Theory -2 (Hsu 1984; Hsu & Mo 1985)

$$T_c = \left(\frac{x^2 y}{3}\right)(0.85)\left(\sqrt[7.5]{f_c'}\right) \quad (19)$$

Where

x	=	b	=	width of the beam
y	=	h	=	overall Depth of the Beam
		α	=	angle of Crack in radians
		Ac	=	area of Concrete Section
		Pc	=	perimeter of Concrete Section
		f_c'	=	cylindrical Characteristic Concrete strength

2.2.2 Torsion of Structural Concrete [Thomas T. C. Hsu (1968)]

A simplified equation given by [Thomas T. C. Hsu (1968)] as follows

$$\boldsymbol{T_u = \frac{2.4}{\sqrt{x}}\, x^2 y\sqrt{f_c'} + \left(0.66 + 0.33\frac{y_1}{x_1}\right) x_1 y_1 \frac{A_s f_{sy}}{s}} \quad \textbf{(20)}$$

2.3 Torque in Strengthened RC Beams with FRP

Following are the theoretical studies for calculating the Torque in RC strengthened beams with FRP

2.3.1 FIB (2001)

The model assumed that there is no interaction between the steel and FRP contribution to the torsion resistance of the section. The contribution of the FRP to the torsion capacity of the beam (T_f) was computed as:

For Full Wrapping

$$T_f = \frac{2E_f \varepsilon_f t_f w_f bh \cot(\theta)}{s_f} \quad (21)$$

For U-Wrapping

$$T_f = \frac{E_f \varepsilon_f t_f w_f bh \cot(\theta)}{s_f} \quad (22)$$

Where E_f is Young's modulus of the FRP, t_f is the thickness of the FRP, b and h is the width and depth of the concrete section, respectively, w_f is the width of the FRP strip, s_f is the spacing between strips, θ is the angle of inclination of the diagonal cracks to the longitudinal axis of the beam. The effective FRP strain ε_f is calculated for CFRP and GFRP using the formulas:

$$\varepsilon_f = 0.17 \left(\frac{f_{cm}^{2/3}}{E_{fu} \rho_f} \right)^{0.3} \varepsilon_{fu} \quad (23)$$

Where ε_{fu} is the ultimate is strain in the FRP and ρ_f is FRP reinforcement ratio with respect to concrete calculated as:

$$\varepsilon_f = 0.048 \left(\frac{f_{cm}^{2/3}}{E_{fu} \rho_f} \right)^{0.47} \varepsilon_{fu} \quad (24)$$

$$\rho_f = \frac{2 t_f w_f}{b s_f} \quad (25)$$

2.3.2 Simplified Analysis [Deifalla A and Ghobarah (2005)]

Assuming no interaction between the internal steel reinforcement and the external FRP reinforcement, the total contribution of the reinforcements (T_r) to the torsion capacity of the RC beam can be computed by:

$$T_r = T_s + T_f \quad (26)$$

Where T_s and T_f are the steel and the FRP contribution is to the torsion capacity of the cross section, respectively. The assumption implied in Equation (6) that there is no interaction between the steel and the FRP is not entirely accurate. However, in most of the cases that require strengthening internal steel reinforcement are yielding or deteriorated. Therefore, this assumption may be used for the purpose of simplifying the analysis. Using the Mohr circle equilibrium space truss along with the hollow tube analogy, Deifalla and Ghobarah (2005) proposed that the torsion contribution of inclined steel reinforcements (T_s) to the total torsion capacity of RC beam be computed as:

$$T_s = \frac{2\,A_0 f_y A_t [\cot(\beta_s)+\cot(\theta)]\sin(\beta_s)}{s_s} \quad (27)$$

Where A_0 is area enclosed inside the centre line of the shear flow path, f_y is the yield stress of the reinforcement, A_t is area of the reinforcement resisting torsion, θ is the angle of inclination of the principal cracks and β_s is the angle of inclination of the steel reinforcement. Similarly, the FRP contribution (T_f) to the torsion capacity can be calculated by:

$$T_f = \frac{2\,A_{0f} f_f A_f [\cot(\beta_f)+\cot(\theta)]\sin(\beta_f)}{s_f} \quad (28)$$

where A_{0f} is area enclosed inside the critical shear flow path due to the strengthening, f_f is the stress in the FRP sheets at failure, β_f is angle of orientation of the fiber direction to the longitudinal axis of the beam and s_f is the spacing between the centre line of the FRP strips, and A_f is the effective area of the FRP resisting torsion calculated using:

$$A_f = n_f t_f w_f \quad (29)$$

Where n_f is the number of FRP layers and w_f is the width of the FRP strips. Equation 15 implies that using a number of FRP layers is equivalent to using one FRP layer with the same total area. For the purpose of simplifying the design, this assumption will be used. Using equations (27), (28), (29), will account for the effect various

parameters such as strengthening techniques, number of FRP layers, thickness of each layer, spacing between FRP strips, fiber orientation of FRP sheets, average stress level of the FRP sheets, and angle of principal crack. In order to use the above-mentioned equations, the FRP effective stress has to be computed.

2.3.3 Ultimate and cracking moment strengthened by FRP under Pure Torsion [S. Panchacharam and A. Belarbi (2002)]

S. Panchacharam and A. Belarbi (2002) proposed to calculate the ultimate and cracking moment strengthened by FRP under pure torsion. The increase in cracking torsional moments of the strengthened test beams was modelled as reinforced concrete beams subjected to prestress. The strain in the FRP is gradually varying due to the tensile stresses in surface of the beam. The resistance of FRP to the tensile stresses and strains at the surface of the beam can be considered as applying a passive prestressing force acting in the direction of fibers on the RC beams. Due to the gradual variation of strain in the FRP, the effective prestress is determined based on average strain in the FRP sheets at the instant of cracking in Eq. (30).

$$\text{effective prestress} = \frac{\varepsilon_f E_f}{2} \tag{30}$$

Cracking torque can be determined using the effective prestress as given in Equation (31).

$$T_{cr} = c_1 b^2 h d_t \sqrt{1 + \frac{\text{effective prestress}}{f_t}} \tag{31}$$

where c_1 is St. Venant's constant, which is based on elastic theories, b and h are the dimensions of the beam, ε_f and E_f are the tensile strain and tensile elastic modulus of the FRP sheets, respectively, and ft is the tensile strength of concrete at rupture. Ultimate torque calculations are based on the fiber orientation and the mode of failure. When the failure of the test beam is controlled by FRP rupture and the fibers are oriented in the 90-degree direction, the contribution of FRP sheets to ultimate strength is determined by using the effective strain in the fibers. The effective strain in the

fibers is determined by using the empirical equations proposed in FIB (CEBFIP) Technical Report [FIB (2001)]. If the rupture of fibers does not govern the failure mode, design approach based on effective bond length is used to calculate the ultimate strength. When the fibers are oriented in 0-degree direction, the ultimate strength was not much greater than its cracking strength. Hence, the cracking torque calculated is taken as the predicted ultimate torque.

For Complete wrap and strips

$$T_{u,frp} = \frac{2\, E_{fu}\varepsilon_{ke,f}t_f b_f bh\cot(\alpha)}{s_f} \quad (32)$$

For U-wrap with anchors

$$T_{u,frp} = \frac{E_{fu}\varepsilon_{ke,f}t_f b_f bh\cot(\alpha)}{s_f} \quad (33)$$

where $\varepsilon_{ke,f}$ is the characteristic value of effective FRP strain (corresponding equation to calculate the effective strain in FRP is available in FIB (2001), E_{fu} is the elastic modulus of FRP in the principal fiber orientation, t_f is the thickness of the FRP sheet, s_f is the center-to-center spacing of FRP strips, b_f is the minimum width of the cross section over the effective depth of the cross section, b and h are the cross sectional dimensions of the beam, and α is the angle of diagonal crack with respect to the member axis, assumed equal to 450 based on the reinforcement of the test beams.

The design equations to calculate the ultimate torsional strength of a reinforced concrete beam, recommended by ACI 318-99 is

$$T_{u,RC} = \frac{2A_o A_t f_{yv}}{s_f}\cot(\alpha) \quad (34)$$

Where, A_o is the cross sectional area bounded by the center line of the shear flow, $A_t$is the area of the transverse steel reinforcement (stirrups) provided, f_{yv} is the yield strength of transverse steel reinforcement, s_f is the spacing of stirrups, and α is the angle of diagonal crack with respect to member axis. Hence, the ultimate torsional strength for the FRP strengthened test beams can be obtained by adding the contribution due to fibers and due to reinforced concrete beam as follows:

$$T_u = T_{u,RC} + T_{u,frp} \quad (35)$$

2.3.4 Ultimate and Cracking Torsional Moment [Constantin E. Chalioris (2007)]

The method employs the combination of two different theoretical models. A typical experimental curve of an FRP strengthened RC beam under torsion consists of a pre-cracking and a post-cracking region and justifies this twofold simulation. The elastic till the first cracking response and the cracking torsional moment are predicted by a smeared crack analysis for plain concrete in torsion. The calculation of the post-cracking behaviour and the ultimate torsional moment is based on the well-known softened truss theory, which is properly modified herein in order to take into account the contribution of the FRP materials.

Elastic response and torsional moment at cracking

It is justified that for the elastic till the first cracking response the percentage of reinforcement has a minor effect on the torsional behaviour and RC elements behave, more or less, as plain concrete members. The analytical smeared crack model for plain concrete in torsion proved to be successfully applicable to RC beams for the prediction of the first elastic part till the developing of concrete cracking. The model is based on an analytical technique that employs constitutive relations expressed in terms of normal stress and crack width for the behaviour of the crack process zones.

Post-elastic response and ultimate torsional moment

For the calculation of the post-elastic torsional behaviour and the estimation of the ultimate torque strength the basic equations and considerations of the softened truss model are initially adopted and properly modified to include the influence of FRP. The well-known softened truss theory, which was first developed by Hsu and Mo [1985] and later modified and unified by Hsu [1993], relies on solving equilibrium and compatibility equations along with the constitutive laws of an element taken from a member subjected to pure torsion. Especially for the concrete in compression, it is considered that the concrete strut strength is greatly reduced by the diagonal cracking

caused by tension in the perpendicular direction (concrete softening). The influence of the epoxy-bonded FRP materials as external reinforcement is implemented as an additional component that contributes to the torsional resistance along with the steel reinforcement. Further, the developed confinement due to the wrapping FRP is also taken into account in the analysis using specially developed compressive stress–strain curves for softened and FRP-confined concrete. Moreover, the effective tensile strain of the fibres is estimated based on two analytical procedures, depending on the material and the failure mode of the FRP. An efficient trial-and-error algorithm procedure has also been developed in order to solve the following equations and to calculate the torsional moment versus angle of twist data points.

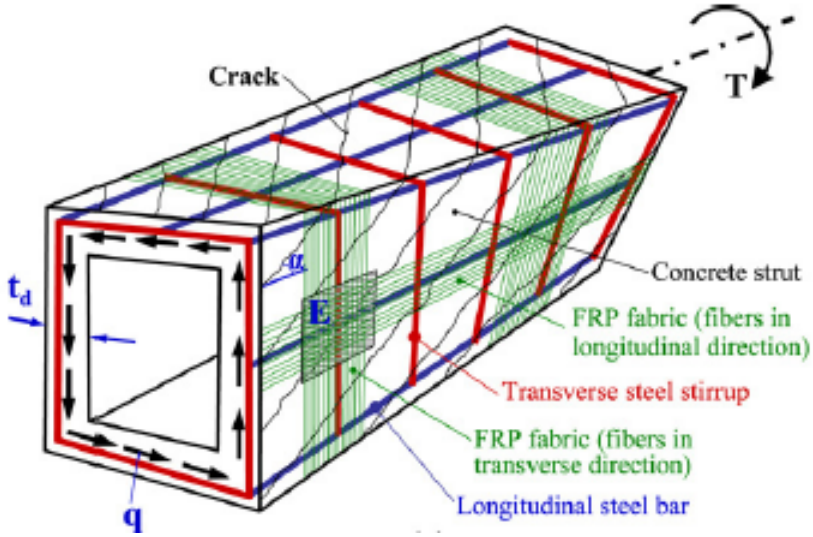

(a)

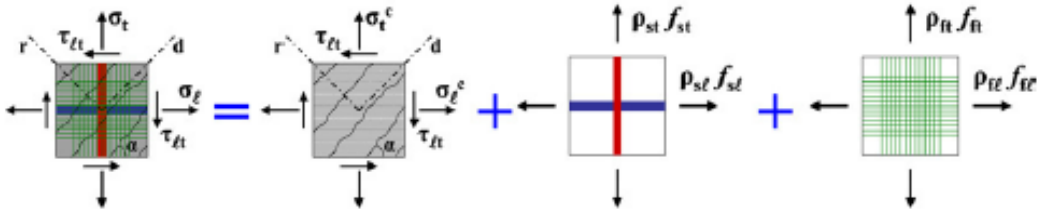

(b)

Fig. 8 (a) & (b) Space truss for the torsional analysis of RC beam strengthened with FRP materials (Constantin E.Chalioris (2007))

Equilibrium equations

When the torsional strength at cracking is reached, diagonal helical cracks are developed around the cross-section of the beam. After concrete cracking, the beam can be idealized as a space truss as shown in Fig. 8 (a), where the external torsional moment T is resisted by an internal torque resulting from the shear flow q, which is developed in the centre of a shear flow zone with an effective wall thickness t_d. Considering the state of stress in a finite concrete element E of the cracked beam, which is assumed to lie in the plane of the shear flow, it is subjected to a set of stresses in the plane represented by Mohr's circle [Hsu (1993)]. Thus, from the stresses equilibrium the following relationships that include the effect of FRP are deduced.

$$\sigma_l = \sigma_d \cos^2 \alpha + \sigma_r \sin^2 \alpha + \rho_{sl} f_{sl} + \rho_{fl} f_{fl} \tag{36}$$

$$\xrightarrow{\sigma_l=\sigma_r=0} -\sigma_d \cos^2 \alpha = \rho_{sl} f_{sl} + \rho_{fl} f_{fl} \tag{37}$$

$$\sigma_t = \sigma_d \sin^2 \alpha + \sigma_r \cos^2 \alpha + \rho_{st} f_{st} + \rho_{ft} f_{ft} \tag{38}$$

$$\xrightarrow{\sigma_t=\sigma_r=0} -\sigma_d \sin^2 \alpha = \rho_{st} f_{st} + \rho_{ft} f_{ft} \tag{39}$$

$$\tau_{lt} = (-\sigma_d + \sigma_r \sin \alpha \cos \alpha \xrightarrow{\sigma_r=0} \tau_{lt} = -\sigma_d \sin \alpha \cos \alpha \tag{40}$$

where σ_l and σ_t are the normal stresses of the element in longitudinal and transverse direction, respectively; σ_d and σ_r are the principal compressive and tensile stresses, respectively; α is the inclination angle of the diagonal compression struts (crack angle); τ_{lt} is the shear stress; ρ_{sl} and ρ_{st} are the longitudinal and transverse steel reinforcement ratio, respectively; ρ_{fl} and ρ_{ft} are the ratio of the FRP materials in longitudinal and transverse direction, respectively; f_{sl}, f_{st} , f_{fl} and f_{ft} are the stresses of steel reinforcement and FRP in longitudinal and transverse direction. It is noted that for the tensile stress of concrete has been neglected (σ_r = 0). Also, since only shear stresses develop on a cross section of an element subjected to pure torsion

without skew restraint, an infinitesimal element on this cross-section is in pure shear stress state without normal stresses ($\sigma_l = \sigma_t = 0$). The crack angle α can be calculated

$$\tan\alpha = \sqrt{\frac{\rho_{st} f_{st} + \rho_{ft} f_{ft}}{\rho_{sl} f_{sl} + \rho_{fl} f_{fl}}} \tag{41}$$

The shear flow derived from the Bredt equation has the form

$$q = \frac{T}{2\,A_o} \xrightarrow{q=\tau_{lt} t_d} \tau_{lt} = \frac{T}{2\,A_o t_d} \tag{42}$$

$$T = -\sigma_d\, A_o t_d \sin\alpha \cos\alpha \tag{43}$$

Where T is the torsional moment; A_o is the area enclosed by the centre line of the shear flow.

2.3.5 Ultimate and Cracking torsional moment [A. Ghobarah et al (2002)]

The relationship between the ultimate torsional moment T_u and the ultimate shear stress in concrete υ_u is

$$T = 0.67\left(A_c^2 / P_c\right) \upsilon_u \tag{44}$$

Where A_c = gross area of the concrete cross section; and P_c = perimeter of the outer dimensions of the concrete cross section. The shear strength of concrete υ_u is calculated as a fraction of the compressive strength f_c' by taking into account the longitudinal and transverse steel ratios. The ultimate applied central load P_u is calculated using the expression

$$P_u = 2\,T_u / a \tag{45}$$

Where the moment arm a = lever arm

The difference between the recorded ultimate torque for strengthened beams and the torsional moment capacity of the provided longitudinal reinforcement provided in compression as well tension zone was assumed to represent the contribution of the FRP.

From the torque taken by the FRP, T_f, the strain in the fiber ε_f , was calculated as

$$\varepsilon_f = \frac{T_f\left(\frac{A_f}{s}\right)^{-1}}{(A_c E_f)} \quad (46)$$

Where A_f area of the fiber material; s=length along the beam over which the fiber area is distributed (in order to obtain area per unit length of fiber); and E_f modulus of elasticity of the CFRP fiber material. For the case of 45° spiral wrapping of CFRP strips, the strain along the fibers in the spiral direction can be calculated using Eq. (46) as ε_f /cos 45°.

Accordingly, the maximum additional torsional moment contribution of the CFRP T_f may be estimated from Eq. (47) by assuming the average ultimate fiber strain to be approximately 0.003; thus

$$\boldsymbol{T_f = 0.006\, A_f A_c E_f / s} \quad \textbf{(47)}$$

The total torsional moment capacity of the strengthened beam T can be calculated by adding the contribution of the reinforced concrete section given by Eq. (48) plus the contribution of the CFRP given by Eq. (47)

$$T = T_u + T_f \quad (48)$$

It should be noted that Eq. (47) is applicable for the case of fiber wrap with the fibers in the (vertical) transverse direction of the beam.

2.4 Ductility

The ductility ratio, $\mu_{\emptyset}$ is usually defned as:

$$\boldsymbol{\mu_{\emptyset} = \frac{\emptyset_p}{\emptyset_y}} \quad \textbf{(49)}$$

Where $\emptyset_p$ is the twist angle at the ultimate torque and $\emptyset_y$ is the yield twist angle. This ratio indirectly represents the amount of energy that a member can store during plastic deformations and so represents the ductility or energy absorbing capacity of the member. This concept of ductility can be applied to strengthened reinforced concrete members in a similar manner.

Some other researchers have proposed the following relation for computing the ductility ratio.

$$\boldsymbol{\mu_{\emptyset,0.85P} = \frac{\emptyset_{0.85p}}{\emptyset_y}} \quad \textbf{(50)}$$

Where $\boldsymbol{\emptyset_{0.85p}}$ is the twist angle at 85% of the peak torque beyond the peak point.

CHAPTER – 3

MATERIAL PROPERTIES
AND
MIX DESIGN

CHAPTER - 3

3.0 MATERIAL PROPERTIES AND MIX DESIGN

3.1 CEMENT

Ultratech make 43 Grade OPC Cement used for the experimental work. Before preparing the Mix-Design the following test was carried out to find the various properties of cement according to IS: 4031.

3.1.1 Normal consistency of cement

Consistency means the amount of water needed to prepare a plastic mix. It is a term which describes the state of fresh concrete. It shows the degree of wetness of cement. It also affects the workability of concrete hence determination of consistency is very important. To determine the consistency of cement Vicat's apparatus is used, and tested according to IS: 4031 (Part IV).

Experimental procedure

i. The Vicat's apparatus was set at zero.
ii. The given sample was taken and 90 ml (by assuming a normal consistency 30 by the range 26 – 35) water was added to it.
iii. Cement mixed with water gradually, within 3 to 5 minute then mould is filled with the water cement paste after that mould is vibrating slowly with hand.
iv. Mould is placed on the Vicat's apparatus platform then touch the plunger to the cement surface.
v. Allow the plunger to sink slowly into the paste. Reading is recorded.
vi. Trial paste was taken to five times until the penetration of 5-7 mm achieved.
vii. After the penetration of 5-7 mm achieved the reading was taken that point describe normal consistency of cement.

Fig. 9 Vicat's Apparatus showing Testing of Consistency of Cement

Results

Normal Consistency of Cement = 31.3%

3.1.2 Initial and Final Setting Time of Cement

Initial setting time is the time between which water is added to cement at which Vicat's needle fail to penetrate cement waste paste 5 to 7 mm bottom of mould and final setting time is the time when water is added to cement and an impression was not seen on the paste. It is important to note initial and final setting time of cement because when water is added to cement chemical reaction take place and cement start harden and one time if its hard then paste of water and cement will not used for construction. Procedure and some relevant information related to test are describe in IS: 4031 (Part V).

Fig. 10 Vicat's Apparatus showing Testing of Initial and Final Setting Time of Cement

Experimental procedure

i. Cement and water paste was prepare as per standard consistency and mould is filled with paste.

ii. Mould is placed under calibrated Vicat's apparatus and reading is recorded with the stop watch by lowering the needle.

iii. Every half an hour penetration is checked until a penetration of 5-7mm was not achieved that was initial setting time.

iv. Needle changed and impression was checked at the interval of every one hour until impression disappears.

v. Disappearance of impression was the finial setting.

Results

Initial Setting Time = 140 minutes

Final Setting Time = 325 minutes

3.1.3 Compressive Strength of Cement Mortar Cubes

This test help us to determine the compressive strength of cement mortar cubes as per IS: 4031 (Part VI). Compressive strength test is the final check on the quality of cement. This test is performed in order to determine whether the cement conforms to standard specifications or not. The compressive strength is measured by determining the compressive strength of cement mortar cubes of one part of cement to three part of fine aggregates (standard sand).

Fig. 11 Cement Cube Moulds

Experimental Procedure

i. Sample of 200gm of ordinary Portland cement and sand conforming to IS: 650-1966 (revised) was mixed properly in uniform colour.
ii. After mixing the sample properly water was added to it p/4+3.00% (where P was percentage of water for preparing paste of standard consistency) within 3 minutes
iii. Cleaned cubes moulds are oiled thoroughly.
iv. Clamps of vibrating machine are opened and placed the mould thoroughly.

v. Mould was filled with cement sand paste using hopper attached at the top of mould and tamped 25 times and allow vibrating it for 2 minutes at a specified speed of 12000±400 per minute to achieve full compaction.

vi. Moulds was removed from vibrating machine and keep it in a place with temperature of 27°±2°C and relative humidity of 90% for 24 hrs.

vii. At the end of 24 hours cubes are removed from mould immediately and marked date of manufacturing on it than submerge in fresh water.

viii. 6 cubes were prepared in same manner.

ix. After 7 days three cubes are taken for strength testing and placed it under the compaction machine and load applied for breaking the cubes.

x. All the reading was noted.

xi. Similarly after 28 days remaining cubes taken and repeat above same process of 7 days and determine the strength.

Fig. 12 Vibrating Machine for mixing of Cement Mortar Cubes

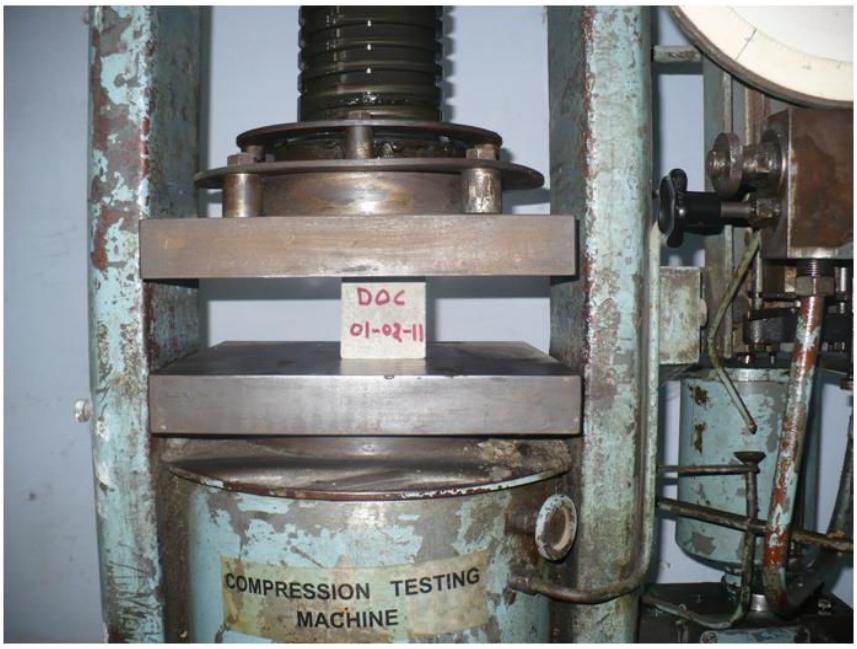

Fig. 13 Testing of Cement Cube

Results

Average strength of 7 days cubes = 388 N/mm²

Average strength of 28 days cube = 495 N/mm²

3.2 AGGREGATES

3.2.1 Specific gravity

3.2.1.1 Fine Aggregate

This test help us to determine specific gravity of fine aggregate as per IS: 2386 (Part III). Specific gravity of fine aggregate is important to determine for moisture contain and volume yield of concrete. It also gives information regarding quality and properties of aggregate.

Fig. 14 Apparatus Pycnometer

Experimental procedure

i. Sample of 500gm fine aggregate was washed with water to remove their silt content in 75μ IS: sieve.
ii. Empty weight of Pycnometer was taken and recorded.
iii. Water was filled in Pycnometer at the tip and weight of water and Pycnometer were taken and noted.
iv. Sample was filled half of the Pycnometer and than water + sample + Pycnometer weight were taken.
v. Drawn the sample and water from Pycnometer in a tray and put it in oven at 100° to 110° C for 24hrs.
vi. Add little water to sample to determine its SSD weight and recorded.
vii. Again sample was put into the oven for 24 hrs and weight of dry sample is taken.
viii. Calculate the specific gravity of fine aggregate.

Results

Specific Gravity = 2.683

Water absorption = 0.826%

Moisture Content = 1.78%

3.2.1.2 Coarse Aggregate – 20 mm down

This test help us to determine the specific gravity of 20 mm aggregate as per IS: 2386 (Part III). Specific gravity is quality of aggregate. It is useful for calculating voids contain in the aggregate. If the specific gravity is above or below for a particular type of aggregate, it is an indication of change of shape and grading.

Fig. 15 Apparatus of Weighing of Aggregate in Water

Experimental procedure

i. Sample of 710 gm was washed to remove finer dust particles and the sample was immersed in water for 24 hr.
ii. After 24hr. wire basket was filled with water and weighted it. Basket +water was the weight (A) noted.
iii. Basket + water + sample were the weight (B).

iv. Sample was taken out from basket and then sample was rubbed by cloth for surface saturated weight.

v. Surface saturated weight (C) was taken and placed it in oven for 24hr.

vi. Sample was taken out from oven and weighted (D) it.

Results

Specific gravity = 2.604

Water absorption = 0.565%

3.2.2 Aggregate Impact Value (AIV)

This test is done to determine the aggregate impact value of coarse aggregate as per IS: 2386 (Part IV)–1963. The 'Aggregate Impact Value' gives a relative measure of the resistance of an aggregate to sudden shock or impact, which in some aggregates differs from its resistance to a slow compressive load. The impact value is the resistance of an aggregate to sudden compressive forces. It is desirable that the aggregate should be able to resist impact well. In this test an Impact Testing Machine is used to determine impact value of aggregates.

Fig. 16 Equipment for finding Impact Value

Experimental Procedure

i. The cylindrical metal measure of the impact testing machine was filled to about one-third with the aggregate and tamped for 25 times with the rounded end of the tamping rod. A further similar quantity of aggregate was added and a further tamping of 25 strokes was given. The net weight of aggregate in the measure was determined to the nearest gram (weight 'A').
ii. The cup of the impact testing machine was filled with the test sample and was fixed firmly in position to the base of the machine.
iii. The hammer of the impact testing machine was raised to 380mm above the upper surface of the aggregate in the cup, and was allowed to fall freely on to the aggregate. The test sample was subjected to a total of 15 such blows, each being delivered at an interval of not less than one second.
iv. The crushed aggregate was then removed from the cup and the whole of it was sieved on the 2.36 mm IS Sieve. The fraction passing the sieve was weighted (weight 'B').
v. The fraction retained on the sieve was also weighed (weight 'C').
vi. Calculate the impact value of aggregate.

Results

Aggregate impact value = 18.6 %

Acceptance Criteria

As per IS: 383:1970, the aggregate impact value shall not exceed 45 percent by weight for aggregates used for concrete other than for wearing surfaces and 30 percent by weight for concrete for wearing surfaces, such as runways, roads and pavements. In our testing result impact value is 18.6%, which satisfied the condition.

3.2.3 Aggregate Crushing Value (ACV)

This test method helps to determine the aggregate crushing value of coarse aggregate as per IS: 2386 (Part IV) – 1963. Crushing strength of aggregate is the résistance of aggregate to compressive forces. In order to know the behaviour of aggregates when subjected to wear the crushing strength value is important.

Fig. 17 Mould for Finding Crushing Value

Experimental Details

i. A coarse aggregate sample, weighing 2813 gm, and passing through 12.5mm and retained on 10 mm IS Sieve was oven- dried at a temperature of 100˚ to 110˚C.

ii. The cylinder of the crushing value apparatus was filled in three layers, and each layer was tamped with the tamping rod for 25 times. The weight of the material comprising the test sample was determined (Weight A).

iii. The surface of the aggregates was then leveled and the plunger of the crushing value apparatus was inserted. The apparatus was then placed in the compression testing machine and loaded at a uniform rate so as to achieve 40 Tons load in 10 minutes. After this, the load was released.

iv. The sample was then sieved through a 2.36mm IS Sieve and the fraction passing through the sieve was collected and weighed (Weight B).

Fig. 18 Testing of Finding Crushing Value

Result

Aggregate crushing value (%) = 22.8%

Acceptance criteria

As per IS: 383:1970, the aggregate crushing value, shall not exceed 45 percent by weight for aggregate used for concrete other than for wearing surfaces, and 30 percent for concrete for wearing surfaces, such as runways, roads and pavements. In our result aggregate crushing value is 22.8%, which satisfied the result.

3.2.4 Aggregate Abrasion Value (ABV)

This test helps us to determine the abrasion value of aggregate as per IS: 2836 (Part IV)-1963. Resistance to abrasion is the resistance of aggregate to wear. It is desirable that the aggregate should be able to resist abrasion well. This quality is ascertained by

finding the abrasion value of the aggregate. LOS Angles Machine is used to find the abrasion value of aggregates.

Fig. 19 LOS Angles Abrasion Machine and Spheres

Table 1 Abrasive Charges Vs Grading of Aggregate

Grading	Number of Spheres	Weight of charge
A	12	5000 ± 25
B	11	4584 ± 25
C	8	3330 ± 20
D	6	2500 ± 15
E	12	5000 ± 25
F	12	5000 ± 25
G	12	5000 ± 25

Table 2 Sieve Size Vs Weight of Test Sample for Abrasion Value (AV) Test

Sieve size		Weight in gm of test sample for grade						
Passing through (mm)	**Retained on (mm)**	**A**	**B**	**C**	**D**	**E**	**F**	**G**
80	63	-	-	-	-	2500*	-	-
63	50	-	-	-	-	2500*	-	-
50	40	-	-	-	-	5000*	5000*	-
40	25	1250	-	-	-	-	5000*	5000*
25	20	1250	-	-	-	-	-	5000*
20	12.5	1250	1250	-	-	-	-	-
12.5	10	1250	1250	-	-	-	-	-
10	6.3	-	-	2500	-	-	-	-
6.3	4.75	-	-	2500	-	-	-	-
4.75	2.38	-	-	-	5000	-	-	-

Experimental procedure

i. Sample of 5kg of aggregate were passed through 20mm IS: Sieve and retained on 12.5 mm IS: Sieve was used.
ii. Sample and abrasive charge was filled in los angle abrasion machine than machine cylinder rotated at the rate of 30 to 33 rpm for 500 numbers of revolutions.
iii. After half hour cylinder was opened and filling was withdrawn from it.
iv. Sample was sieved by 1.7mm IS sieve and weight of aggregate passing through IS sieve 1. 7mm is calculated and express as the percentage of original weight which gives the abrasion value of aggregate.

Results

Weight of sample = 5000gm
Abrasion value = 29%

Acceptance Criteria

According to IS: 2386 (Part IV)- 1963 using Los Angeles machine was not exceed for aggregate to be used in 30% concrete for wearing surfaces and 50% for other concrete surfaces.

3.2.5 Sieve Analysis

3.2.5.1 Sieve of Coarse Aggregate

This method covers the procedure for the determination of particle size distribution of the coarse aggregates. This sieve analysis is important as a well graded aggregate mix would produce a cohesive concrete mix. This is done by sieving the aggregates as per IS: 2386 (Part I) – 1963 (Re-affirmed 2007). In this method, different standard sieves as per the above IS code are taken, and assembled in the decreasing order of the aperture size and a weighed mixture of aggregates are passed through the set of sieves. The aggregates collected on each sieve are weighed.

Experimental procedure

i. The test sample of 3000 gm of 20mm size and 2000 gm of 10 mm size was dried to at a temperature of $110^0 + 5^0$C.
ii. Sieve is filled with cooled sample after weighing the sample correspondingly.
iii. A set of IS Sieve (40mm, 20mm, 10mm, 4.75mm and pan) was used for 3000 gm sample and a set of IS Sieve (12.5 mm, 10 mm, 4.75 mm, 2.36 mm and pan) was used for 2000 gm sample.
iv. A sieve was shaked in varied motion with frequent jarring.
v. On the completion of sieving, the material on each sieve is weighed.
vi. Cumulative weight passing through each sieve is calculated as a percentage of the total sample weight.

Result

Table 3: Results of Sieve Analysis of 20mm Aggregate

Sample no.	Sieve size	% passed	Permissible Limit as per IS: 383
1.	40	100	100
2.	20	96.8	90─100
3.	10	26.10	20─25
4.	4.75	3.96	0─10

Table 4: Results of Sieve Analysis of 10mm Aggregate

Sample no.	Sieve size	% passed	Permissible limit as per IS: 383
1.	12.5	99.5	100
2.	10	96.35	85─100
3.	4.75	22.90	0─25
4.	2.36	5.17	0─5

3.2.5.2 Sieve Analysis of Fine Aggregate

This method covers the procedure for the determination of particle size distribution of the coarse and fine aggregates. This sieve analysis is important as a well graded aggregate mix would produce a cohesive concrete mix. This is done by sieving the aggregates as per IS: 2386 (Part I) – 1963 (Re-affirmed 2007). In these method different standard sieves as per the above IS code are taken, and assembled in the decreasing order of the aperture size and a weighed mixture of aggregates are passed through the set of sieves. The different sieves used are shown in Fig. 20. The aggregates collected on each sieve are weighed.

Experimental procedure

i. Fineness modulus is obtained by adding cumulative percentage the test sample of 1500 gm is dried to at a temperature of 110 + 5^0C and weighed.

ii. After weighing, sample put in cleaned sieve of above size.

iii. The sample is sieved by using a set of IS Sieves (10 mm, 4.75 mm, 2.36 mm, 1.18mm, 600 µm, 300 µm, 150 µm and pan) after properly arranged. Shake the sieve with a varied motion with frequent jarring.

iv. On completion of sieving, the material on each sieve is weighed.

v. Cumulative weight passing through each sieve is calculated as a percentage of the total sample weight of aggregates retained on each sieve and dividing the sum by 100.

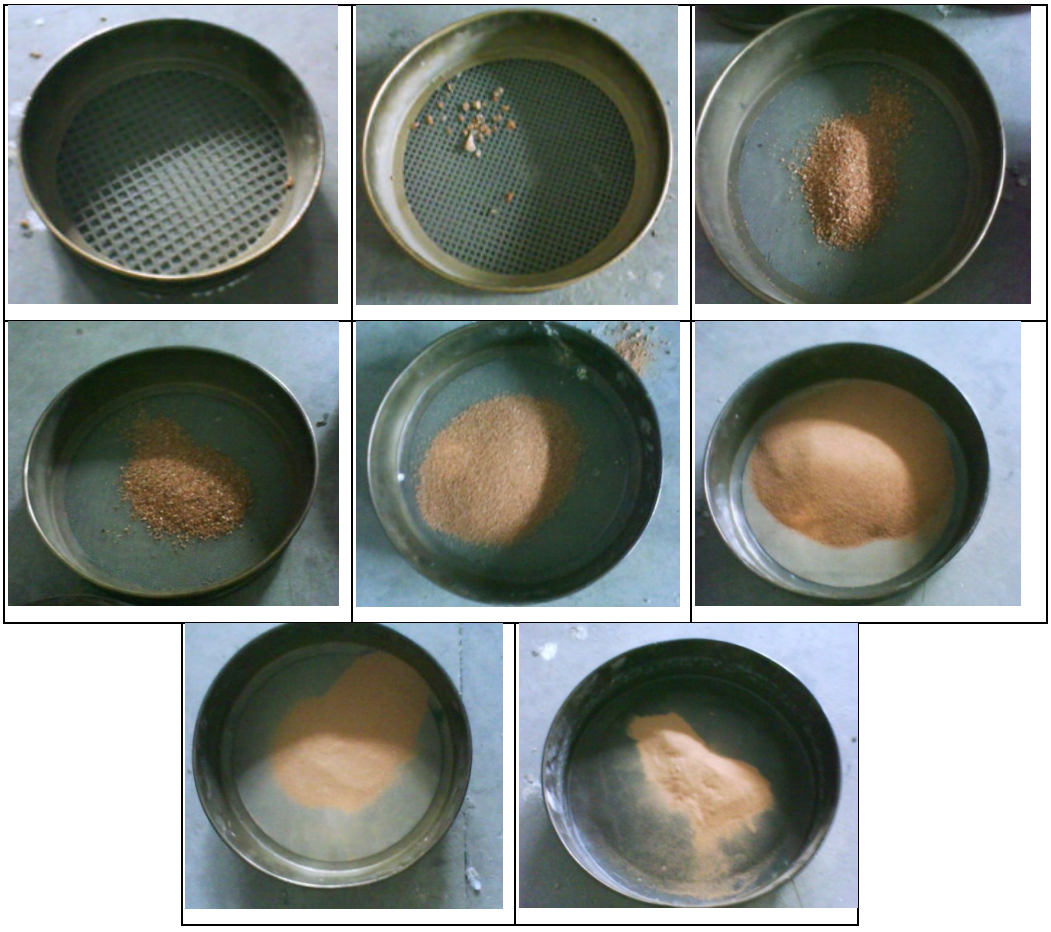

Fig. 20 Aggregates Retain on Various Sieve for Sieve Analysis of Fine Aggregates

Results

Table 5 Results of Sieve Analysis of Fine Aggregate

IS: sieve size (mm)	% passed	% passing for zone		
		I	II	III
10	100	100	100	100
4.75	91.5	90-100	90-100	90-100
2.36	83.6	60-95	75-100	85-100
1.18	74.4	30-70	55-90	75-100
600µm	55.4	5-34	35-59	60-79
300µm	18.2	5-20	8-30	12-40
150µm	6.5	0-10	0-10	0-10

The results passing percentage of 600 µm IS sieve from Table 5 shows that the Fine Aggregate conforms to Zone II.

3.3 Mix Design

Previous chapter we discussed and calculate the material properties of Cement, Coarse Aggregate and Fine Aggregate. For preparing the mix design trials for grade of M30, a spreadsheet was prepared in M.S. Excel with incorporate the all step to step procedure mentioned in IS Code 10262:2009. While giving all the input to the spreadsheet, the following three trials for tested for target strength of 38.25 N/mm^2 as derived from the excel spreadsheet and his composition as follows:

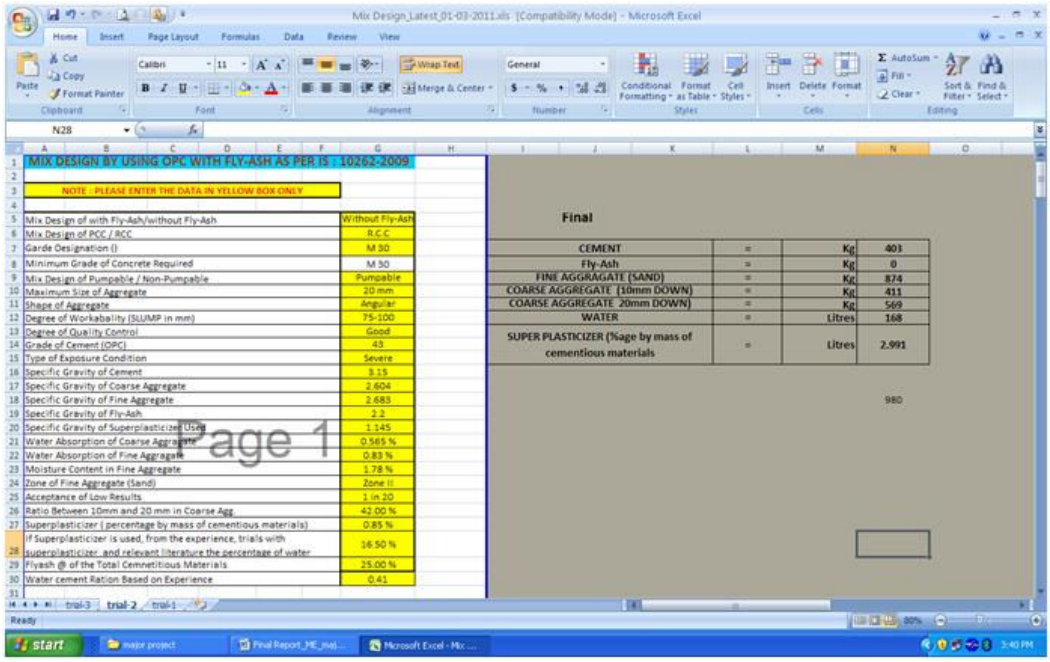

MIX DESIGN BY USING OPC WITH FLY-ASH AS PER IS : 10262-2009

NOTE : PLEASE ENTER THE DATA IN YELLOW BOX ONLY

Mix Design of with Fly-Ash/without Fly-Ash	Without Fly-Ash
Mix Design of PCC / RCC	R.C.C
Garde Designation ()	M 30
Minimum Grade of Concrete Required	M 30
Mix Design of Pumpable / Non-Pumpable	Pumpable
Maximum Size of Aggregate	20 mm
Shape of Aggregate	Angular
Degree of Workability (SLUMP in mm)	75-100
Degree of Quality Control	Good
Grade of Cement (OPC)	43
Type of Exposure Condition	Severe
Specific Gravity of Cement	3.15
Specific Gravity of Coarse Aggregate	2.604
Specific Gravity of Fine Aggregate	2.683
Specific Gravity of Fly-Ash	2.2
Specific Gravity of Superplasticizer Used	1.145
Water Absorption of Coarse Aggregate	0.565 %
Water Absorption of Fine Aggregate	0.83 %
Moisture Content in Fine Aggregate	1.78 %
Zone of Fine Aggregate (Sand)	Zone II
Acceptance of Low Results	1 in 20
Ratio Between 10mm and 20 mm in Coarse Agg.	42.00 %
Superplasticizer (percentage by mass of cementious materials)	0.85 %
If Superplasticizer is used, from the experience, trials with superplasticizer and relevant literature the percentage of water Flyash @ of the Total Cemnetitious Materials	16.50 % 25.00 %
Water cement Ration Based on Experience	0.41

Final

CEMENT	=	Kg	403
Fly-Ash	=	Kg	0
FINE AGGRAGATE (SAND)	=	Kg	874
COARSE AGGREGATE (10mm DOWN)	=	Kg	411
COARSE AGGREGATE (20mm DOWN)	=	Kg	569
WATER	=	Litres	168
SUPER PLASTICIZER (%age by mass of cementious materials	=	Litres	2.991

980

Page 1

(a) Full Sheet View for Data Input

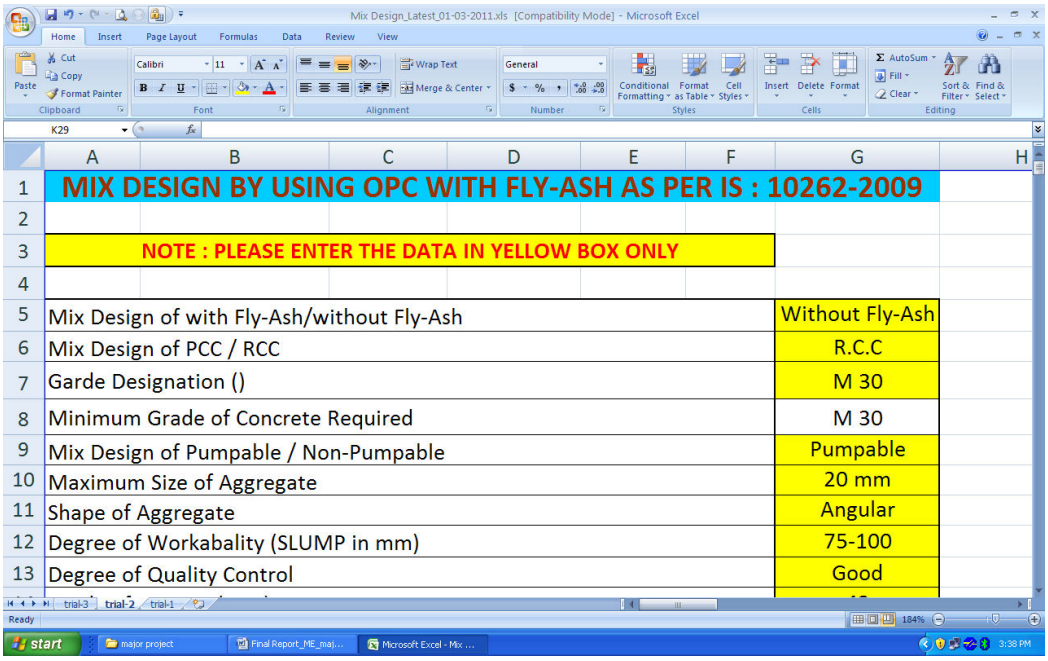

MIX DESIGN BY USING OPC WITH FLY-ASH AS PER IS : 10262-2009

NOTE : PLEASE ENTER THE DATA IN YELLOW BOX ONLY

Mix Design of with Fly-Ash/without Fly-Ash	Without Fly-Ash
Mix Design of PCC / RCC	R.C.C
Garde Designation ()	M 30
Minimum Grade of Concrete Required	M 30
Mix Design of Pumpable / Non-Pumpable	Pumpable
Maximum Size of Aggregate	20 mm
Shape of Aggregate	Angular
Degree of Workability (SLUMP in mm)	75-100
Degree of Quality Control	Good

(b) Close View

Fig. 21 Microsoft Excel Spreadsheet for Mix Design any Grade as per IS 10262: 2009

Table 6 Proportion of Mixes of Trials as per of IS 10262:2009

Grade of Concrete - M30 (Mix Design as per IS 10262:2009)				
Type of Cement – OPC – 43 Grade				
		Trial-1	**Trial-2**	**Trial-3**
Water Cement Ratio (W/C Ratio)		0.41	0.41	0.41
Specific Gravity of Cement		3.15	3.15	3.15
Specific Gravity (Bulk) of Fine Aggregate		2.683	2.683	2.683
Specific Gravity (Bulk) of Coarse Aggregate		2.604	2.604	2.604
Water Absorption of Fine Aggregate		0.83%	0.83%	0.83%
Type of Fine Aggregate		Zone II	Zone II	Zone II
Water Absorption of Coarse Aggregate		0.565	0.565	0.565
Percentage of Coarse Aggregate w.r.t Total Volume of Aggregate in Concrete		0.62	0.62	0.62
Free Water Content in Fine Aggregate		0.00	0.00	0.00
A)	Cement (Kg)	410	403	385
B)	Water (Kg)	171	168	163
C)	Fine Aggregate (Kg)	868	874	885
D)	Coarse Aggregate (Kg) – 10mm	437	411	396
E)	Coarse Aggregate (Kg) – 20mm	536	569	596
F)	Total Weight of Coarse Natural Aggregate (kg)	973	980	992
G)	Super-Plasticizer (Litres)	0.75% - 2.685	0.85% - 2.991	1.00% - 3.414

Table 7 shows the compressive strength of all the three trials after 7 and 28 days.

Table 7 Compressive Strength of Cubes form various Trials after 7 and 28 Days

Description	Trial – 1	Trail - 2	Trail - 3
Cement Contents – (Kg)	410	403	385
Compressive Strength after 7 Days (N/mm^2)	27.10	27.15	25.65
Compressive Strength after 28 Days (N/mm^2)	39.09	38.85	36.75

From the above results Trial-2 was to be selected for the experimental work.

3.4 STEEL

Generally steel was used for provide in longitudinal reinforcement at top and bottom of the beam were provided to resist the bending as well torsion moment in the beams and vertical shear stirrups were provided to resist the shear stress induced in the beams. In our experimental program TMT steel of grade Fe 500 was used and tested as per IS 1786: 2008

3.4.1 Tensile Strength

The tensile test of steel was conducted on UTM machine installed in Bridges Division of Central Road Research Institute. Fig. 22 shows the testing of steel in universal testing machine. The results were presented in the Table 8.

Table 8 Results of Ultimate Tensile Strength of Steel Rebars

Sr. No.	Nominal Diameter of Bar (mm)	Actual Weight (Kg/m)	Actual Cross Sectional Area of Bar (mm^2)	Ultimate Tensile Load (KN)	Ultimate Tensile Strength (N/mm^2)	Avg. Ultimate Tensile Strength (N/mm^2)
1	12	0.893	113.707	70.56	623.87	**623.11**
2	12	0.893	113.707	70.18	620.51	
3	12	0.891	113.554	70.68	624.93	
1	8	0.383	48.820	30.05	597.42	**612.86**
2	8	0.388	49.427	31.18	619.88	
3	8	0.384	48.926	31.25	621.27	

Fig. 22 Testing of Ultimate Tensile Strength of Steel Rebar

3.4.2 Percentage of Elongation

Impressions were marked every 10 mm on the sample by knife edge Blade on the Steel Rebars. After the specimens were failure of the sample in ultimate load, the gauge length was again measured between the marked impressions.

Table 9 Results of Percentage of Elongation of Steel Rebars

Sr. No.	Nominal Diameter of Bar (mm)	Actual Weight (Kg/m)	Actual Cross Sectional Area of Bar (mm^2)	Gauge Length (Lo) (mm)	Elongation (δLo) (mm)	% age of Elongation	Aevarage %age of Elongation
1	12	0.893	113.707	60	13	21.67	**20.56**
2	12	0.893	113.707	60	12	20.00	
3	12	0.891	113.554	60	12	20.00	
1	8	0.383	48.820	40	7	17.50	**17.50**
2	8	0.388	49.427	40	7	17.50	
3	8	0.384	48.926	40	7	17.50	

3.5 FRP

Strengthening proposed to provide U-shaped Carbon Fabric. In case of strips, it is difficult to possible to provide continues U-shaped Strips. So we decided to used Carbon Fabric – 400 g/m^2 in our strengthening scheme, It is very easy to provide in corners of the beam and contact area at corner is also very good in case Carbon Fabric as compared to Strips. Fig. 23 shows the CFRP Fabric – 400 g/m^2

The Carbon Fabric was provided by Dr. Gopal Lalji Rai, Chief Executive Officer, R&M International, Mumbai.

The Technical data sent by the supplier was used in our design calculation

Fig. 23 CFRP-Fabric – 400 g/m^2 (Unidirectional)

The following the technical data provided by the R&M International.

Table 10 Technical Data of CFRP – Fabric

Technical data (Unidirectional)	CFRP-Fabric – 400 g/m^2
Weight per unit area of sheet (g/m^2)	430
Elastic modulus (kN/mm^2)	260
Tensile strength (N/mm^2)	3900
Fibre weight (g/m^2) (main direction)	400
Density (g/cm^2)	1.8
Elongation at rupture (%)	1.55
Design thickness (Fiber weight/density) (mm)	0.234

3.6 Adhesive

When RC beam was strengthen with CFRP Fabric, the Adhesive (R&M Matrix 20) used was also provided by R&M International along with Primer (R&M Resin Primer 11) for better bonding of adhesive to the concrete surfaces.

3.6.1 R&M Resin Primer 11

Primer is the concrete bonding adhesive for use with the Composite Strengthening System. It is a 100% solids low viscosity epoxy resin able to cure in the presence of moisture and at temperatures as low as 2ºC. When applied to sound concrete Composite primer gives high tensile bond strength to the Composite strengthening system.

Method of Application

- In substrata maximum moisture content 4%.
- This may be applied with a brush, a roller or an airless spray.
- Composite Primer must be allowed to cure until tack free (overnight curing is common practice).

The following the technical information provided by the R&M International

Table 11 Technical Data of R&M Resin Primer 11

Properties (Unit)	**Value**
Density (kg/1)	1.10 + 0.01
Packing size (kg)	6
Mix Ratio (Base: Hardener)	100:50
Tensile Strength (N/mm2)	22
Flexural Strength (N/mm^2)	52
Initial tackness (hours)	1.3
Final Set (Days)	1 day
Bond strength in concrete	Failure in Concrete
Coverage	0.25 – 0.35 kg / m^2

3.6.2 R&M Matrix 20

R&M Matrix 20 is a two component solvent free epoxy system for rectifying irregularities on concrete surfaces.

Areas of Application

- Composite FRP system
- Concrete and masonry surface imperfections
- Filling pinholes prior to over coating
- Sealing of surface cracks
- General fair facing over large areas, up to 3 mm thick
- Saturating the dry fiber sheet

The following are the Physical Properties provided by the supplier

Table 12 Physical Properties of Adhesive - R&M Matrix 20

PROPERTY	**TEST METHOD**	**VALUE**
Component	-	Two: Part A- Base
	-	Part B-Hardener
Mixed Form	-	Paste
Colour	-	Off White or Grey
Mixed Density	ASTM D1475	.80 kg/ltr +/- 0.05
Potlife	-	70 +/- 10 mins
Compressive Strength	BS 6319-2	60 N/mm^2 at 7 days
Flexural Strength	BS 6319-3	23 N/mm^2 at 7 days
Tensile Strength	BS 6319-7	20 N/mm^2 at 7 days
Bond Strength	ASTM D4541	> 2.5 N/mm^2 at 7 days
Solid Content	ASTM D1475	100% (Solvent free)
Application Temperature	-	+5°C to +45°C

CHAPTER – 4

ANALYSIS

CHAPTER – 4

4.0 ANALYSIS

4.1 Ultimate Torsional Moment of Test Specimens By IS 456:2000

Excel Spreadsheet was prepared as per IS 456:2000 to calculate the Ultimate Torsional Moment of the Section.

SPAN	=	**1790**	mm
f_y	=	**500**	N/mm^2
f_{ck}	=	**30**	N/mm^2
b	=	**150**	mm
D	=	**250**	mm
clear cover on ten.face	=	**20**	mm
clear cover on com.face	=	**20**	mm
Side Cover		**20**	mm
M_u	=	1	kNm
V_u	=	73	kN
T_u	=	8.5	kNm
Lever Arm	=	**170**	mm
Load (P/2)	=	**50**	kN

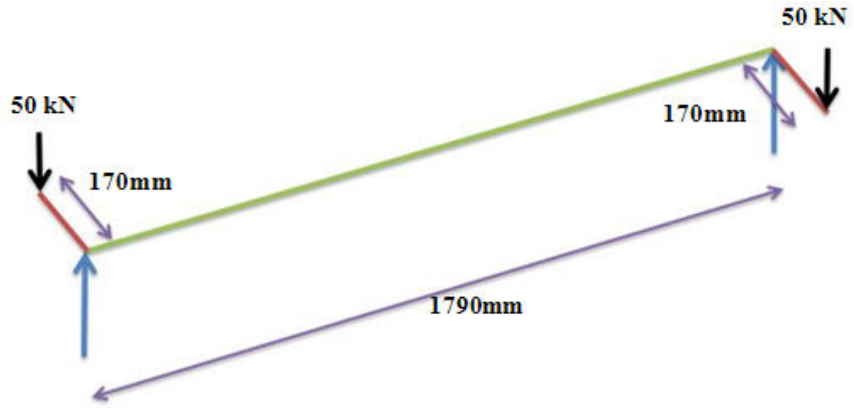

Fig. 24 Line Diagram showing Loading and Span of Reference Beam PTR-1.

Ultimate Torsional Capacity of Test Specimen Reference Beam PTR-1 as per IS 456: 2000 was 8.5 kNm and Fig. 24 shows the line diagram of loading with showing the distance of lever arm.

Ultimate Torsional Capacity of test Specimens Distressed Beam PTT-1 as per IS 456: 2000 was 3.2 kNm.

4.2 Ultimate Torsional Moment By Software STAAD Pro V8i

The beam was also designed in Software STAAD Pro V8i. The Fig. 25 shows the torque applied at end of the beam and Fig. 26 and 27 shows the Torsional moment diagram (TMD) and design of section respectively.

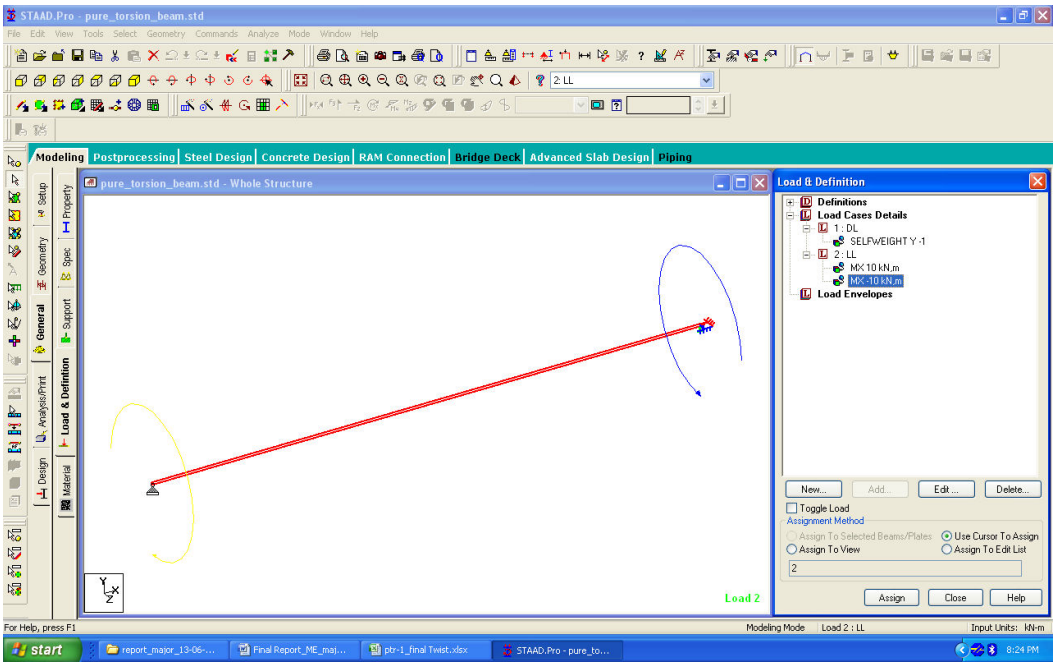

Fig. 25 View of STAAD Software Showing Torque applied at Reference Beam PTR-1.

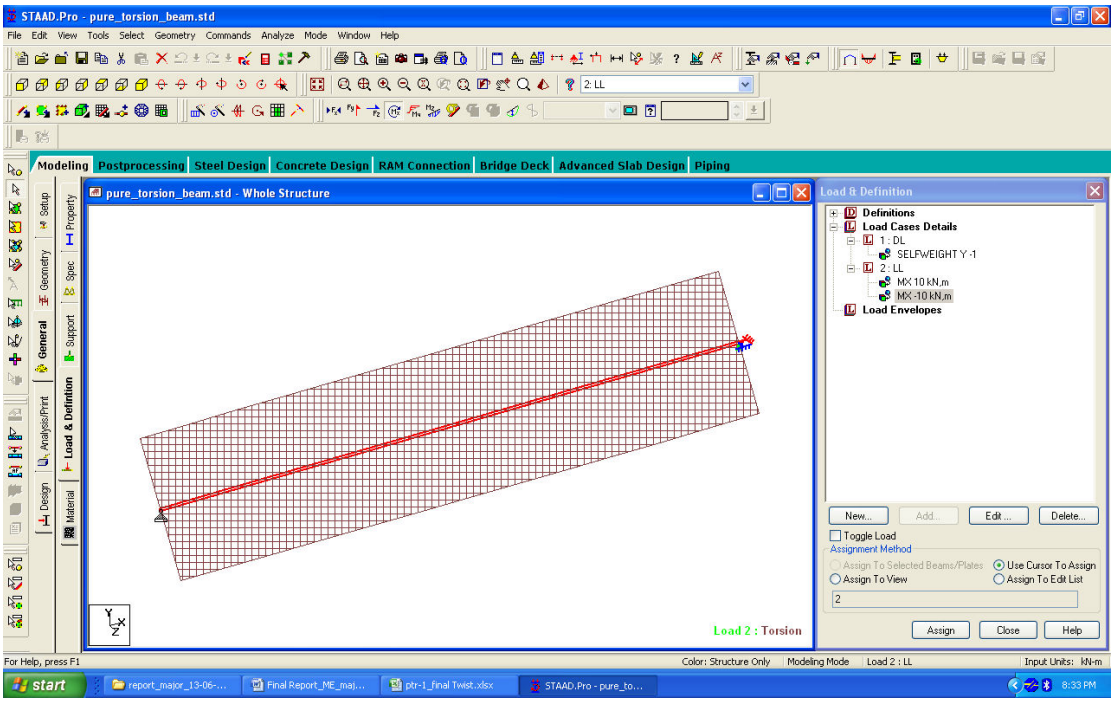

Fig. 26 View of STAAD Software Showing Torsional Moment Diagram (TMD) of Reference Beam PTR-1.

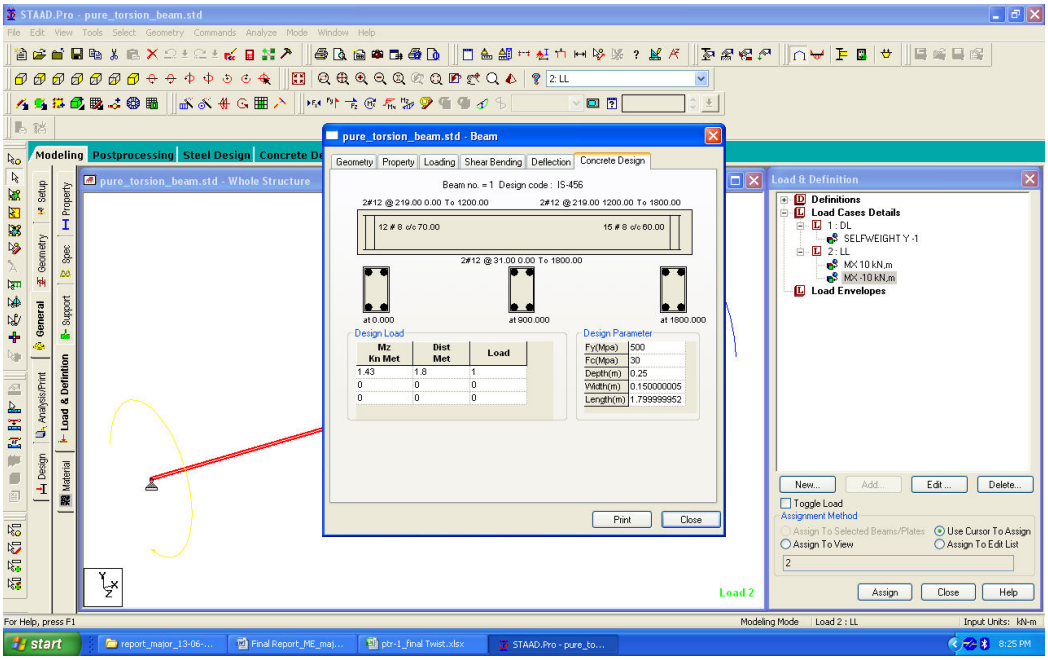

Fig. 27 View of STAAD Software Showing Design of Reference Beam PTR-1.

4.3 Cracking Moment in RC Beams under Pure Torsion [Metin Husem et al (2009)]

Following are the some theory for calculating the cracking moment under pure torsion for reinforced concrete beams [Metin Husem et al (2009)]

Elastic Theory [Timoshenko & Goodier 1969; Popov 1990]
By using the Eq. (15)

$T_c = \alpha\,(x^2 y)\left(\sqrt[6]{f_c'}\right)$ = 7.55 kNm

TS 500: 2000 [Turkish Standards Institutions]
By using the Eq. (18)

$T_c = (1.35)\left(\sqrt[0.35]{f_c'}\right)\left(\left(\frac{b^2 h}{3}\right)\right)$ = 7.81 kNm

Where

x	=	b	=	width of the beam
y	=	h	=	Overall Depth of the Beam
		α	=	Angle of Crack in radians
		Ac	=	Area of Concrete Section
		Pc	=	Perimeter of Concrete Section
		f_c'	=	Cylindrical Characteristic Concrete strength

4.4 Torsion of Structural Concrete [Thomas T. C. Hsu (1968)]

A simplified Eq. (20) given by [Thomas T. C. Hsu (1968)] as follows:

$$T_u = \frac{2.4}{\sqrt{x}}\, x^2 y \sqrt{f_c'} + \left(0.66 + 0.33\frac{y_1}{x_1}\right) x_1 y_1 \frac{A_s f_{sy}}{s}$$

x	150 mm
y	250 mm

x1	124 mm
y1	224 mm
f'c	25 mm
As	100 mm^2
fsy	500 N/mm^2
s	75 mm

The Ultimate Strength of the Reference Beam of the above dimension and properties by using eqn. (20) was

$T_{u,RC}$ = 17.31 kNm

For the analysis of distressed beam PTT-1, properties and dimensions are same Refence Beam PTR-1 except the Shear Strip spacing is 432.5 mm

The Ultimate Strength of the Distressed Beam PTT-1 (Without the effect of CFRP) of the above dimension and properties by using eqn. (20) was

$T_{u,RC}$ = 7.42 kNm

4.5 Ultimate Torsional Moment Contribution from CFRP [Ghobarah A et al (2002)]

The maximum additional torsional moment contribution of the CFRP T_f may be estimated from Eq. (47) by assuming the average ultimate fiber strain to be approximately 0.003; thus

$$T_f = 0.006\, A_f A_c E_f / s$$

It stated that if we used 20% of the ultimate strain i.e. 1.55% then eqn. (47) will be valid.

b	=	150	mm
d	=	250	mm
Ac	=	37500	mm^2

Pc	=	800	mm
f'c	=	25	mm^2
Ef	=	260000	N/mm^2
nf	=	15	
bf	=	50	mm
Af	=	351	mm^2
sp	=	125	mm
tf	=	0.234	mm
s	=	1730	mm

By assuming the average strain in CFRP fabric 0.003, the Ultimate torque contribute by the our strengthening scheme by using Eqn. (47)

Tf = 11.86 kNm

Ultimate Torsional Moment of the Strengthened Beam PTT-1 was

$T_u = T_{u,RC} + T_f$ = 7.42 + 11.86 = 19.28 kNm

CHAPTER – 5

FABRICATION, CASTING AND INSTRUMENTATION TEST SPECIMENS

CHAPTER – 5

5.0 FABRICATION, CASTING AND INSTRUMENTATION OF TEST SPECIMENS

Two Nos. of RC Beams, Thirty Nos. of Cubes, Fifteen Nos. of Cylinders and Nine Nos. Prisms were casted by using M30 Grade of Concrete. Mix design of Trials No. 2 was used for the casting.

A first beam PTR – 1 (Pure Torsion Reference Beam) beams having an effective span of 1.79 m was designed for 8.5 kNm Torsion as per IS 456: 2000, 10 kNm on STAAD software and 17.31 kNm by using Eq. (20). For designing of beams by using IS 456: 2000, Microsoft Office Excel Spreadsheet was prepared. 2 Nos. 12 mm dia bars provided at bottom and 2 Nos. 12 mm dia bars provided at top of the beam. 2-Legged Shear Stirrups 75 mm c/c spacing were also provided. Fig. 28 and 29 shows the caging of rebars.

Electric Strain Gauges having Resistance 120±0.4 Ω were provided on steel reinforcement to measuring the strains during testing of the beam. Electric Strain Gauges were provided at Quarter, Middle and Three Quarter span on Top, Bottom and Vertical Stirrups. The locations of the Electric Strain Gauges were shown in Fig. 27 and 29.

For Torsional Loading arrangement, the steel plate 150 mm x 150 mm x 6 mm was welded on the extra provided steel stirrups on either end at opposite faces as shown Fig. 28 and 30.

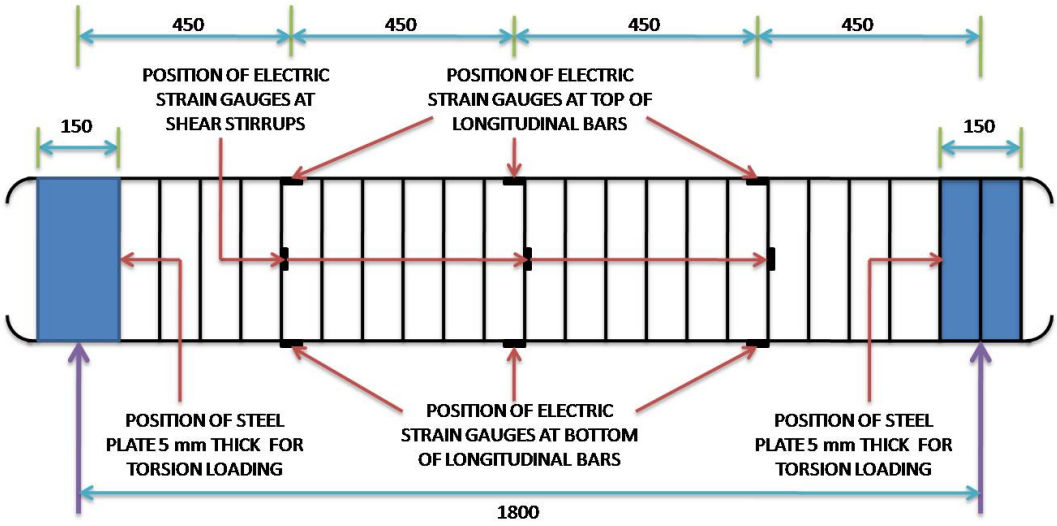

Fig. 28 Schematic Diagram Beam PTR – 1 showing Reinforcement, Electric Strain Gauges and Steel Plates at Both Ends for Torsion Loading

Fig. 29 Caging of RC Beam PTR – 1

Fig. 30 Caging of RC Beam PTR – 1 Showing Reinforcement, Electric Strain Gauges and Steel Plates at Both Ends for Torsion Loading

Second beams Beam PTT-1 (Pure Torsion Test Beam) beams having an effective span of 1.73 m was designed for 7.42 kNm by using Eq. (20). The torque carrying capacity was too less as compared to PTR-1 because this beams was distressed by not provided the vertical shear stirrups. Only three nos. of vertical shear stirrups were provided for installation of Electric Strain Gauges for comparing the results with PTR-1 at Quarter, Middle and Three Quarter position of the Beam. Rest of the reinforcement was same as PTR-1.

Electric Strain Gauges having Resistance 120±0.4Ω were fixed on steel reinforcement. Electric Strain Gauges were provided at Quarter, Middle and Three Quarter Span on Tension, Compression steel and Vertical Shear Stirrups. The locations of the Electric Strain Gauges were shown in Fig. 31 and 32.

For Torsional Loading arrangement, the steel plate 150 mm x 150 mm x 6 mm was welded on the extra provided steel stirrups on either end at opposite faces as shown Fig. 31 and 32.

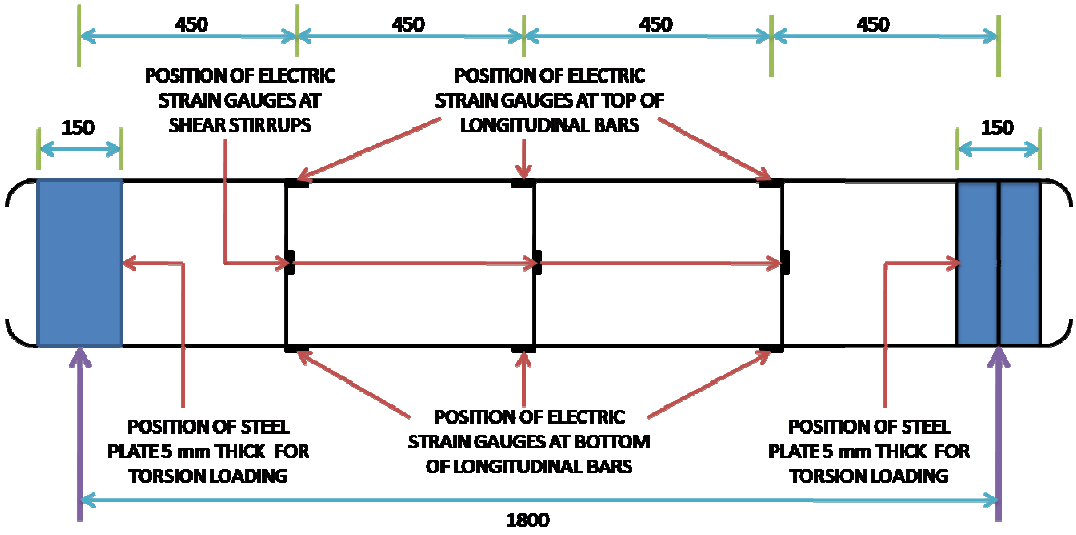

Fig. 31 Schematic Diagram Beam PTT – 1 showing Reinforcement, Electric Strain Gauges and Steel Plates at Both Ends for Torsion Loading

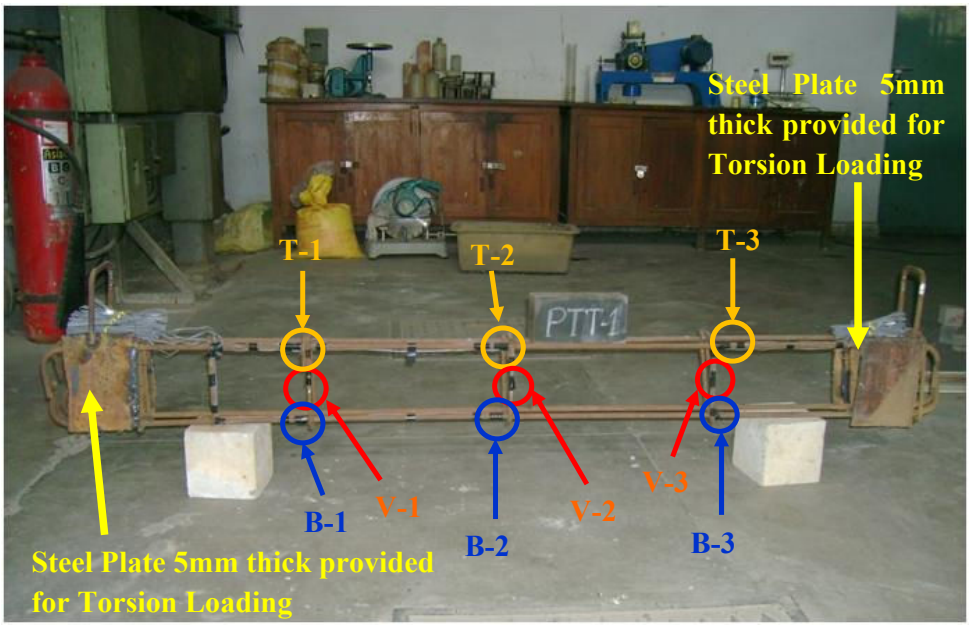

Fig. 32 Caging of RC Beam PTT – 1 Showing Reinforcement, Electric Strain Gauges and Steel Plates at Both Ends for Torsion Loading

Beam mould was fabricated in the Workshop Division in Central Road Research Institute, New Delhi. Casting of Beams, Cubes, Cylinders and Prism were casted in the Bridges Division of Central Road Research Institute, New Delhi

Fig. 33 Beam Mould

Fig. 34 Cubes and Cylinders Moulds

Fig. 35 Table Vibrator and Prism Moulds

Fig. 36 Mechanical Mixer Capacity 0.5 cum and Curing Tank

Fig. 37 Reinforcement Cage inside the Beam Mould

Fig. 38 Casting of Beam on Table Vibrator

Fig. 39 Protecting the Electric Strain Gauges for Damaging during Concreting

Fig. 40 Lifting of Beams from Table Vibrator after casting

Fig. 41 Finishing of Top Surface of Beams

Fig. 42 Filling of Cylinders on the Table Vibrator

Fig. 43 View of Cubes, Cylinders and Prism after Concreting

CHAPTER – 6

TESTING OF HARDENED CONCRETE

CHAPTER - 6

6.0 TESTING OF HARDENED CONCRETE

As we, all know that the properties of concrete are a function of time and ambient humidity and his way in order to be of value, test on concrete have to be performed under specified or known conditions. The most common on all tests on hardened concrete is the compressive strength test, partly because it is an easy test to make, and partly because many, though not all, of the desirable characteristics of concrete are qualitatively related to its strength, but mainly because of the intrinsic importance of compressive strength of concrete in construction.

The strength test can be broadly classified into mechanical tests to destruction and non-destructive test tests, which allow repeated testing of the same specimen and thus make possible a study of the variation in properties with time.

The test to destruction has been in use for great no. of years, but no universally accepted standard is available. Different methods and techniques are used in different countries and sometimes used in the same country. As many of these tests are encountered in laboratory work, and especially in research, knowledge of the influence of the test methods on strength as measured is desirable.

Tests can be made for different purposes but the main two objectives of tests are control of quality and compliance with specifications. It should be remembered that tests are not end to themselves, In the case of concrete; they seldom lend themselves to a neat concise interpretation, so that in order to be of real value tests should always be used against the background of experience.

6.1.1 Test for Compressive strength

6.1.1.1 Cubes Test

The compressive strength of the concrete was tested as per IS: 516 – 1959. Six cubes of 150mm x150mm x 150mm size were tested in the laboratory. Three cubes each were tested under a compression testing machine on the day of testing to have the concrete strength at the day of testing (7 Days & 28 Days). Loading was done at the rate prescribed in the 140 kg/cm²/min i.e. 31.5 t/min. The setup is as shown in following Fig. 44.

Fig. 44 Testing of Cubes for Compressive Strength

Results

Compressive Strength of Cube after 7 days = 24.26 N/mm^2

Compressive Strength of Cube after 28 days (f_c) = 34.58 N/mm^2

6.1.1.2 Cylinders Test

The standard cylinder is 150 mm diameter & 30 cm long and was cast in a mould generally made of steel or cast iron, preferably with a clamped base. Three cylinders each were tested as per IS 516:1959, under a compression testing machine on the day of testing to have the concrete strength (7 Days & 28 Days). Loading was done at the rate prescribed in the 140 kg/cm²/min i.e. 31.5 t/min.

A correction factor according to the height/diameter ratio of specimen after capping shall be obtained from the curve shown in Fig. 45. The product of this correction factor and the measured compressive strength shall be known as the corrected compressive strength, this being the equivalent strength of a cylinder having a height/diameter ratio of two.

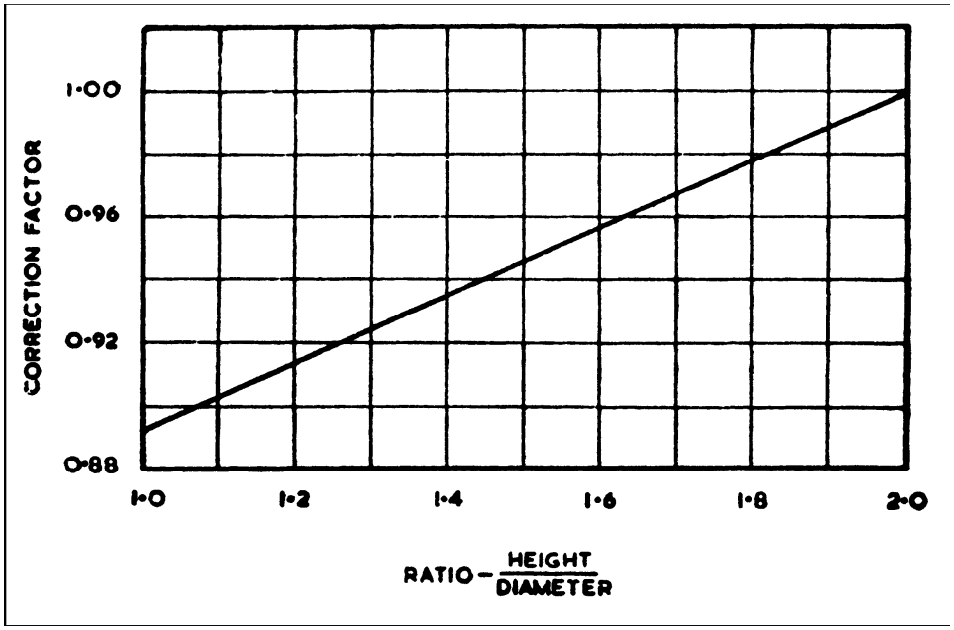

Fig. 45 Correction Factor for Height-Diameter Ratio of a Core

Results

Cylindrical Compressive Strength of Concrete after 28 days (f'_c) = 24.98 N/mm2

6.1.2 Test for Tensile Strength of Concrete

For tensile strength of the concrete "Brazilian tensile strength" (split cylinder test) was conducted on the cylinders under a compression testing machine. Loading was done at the rate prescribed in the 140 kg/cm²/min. i.e. 31.5 t/min. The cylinder is kept in laid position and load is applied along its diameter till the cylinder splits into two parts. The setup of the test is shown in Fig. 46.

Tensile strength (ft) is given by the following equation (51)

$$f_t = 2F / \pi L d \qquad (51)$$

Where F is the load at which cylinder splits in Newton,
L is the length of cylinder and
d is the diameter of the cylinder

Fig. 46 Test Setup of Split Cylinder

Results

Tensile Strength of Concrete 28 days (f_b) = 2.64 N/mm^2

Fig. 47 Split Surface of Cylinder after Testing

6.1.3 Test for E (Modulus of Elasticity) of Concrete

This test was conducted on a cylinder as described in the test no. 9 in code IS: 516 – 1959. The cylinder were tested for "E" of concrete and was later was used as the specimen for the split cylinder test. Test was conducted by means of an extensometer.

The test procedure is as the following:

i. First wet the cylinder for a while.
ii. Then attach the extensometer parallel to its axis
iii. Now place the cylinder in the testing machine. The top and bottom surface of the cylinder should be plane.
iv. Now the load is applied at a rate of 140 kg/cm²/min. (14 MPa), which in our case was 24.7 t/min.
v. First the load is applied upto (C+5) kg/cm² which in our case was 178.3kg/cm² i.e. 31.5 Tons
vi. Now the load was reduced to 1.5 kg/cm² and the dial gauge reading attached to extensometer was recorded as the initial reading.

vii. Now another cycle of the loading was done and load was raised to (C+1.5) kg/cm². The reading at the dial gauge is recorded as the final reading.

viii. Following the above cycle load is again reduced to 1.5 kg/cm² and another cycle of loading and unloading is carried out.

ix. The dial gauge readings are recorded in 10 to 12 equal intervals.

x. And if the readings of 2nd and 3rd cycle are same graph between stress and strain is plotted and the slope of the graph is calculated.

The modulus of elasticity is calculated as following

$$E = \frac{stress}{strain} = \frac{w\,L}{A\,.\Delta\,L} \tag{52}$$

Where w = load (C+1.5) – 1.5 kg/cm² and

$$C = \frac{f_{ck}}{3} \tag{53}$$

Where f_{ck} is characteristic strength of the concrete.

L = Gauge length of the cylinder = 250mm in our case

ΔL = Total deflection of the cylinder

= final gauge reading – initial gauge reading in mm.

A = cross-sectional area of the cylinder mm²

(a)

(b)

Fig. 48 (a) and (b) Test Setup for the "E" of Concrete using Extensometer

Results

Modulus of Elasticity of Concrete after 28 days ($\boldsymbol{E_c}$) = 30060 N/mm^2

6.1.4 Test for Flexure Strength

Although concrete is not normally designed to resist direct tension, the knowledge of tensile strength is of value in eliminating the load under which cracking will develop. The absence of cracking is of considerable importance in maintaining the continuity of concrete structure and in many cases in the prevention of corrosion of the reinforcement. Cracking problem occur, for instance, when high tensile steel reinforcement is used.

So, to measure the tensile strength of concrete, a plain concrete beam is subjected to flexure. This is, infect the only standard test. The theoretical maximum tensile stress reached in the bottom fiber of the test beam is known as the modulus of rupture.
The flexure strength of the concrete was tested as prescribed in test no. 8 in code IS: 516 – 1959.

The test procedure is as the following:

i. Test specimens stored in water at a temperature 24° to 30°C for 48 hours before testing, were to be tested immediately on removal from the water whilst they are still in a wet condition.
ii. The specimen shall then be placed in the machine in such a manner that the load shall be applied to the uppermost surface as cast in the mould, along two lines spaced 20.0 or 13.3 cm apart.
iii. The axis of the specimen shall be carefully aligned with the axis of the loading device. No packing shall be used between the bearing surfaces of the specimen and the rollers.
iv. The load shall be applied without shock and increasing continuously at a rate such that the extreme fiber stress increases at approximately 7 kg/cm^2/min, that is, at a rate of loading rate of 180 kg/min.
v. The load shall be increased until the specimen fails, and the maximum load applied to the specimen during the test shall be recorded.
vi. The appearance of the fractured faces of concrete and any unusual features in the type of failure shall be noted.

The flexural strength of the specimen were expressed as the modulus of rupture (*f*b), which, can be calculated as

$$f_b = \frac{P \times L}{b\, d^2} \qquad (54)$$

If a = the distance between the line of fracture and the nearer support, measured on the centre line of the tensile side of the specimen is less than 13.3cm or

$$f_b = \frac{3\,Pa}{b\,d^2} \qquad (55)$$

If a = less than 13.3 Cm, but more than 11 Cm.

Where,

b = measured width in cm of the specimen,

d = measured depth in cm of the specimen at the point of failure,

L= length in cm of the span on which the specimen was supported,

P = maximum load in kg applied to the specimen.

If a= less than 11 cm, then the results will be discarded

(a)

(b)

Fig. 49 (a) and (b) Test set up for Flexural Strength

Fig. 50 Failure of Prism after Flexural Test

Results

Flexural Strength or Modulus of Rupture (f_b) = 4.56 N/mm^2

6.1.5 Summary of Test Results of Hardened Concrete

All the values of the cube (150mm x150mm x 150mm) compressive strength (f_c), Brazilian tensile strength (f_t) ,(cylinder of150 mm diameter and 300 mm length) and the elastic modulus (E_c) & Modulus of Rupture (f_b) are listed in Table 13.

Table 13 Summary of Results of Hardened Concrete after 28 days

Characteristic Compressive Strength (f_c)	34.58 N/mm^2
Cylindrical Compressive Strength (f_c')	24.98 N/mm^2
Modulus of Rupture / Flexural Strength of Concrete (f_b)	4.56 N/mm^2
Modulus of Elasticity(E_c)	30060 N/mm^2
Brazilian Tensile Strength (f_t)	2.64 N/mm^2

CHAPTER – 7

STRENGTHENING SCHEME
AND
APPLICATION PROCEDURE

7.0 STRENGTHENING SCHEMES AND APPICATION PROCEDURE

7.1 Strengthening Scheme

The original Torque capacity of the distress beam PTT-1 was 7.42 (By using Eq. (20)). The strengthening scheme was designed for increase the torque capacity of the distressed beam PTT-1 by 11.86 kNm (By using Eq. (47)), assuming the design effective strain 20% of the ultimate strain 1.55%). The spacing of U-Shaped CFRP Fabric Strips 50 mm wide was 125 mm c/c (Clear Distance between the Strip = 75mm) as shown in Fig. 57. The End Strip was 100 mm thick and fully wrapped to avoid the failure at ends.

7.2 Application Procedure

During the application, strengthening procedure, special attention was paid to the bond between the reinforced concrete beam and CFRP. Preparation of the concrete surface and the application of the CFRP were conducted using the same standard procedure each time. A handheld grinder was used to level the concrete surface exposing the aggregate, which is beneficial for the bonding between the FRP and the concrete. Additionally, the grinder was used to round the concrete edges to a minimum radius of 25 mm in order to minimize the stress concentration in the fibers at the edges. Finally, the concrete surface was cleaned from any loose particles and dust by using compressed air as shown in Fig. 51. Applying the CFRP to the concrete surface was conducted in steps. First, the concrete surface was impregnated with R&M Resin Primer 11 and allowed to cure for one day as shown in Fig. 52. Second the concrete surface was impregnated with the adhesive R&M Matrix 20. Third, CFRP fabric layer was impregnated with the R&M Matrix 20 as shown in Fig. 53. Then, each CFRP layer was rolled over the concrete surface and pressed using a roller to eliminate air bubbles as shown in Fig. 54. Beam was allowed to cure for at least 7 days before testing.

Fig. 51 Removing Loose Particles by Compressed Air

Fig. 52 Concrete Impregnated with R&M Resin Primer 11

Fig. 53 Applying R&M Resin Matrix 20 on Concrete surface where CFRP was to be placed

Fig. 54 Applying Roller on CFRP-Fabric to remove air bubbles between the CFRP and Concrete Surface

Fig. 55 Beam PTT-1 Strengthen with U-Shaped Wrapped of CFRP Fabric 50 mm Width 125 mm c/c with anchors and Longitudinal Strips

7.3 Instrumentation

The 11 Electric Strain Gauges were fixed on the Surface of the Vertical U-Shaped CFRP Fabric Strips and 2 Electric Gauges on Longitudinal CFRP Fabric Strips. The locations were decided after from viewing the crack pattern of testing of the Reference Beam PTR-1 as shown in Fig. 56 and 57.

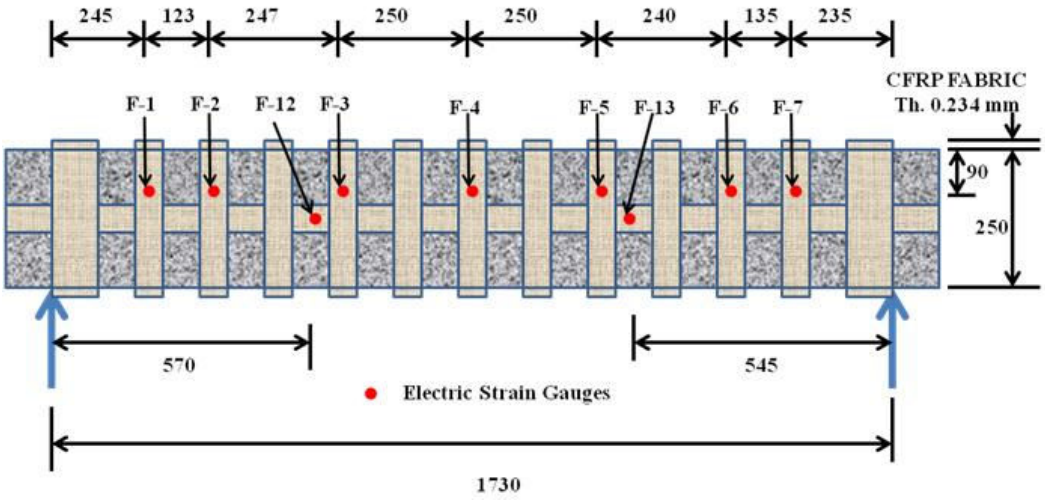

Fig. 56 Position of Electric Strain Gauges on Face F-1 of PTT-1

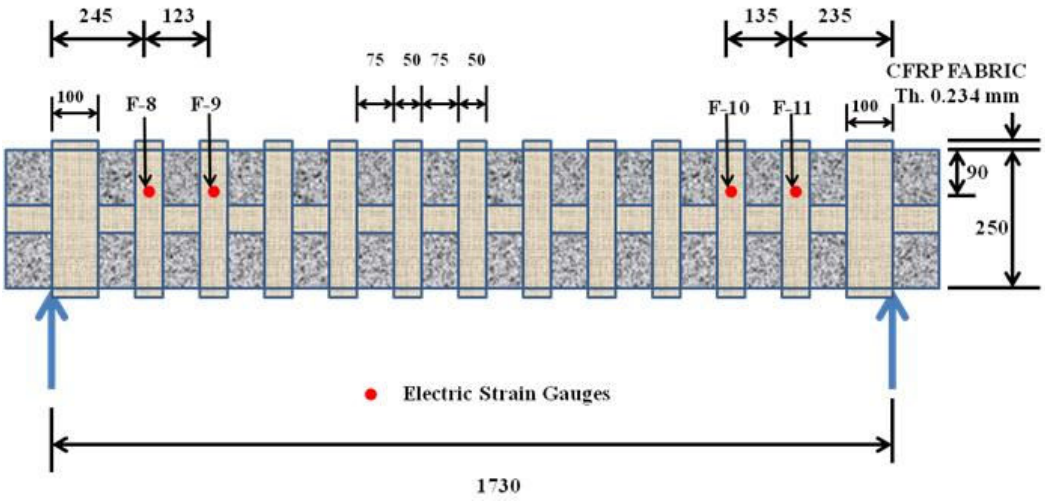

Fig. 57 Position of Electric Strain Gauges on Face F-3 of PTT-1

Fig. 58 Position of Electric Strain Gauges on Surface of CFRP Fabric

CHAPTER – 8

EXPERIMENTAL SETUP
AND
TESTING OF TEST SPECIMENS

CHAPTER – 8

8.0 EXPERIMENTAL SETUP AND TESTING OF TEST SPECIMENS

8.1 Experimental Setup

The rectangular RC beam specimen was tested under a torsion loading. To conduct this test the specimens was simply supported over the span of 1.79m for beam PTR-1 and 1.73m for beam PTT-1. For the application of torsion loading, Steel Section ISWB 150 Length 250mm was welded on the plate shown in Fig. 59 at support section. The strength of the welding was enough that no failure will occur.

Fig. 59 Position of ISWB 150 Welded at End Plates for Torsional Loading

For loading arrangement a 50 Tons static loading capacity Frame was used at Bridges and Structures Division of Central Road Research Institute as shown in Fig. 60

Fig. 60 Static 50 Tons Capacity Loading Frame

Two Load Cells were positioned on the I-section ISWB 150 on either end as shown in Fig. 61, So that the eccentricity of the Loading if any will be detected. To transfer the load from Loading Frame to Load Cell, ISMB150 which was already stiffened by provided 5 mm thick plate at top and bottom flange was placed as shown in Fig. 61. A hydraulic Jack 50 Tons capacity of was placed on the ISMB150 at the mid span such that an equal loading could be transferred at both the ends. To measure the twist angle in beam PTR-1 and PTT-1, 8 Dial Gauges were fixed at distance of 200 mm and 180mm from both the support as shown in Figs. 61,62 63 and 64. The Dial Gauges were fixed at a distance of 50 mm from top and bottom fibre of the beam to give the complete profile of twist at any cross section of the beams as shown in Figs. 63 and 64.

Fig. 61 Experimental Setup of Beam PTR-1

Fig. 62 Experimental Setup of Beam PTT-1

Fig. 63 Position of Dial Gauges to Measure the Twist Angle of and Load Cells of PTR-1

Fig. 64 Position of Dial Gauges to Measure the Twist Angle and Load Cells of PTT-1

A 32-Channel Dynamic Data logger "DEWETRON" was used to record the strains in longitudinal steel reinforcements and shear reinforcements at 9 different locations as well as the data of twist angle at 8 locations were also recorded through DEWETRON as shown in Fig. 65.

Fig. 65 Dynamic Data Logger "DEWETRON"-32 Channels

8.2 Testing of Reference Beam (PTR-1)

The properties of concrete as shown in Table 14 were determined on the same day to know the exact material propertied on the day of testing.

Table 14 Results of Hardened Concrete on Day of Test of Beam PTR-1

Characteristic Compressive Strength (f_c)	37.55 N/mm^2
Cylindrical Compressive Strength (f_c')	26.09 N/mm^2
Modulus of Rupture / Flexural Strength of Concrete (f_b)	6.37 N/mm^2
Modulus of Elasticity(E_c)	30374 N/mm^2
Brazilian Tensile Strength (f_t)	2.71 N/mm^2

The lever arm of the load was at both the ends was kept as 170mm. The four faces of the beam were marked as F-1 for Front Vertical Face, F-2 for Bottom face, F-3 for Back Face and F-4 for Top Face. The connection of the Electric Strain Gauges, Load Cells and Dial Gauges were properly checked and properly connected to the Data Logger "DEWETRON" as per our Testing Scheme. Nineteen Channels were used of Data Logger, Two Channels for Load Cells, Nine channels for Electric Strain Gauges and Eight channels for Dial Gauges. Ten Reading were recorded at every one second in Computer attached with Data Logger and also simultaneously Dial Gauge reading were recorded every 0.5 kN for safety purposes if anything goes wrong with Data Logger during test.

8.2.1 Crack Development and Failure Mode

There first crack was observed 200mm distance from Rocker End and in the middle depth of the front face F-1 of the beam towards roller end, top of the face F-2 at middle, two crack formed from long the full face near rocker end and middle at back face F-3 when Torque was 9.78 kNm (Load was 115 kN (68 kN at Rocker End and 47 kN at Roller End) as shown in Fig. 66 (a) and (b). T**he torque 9.78 kNm was observed as Cracking Torque and recorded yielded Angle of Twist was 0.120 °/m.**

(a) Face F-1 and F-3

(b) Face F-3

Fig. 66 (a) & (b) Crack was Initiate at Face F-1, F-3 and Face F-4 (Torque 9.8 kNm)

When the applied Torque increased to 10.68 kNm (Pu = 125 kN, P1=72.5 kN at Rocker End and P2=52.5 kN at Roller End), at the existing cracks were widen and two new cracks were developed 250mm at quarter span on Face F-1 Roller End and quarter span on Face F-3 as shown Fig. 67 (a) and (b). Fig. 68 shows the twisting of Rocker End.

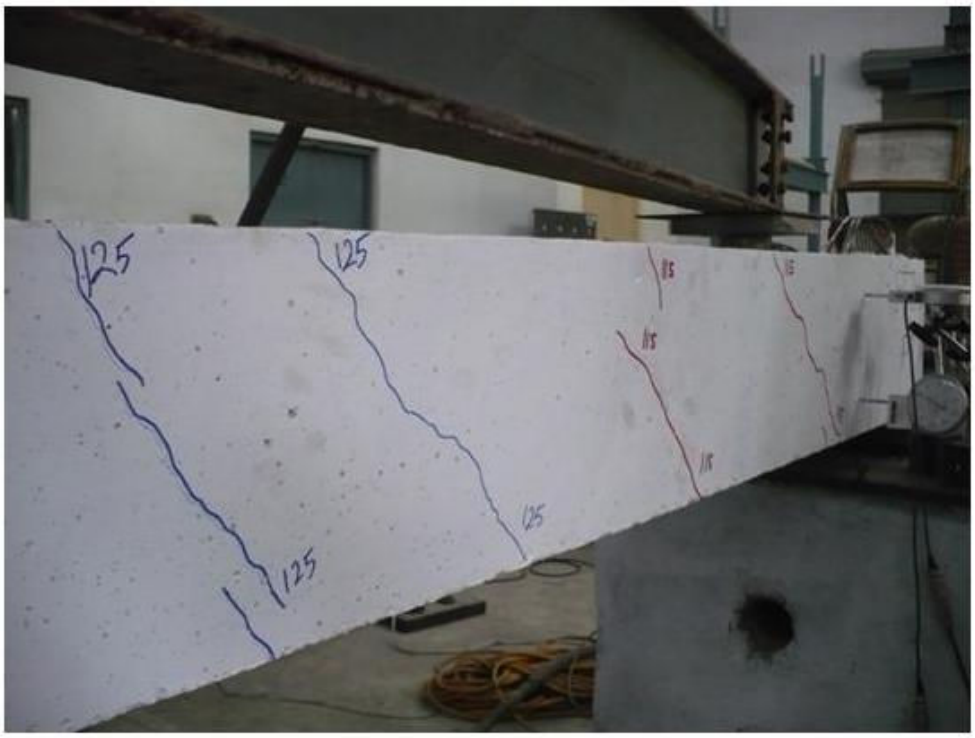

(a) F-1

(b) Face F-3

Fig. 67 (a) and (b) Position of Cracks were formed at Face F-1 and F-3 (Torque was 10.68 kNm)

Fig. 68 Position of Twisted of Beam at Rocker End Cracks were formed (Torque was 10.68 kNm) at Face F-3

When the load was further increase, the cracks near the Roller end were widened as compared to Rocker End. The crack formation at applied torque 11.05, 11.90 and 12.75 kNm (Pu at 130kN, 140 kN and 150 kN respectively) as shown in Fig. 69 a) and (b)

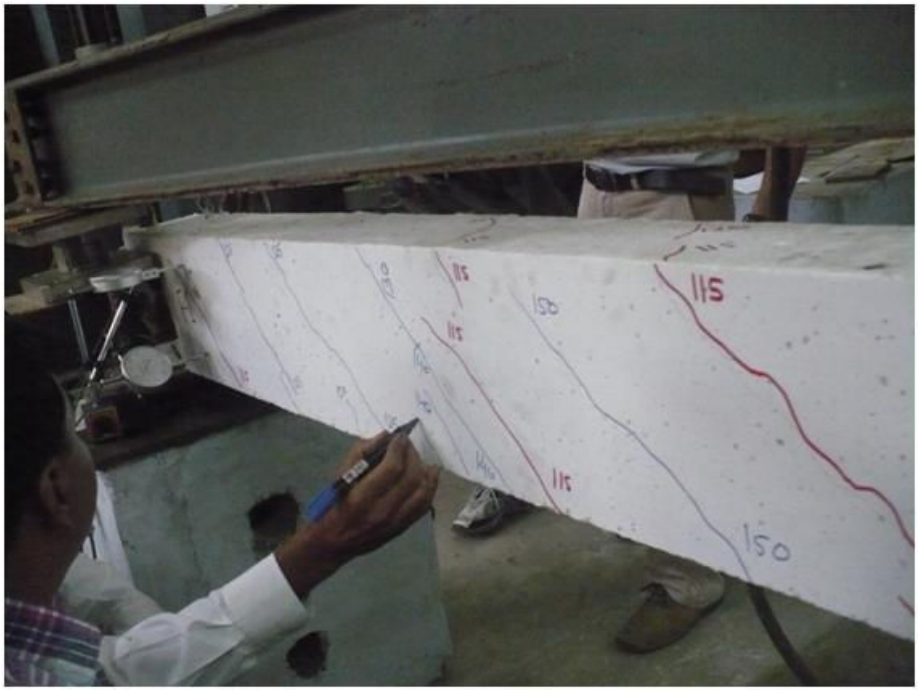

(a) Face F-1

(b) Face F-3

Fig. 69 (a) and (b) Position of Cracks Total Load of 130, 140, 150 and 155 kN (Torque 11.05, 11.90 and 12.75 kNm respectively) at Face F-1 and F-3

The maximum toque was 14.14 kNm (Pu=165) and The crushing of concrete initiated in the vicinity of the roller end on Face F-1, F-3 and F-4 as shown in Fig. 70 and 71. The ultimate angle of Twist was recorded 1.032 °/m.

Fig. 70 Position of Cracks Total Load of 165 kN (Torque was 14.14 kNm) Face F-1 and F-4

On further application of load, the beam could not sustain more load and the load reduced to 100 kN (applied torque = 8.5 kNm). The close view the crack pattern as shown in Fig. 71

Fig. 71 Position of Cracks Total Load of 100 kN on Reversal of Loading at Face F-1

The strain was also recorded in steel reinforcement provided in compression and tension as well as shear. The tension steel reinforcement yielded in the quarter span towards roller end as the magnitude of strain was more than the yield strain of steel (2380 μm). The crack which causes the ultimate failure of the beams was also in the vicinity of the quarter span.

The Fig. 72 shows the complete crack pattern of all the four side in one plane after testing.

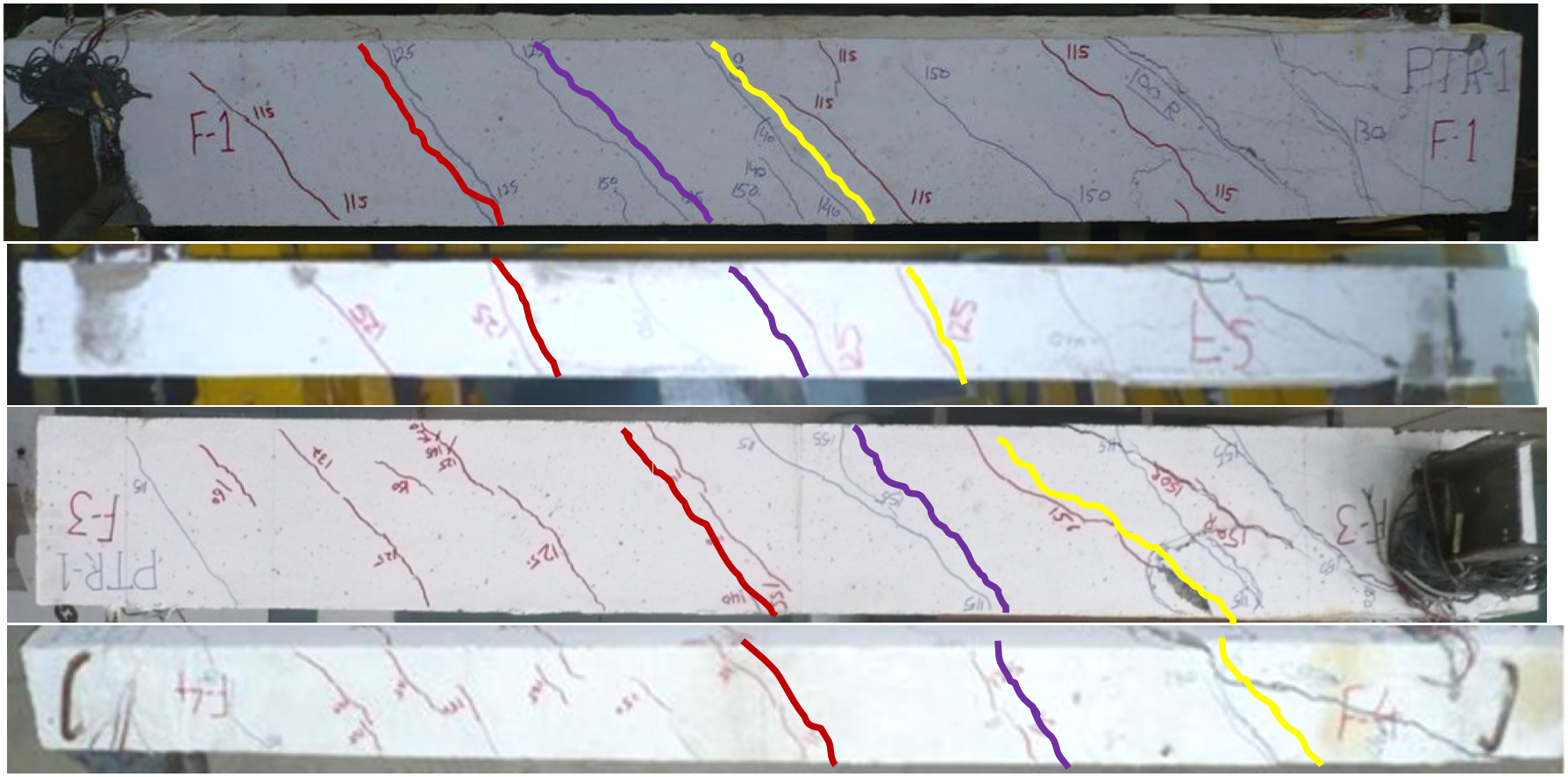

Fig. 72 Typical Crack Pattern of PTR-1 at failure (All Four Faces in One Plane under Pure Torsion)

8.2.2 Strain Variation in Steel Reinforcement

The Figures 73 to 78 shows the relationship between recorded strain (microstrain) and avearge applied torque (kNm) .

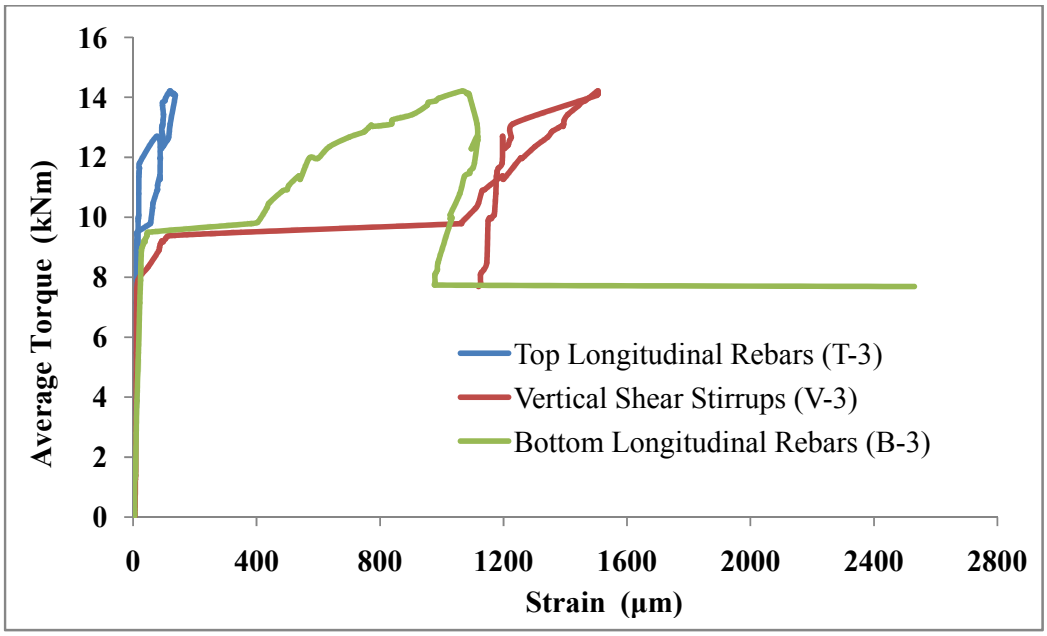

Fig. 73 Strain Vs Average Torque in Steel Reinforcement Provided at Quarter Span towards Roller End

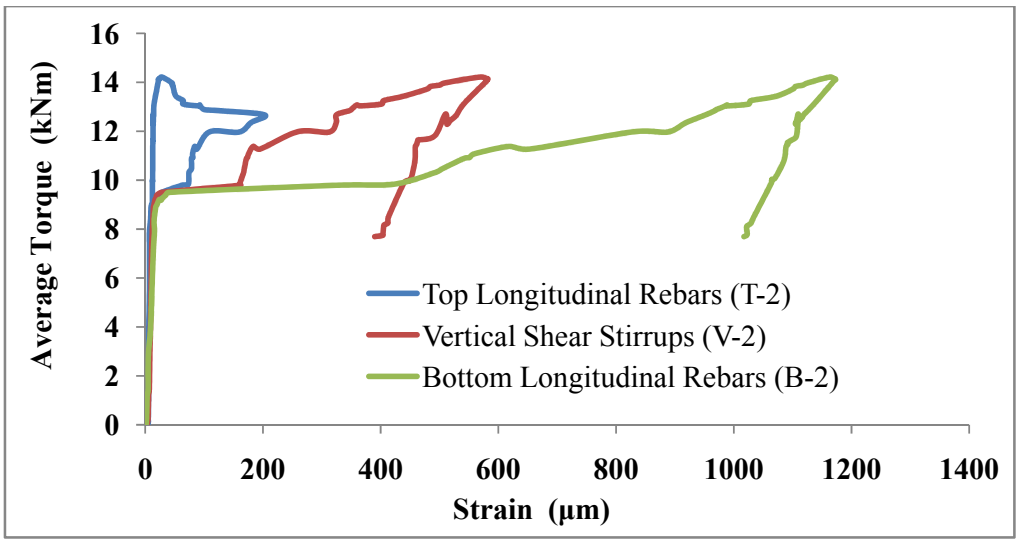

Fig. 74 Strain Vs Average Torque in Steel Reinforcement Provided at Middle Span

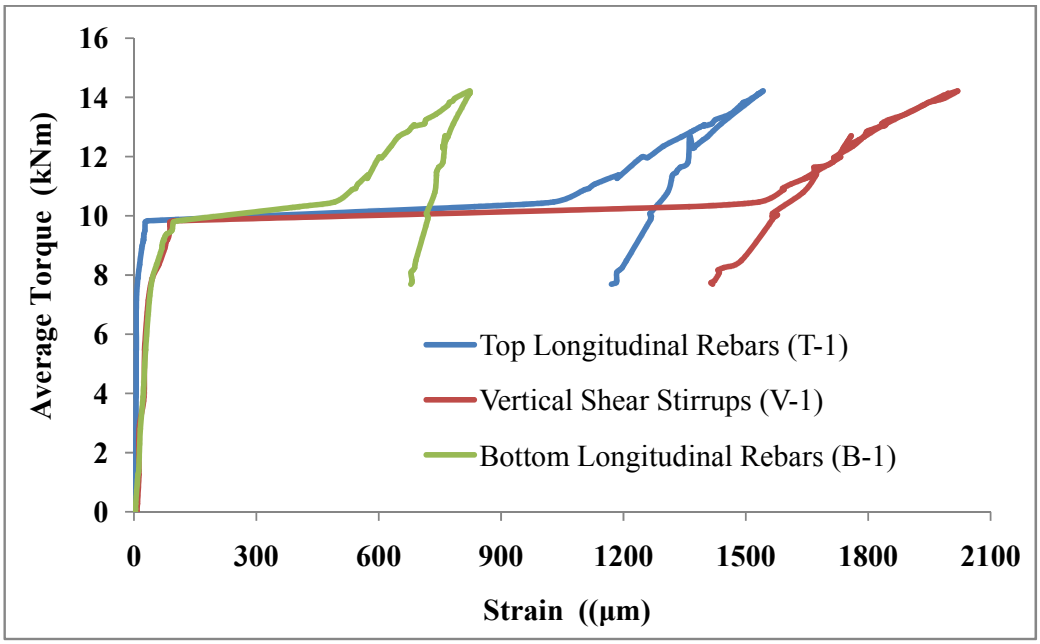

Fig. 75 Strain Vs Average Torque in Steel Reinforcement Provided at Quarter Span towards Rocker End

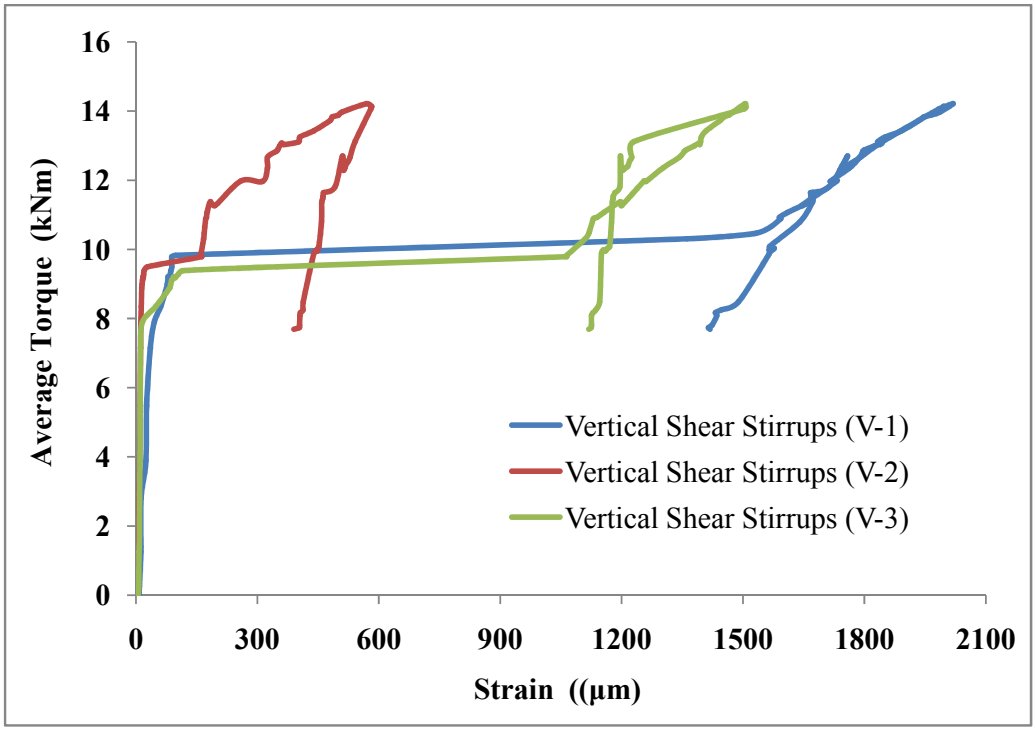

Fig. 76 Strain Vs Average Torque at Vertical Shear Stirrups

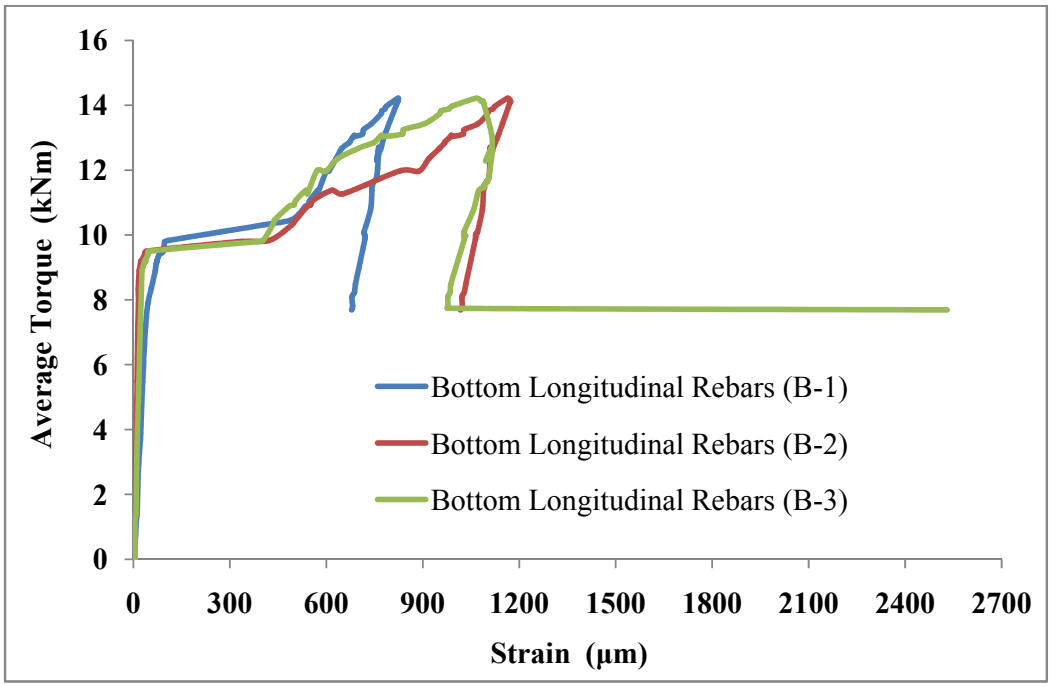

Fig. 77 Strain Vs Average Torque at Bottom Longitudinal Reinforcement

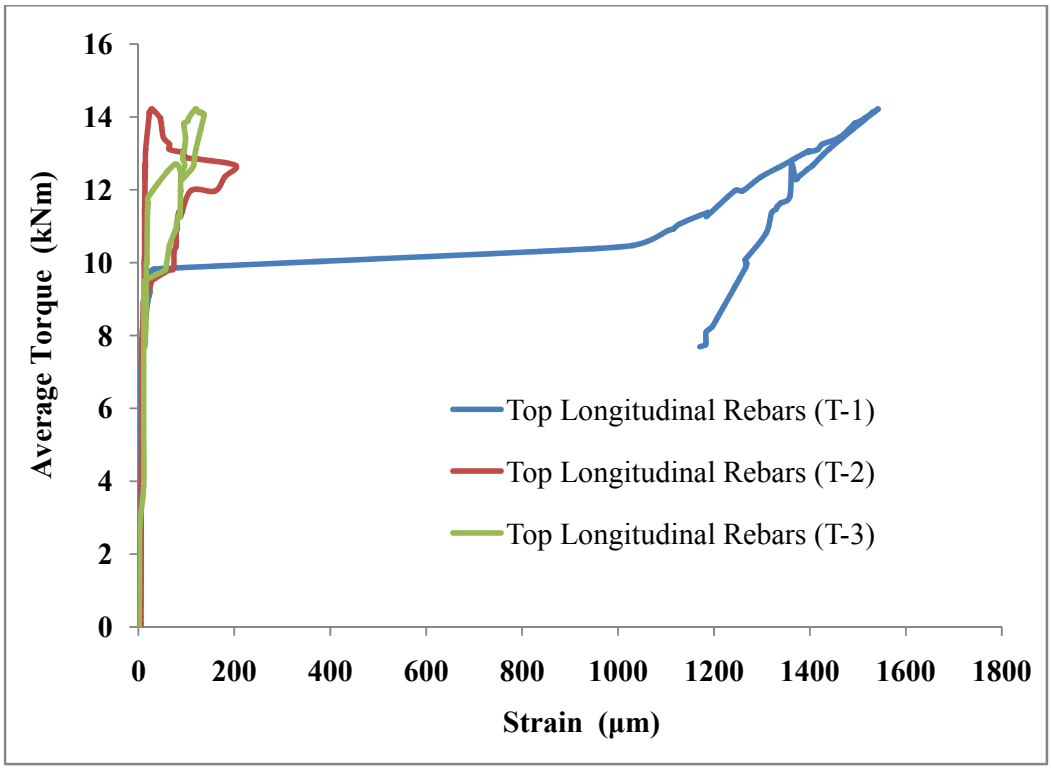

Fig. 78 Strain Vs Average Torque at Top Longitudinal Reinforcement

The test values of the recorded strains are presented in Table 15.

Table 15 Maximum Strain Recorded in Tension, Compression Steel and Vertical Shear Stirrups

Position of Strain Gauge	Maximum Strain (μm)	Remarks
Steel in Compression at Quarter Span Towards Rocker End (T-1)	1541	
Steel in Compression at Mid Span (T-2)	202	
Steel in Compression at Quarter span Toward Roller End (T-3)	137	
Steel in Tension at Quarter Span Towards Rocker End (B-1)	823	
Steel in Tension at Mid Span (B-2)	1173	
Steel in Tension at Quarter span Toward Roller End (B-3)	2531	Yielded
Vertical Shear Stirrups at Quarter Span Towards Rocker End (V-1)	2019	
Vertical Shear Stirrups at Mid Span (V-2)	583	
Vertical Shear Stirrups at Quarter Span Towards Roller End (V-3)	1506	

8.3 Testing of Strengthened Beam (PTT-1)

The properties of concrete as shown in Table 16 were determined on the same day to know the exact material propertied on the day of testing.

Table 16 Results of Hardened Concrete on Day of Test of Beam PTT-1

Characteristic Compressive Strength (f_c)	37.42 N/mm^2
Cylindrical Compressive Strength (f_c')	26.15 N/mm^2
Modulus of Rupture / Flexural Strength of Concrete (f_b)	6.32 N/mm^2
Modulus of Elasticity(E_c)	30265 N/mm^2
Brazilian Tensile Strength (f_t)	2.80 N/mm^2

The Fig. 79 shows the setup for the testing of Strengthened Beam (PTT-1) with CFRP Fabric.

Fig. 79 Setup of the Test of the PTT-1 Beam

The lever arm at both ends were 170 mm. Each face of the beam were marked as F-1 for Front Vertical Face, F-2 for Bottom face, F-3 for Back Vertical Face and F-4 for Top Face. The connection of the electric strain gauges, Load Cells and Dial Gauges were properly checked and given to Channel Nos. of Data Logger "DEWETRON" as per our Testing Scheme. Thirty Two Channels were used of Data Logger, Two Channels for Load Cells, Nine channels for Electric Strain Gauges of Reinforcements, Eight channels for Dial Gauges and Thirteen Channels for CFRP –Strips as shown in Fig 79. Ten Reading were recorded at every one second in Computer attached with Data Logger and also simultaneously Dial Gauge reading were recorded every 0.5 kN for safety purposes if anything wrong with data logger during test.

8.3.1 Crack Development and Failure Mode

First crack was observed in quarter span (Rocker End) and also middle of the front face F-1, top of the face F-4 at middle and two crack were developed from the full face near rocker end and middle at back face F-3 when Torque was 8.50 kNm (Load was 100 kN (45 kN at Rocker End and 55 kN at Roller End) as shown in Fig. 80 (a), (b) and (c). T**he torque 8.50 kNm was observed as Cracking Torque and recorded rotation was 0.30 ^{0}/m.**

(a) Face -1

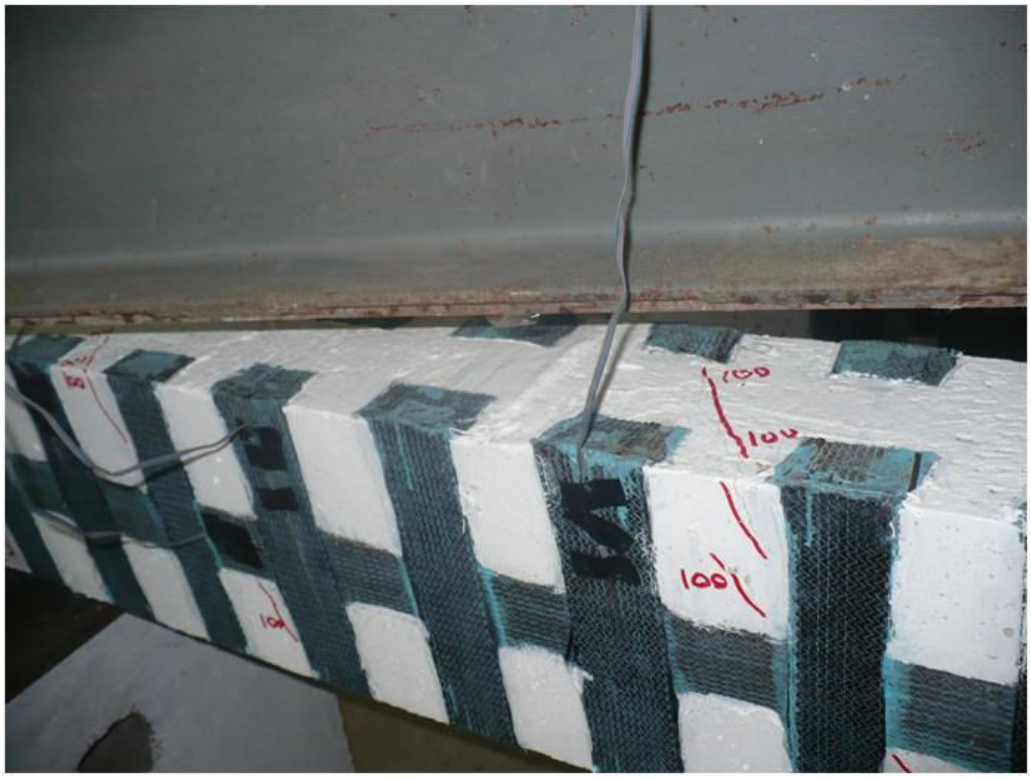

(b) Face F-1 and Face F-4

(c) Face F-3

Fig. 80 (a), (b) & (c) First Crack observed at Average Torque 8.50 kNm (Total Load 100 kN) on Face F-1, F-3 and F-4

Further cracks were developed at Face F-2 (Bottom) quarter span near to roller end, at middle on face F-3 when the torque was 9.35 (Total Load 110 kN) as shown in Fig. 81 (a) and (b).

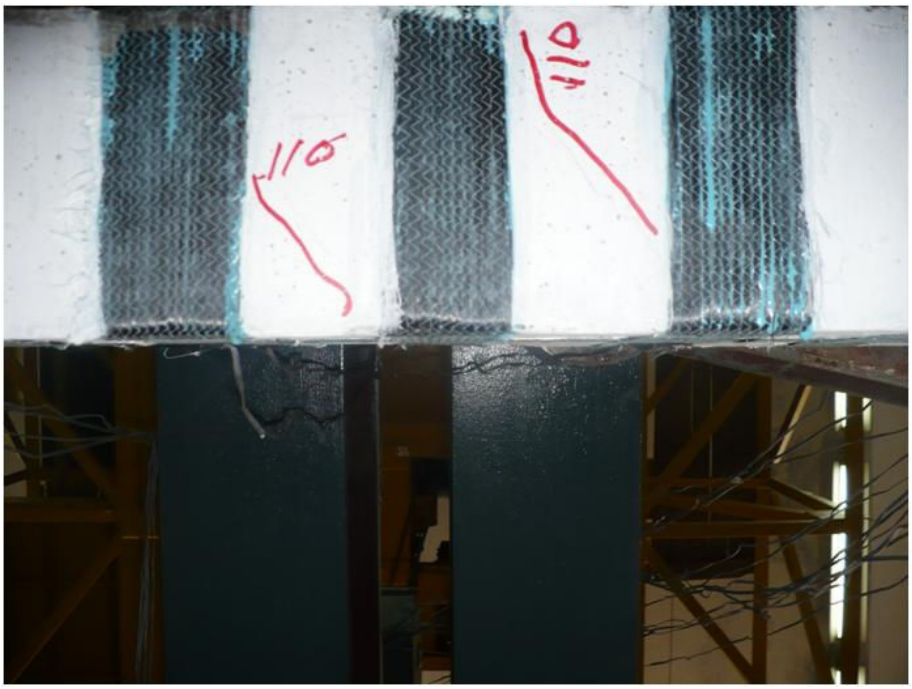

(c) Face F-2

(c) Face F-3

Fig. 81 (a), (b) & (c) Cracks formation at Average Torque 9.35 kNm (Total Load 110 kN) on Face F-2 and F-3

The existing cracks were widen as the torque was further increased to 10.2 kNm (Total Load is 120 kN). New cracks were also initiated near the quarter span towards roller end in Face F-3 as shown in Fig. 82.

Fig. 82 Cracks formation at Average Torque 10.2 kNm (Total Load 120 kN) on Face F-1

The anchorage failure was observed on U-shaped strip and further debonding of the U-shaped strips were first initiated when torque was 11.48 kNm (Total Load was 130 kN) at Strips near the Middle towards to the rocker end as shown in Fig. 83 (a) and (b).

(a)

(b)

Fig. 83 (a) & (b) Anchorage failure and Initiating of Debonding of Strips on Face F-1, F-4 (Torque 11.48 kNm and Total Load 135 kN)

The peak load was observed as 135.9 kN with lever arm 170 mm. The maximum toque was 11.55 kNm and Ultimate Average Twist angle 1.49 ^{0}/m was recoded. Finally the beam was failed by crushing of concrete and first anchor failed afterwards the debonding of CFRP fabric strips as shown different failure views in Fig. 84 to 88.

The strain was also recorded in Steel provided in compression and tension as well as shear and CFRP Fabric Strips at various locations as shown in Fig. 56 and 57. The yielding of steel reinforcement takes place which was provided in Top reinforcement at mid-span.

Fig. 84 Crushing Failure View from Roller End

Fig. 85 Close View Crushing Failure of Concrete and Deboning of CFRP Fabric Strips

Fig. 86 Close View Debonding of Fabric Strips from Concrete

Fig. 87 Top View Failure of Crushing of Concrete

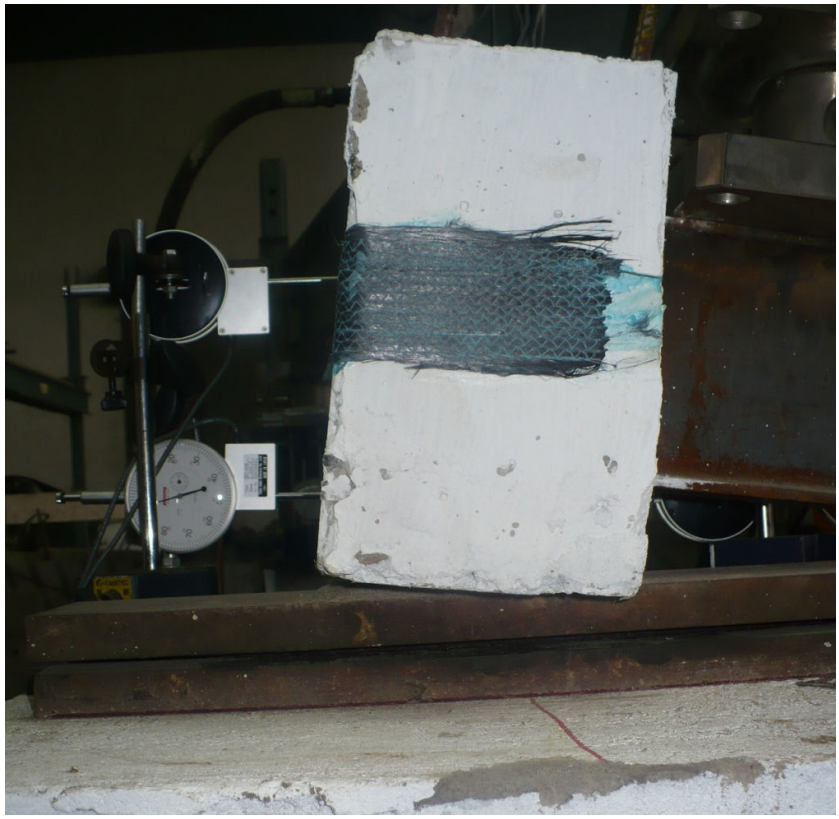

Fig. 88 View of Failure Beam from Rocker End

8.3.2 Strain Variation in Reinforcement

The Figs. 89 to 94 shows the relationship between recorded strain (microstrain) and avearge of applied torque (kNm) .

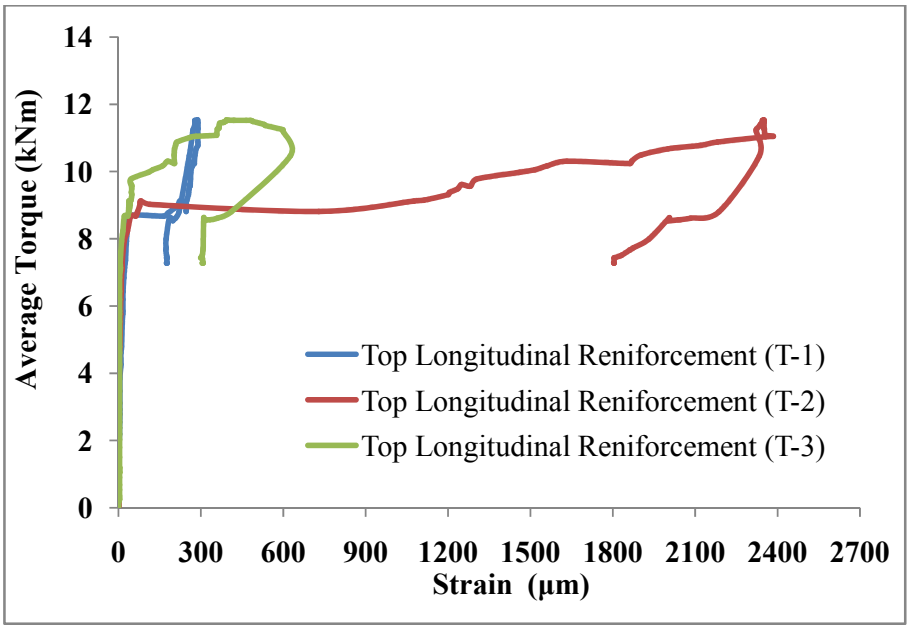

Fig. 89 Strain Vs Average Torque at Top Longitudinal Reinforcement

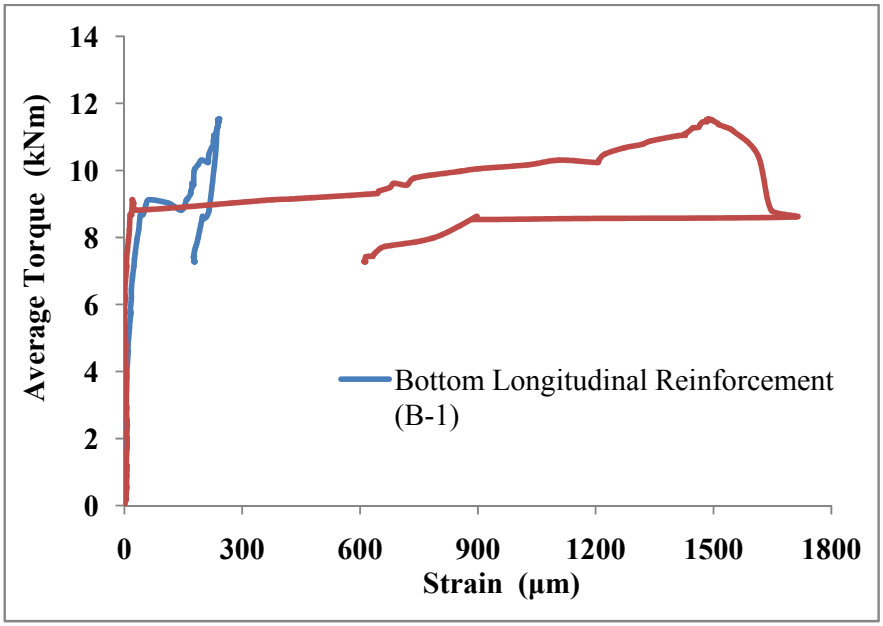

Fig. 90 Strain Vs Average Torque at Bottom Longitudinal Reinforcement

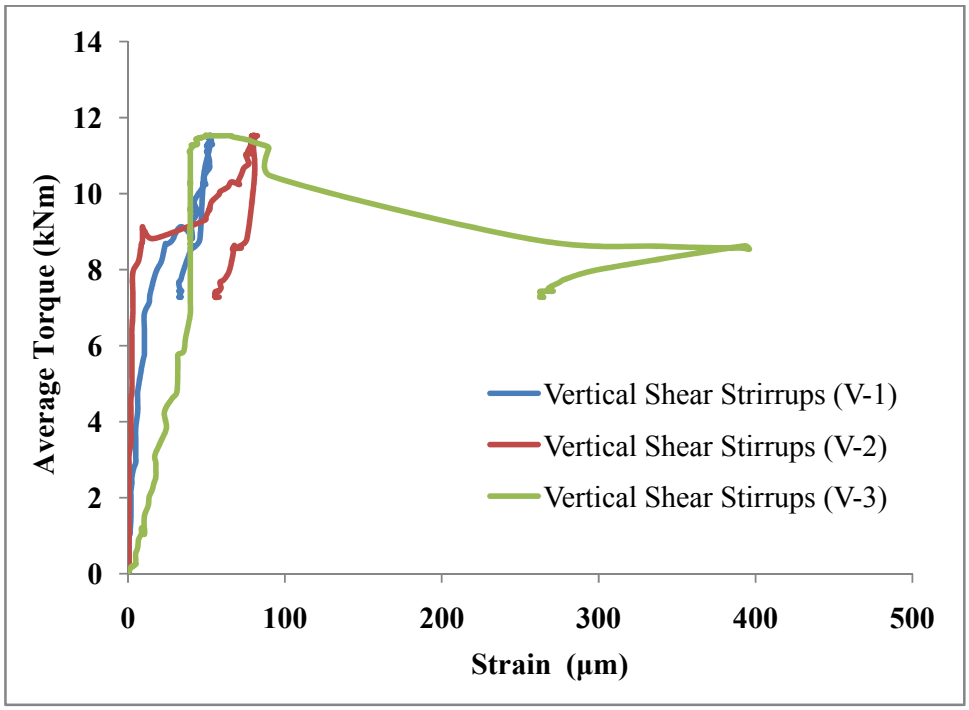

Fig. 91 Strain Vs Average Torque at Vertical Shear Stirrups

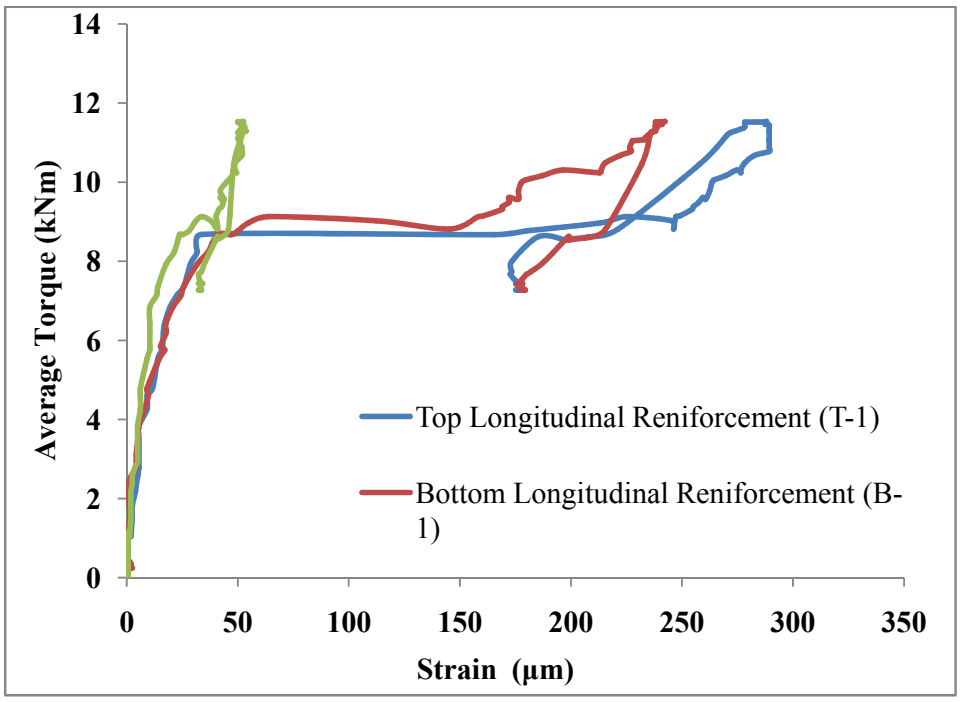

Fig. 92 Strain Vs Average Torque at Reinforcement provided in Quarter Span Near to Rocker End

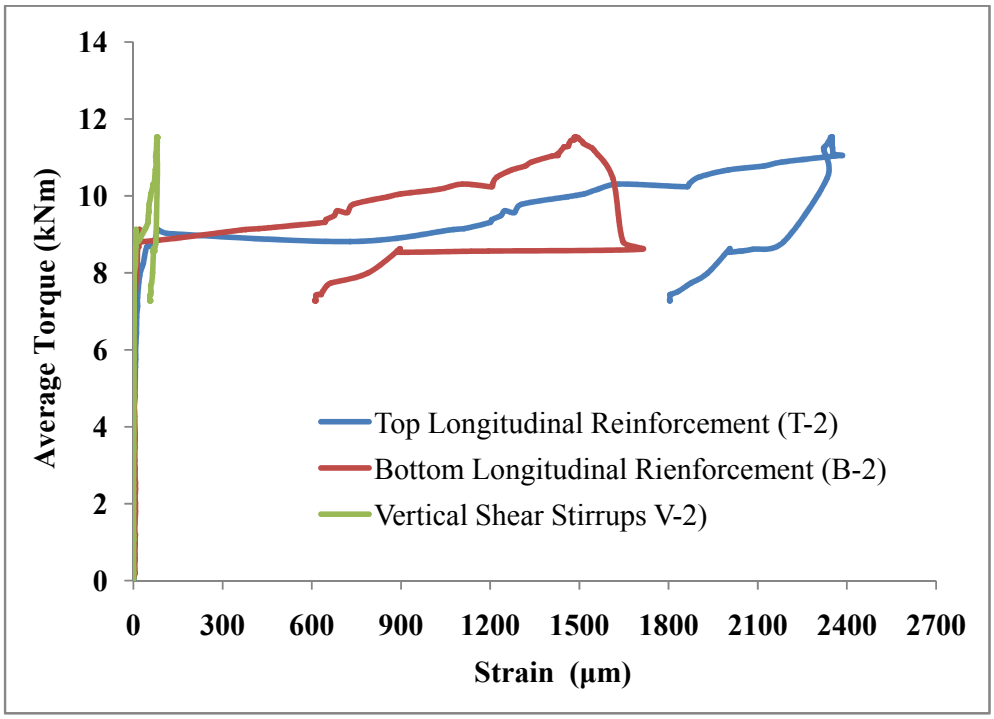

Fig. 93 Strain Vs Average Torque at Reinforcement provided in Mid Span

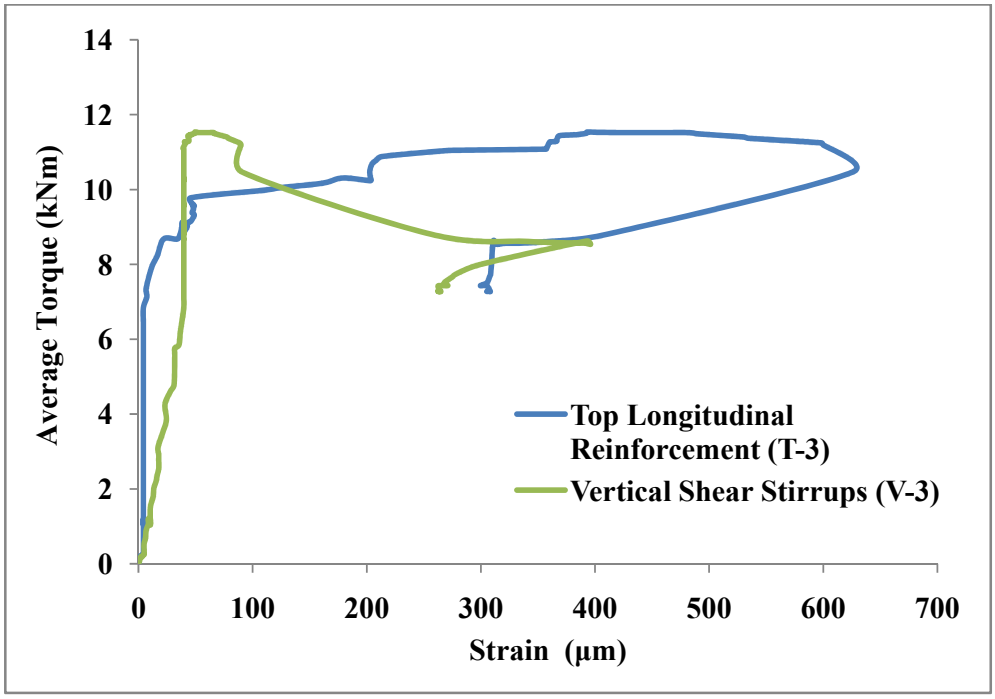

Fig. 94 Strain Vs Average Torque at Reinforcement provided in Quarter Span Near to Roller End

The test values of the recorded strain are presented in Table 17.

Table 17 Maximum Strain Recorded in Tension, Compression Steel and Vertical Shear Stirrups

Position of Strain Gauge	Maximum Strain (μm)	Remarks
Steel in Compression at Quarter Span Towards Rocker End (T-1)	289	
Steel in Compression at Mid Span (T-2)	2385	Yielded
Steel in Compression at Quarter span Toward Roller End (T-3)	626	
Steel in Tension at Quarter Span Towards Rocker End (B-1)	242	
Steel in Tension at Mid Span (B-2)	1708	
Steel in Tension at Quarter span Toward Roller End (B-3)	N.A.	
Vertical Shear Stirrups at Quarter Span Towards Rocker End (V-1)	54	
Vertical Shear Stirrups at Mid Span (V-2)	82	
Vertical Shear Stirrups at Quarter Span Towards Roller End (V-3)	396	

8.3.3 Strain Variation in CFRP Fabric

The Fig. 95 to 97 shows the relationship between recorded strain (microstrain) and avearge applied torque (kNm). Fig 95 shows the relationship of strain in U-shaped strips near the Rocker Ends of Face-1 and Face F-3. Fig 96 shows the realtion

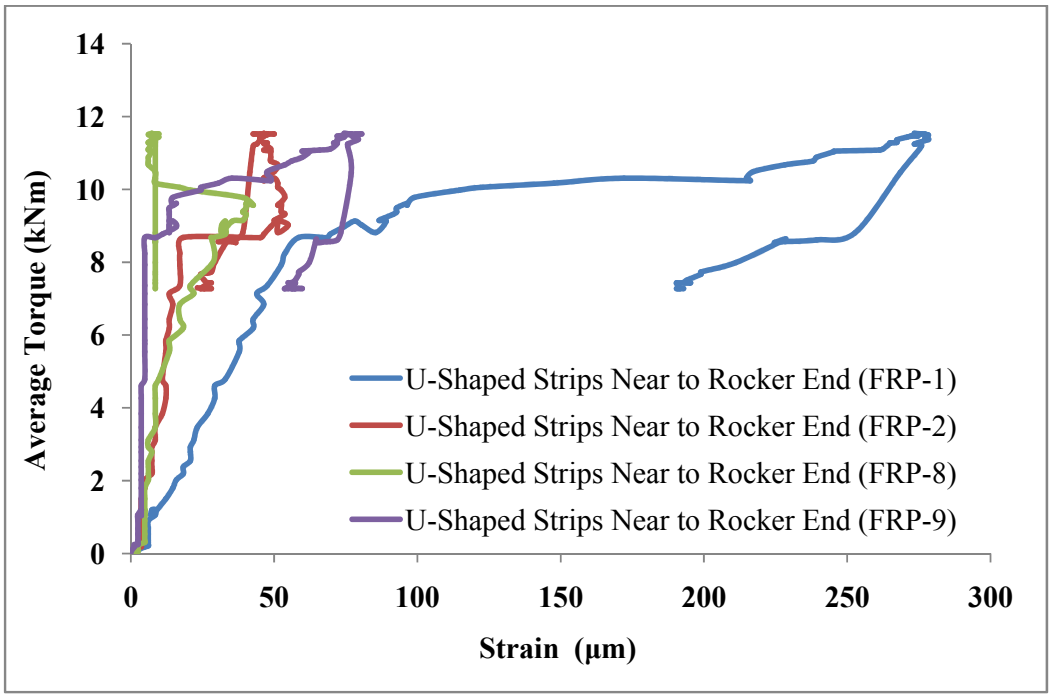

Fig. 95 Strain Vs Average Torque at U-Shaped CFRP Fabric Strips provided in Quarter Span Near to Rocker End

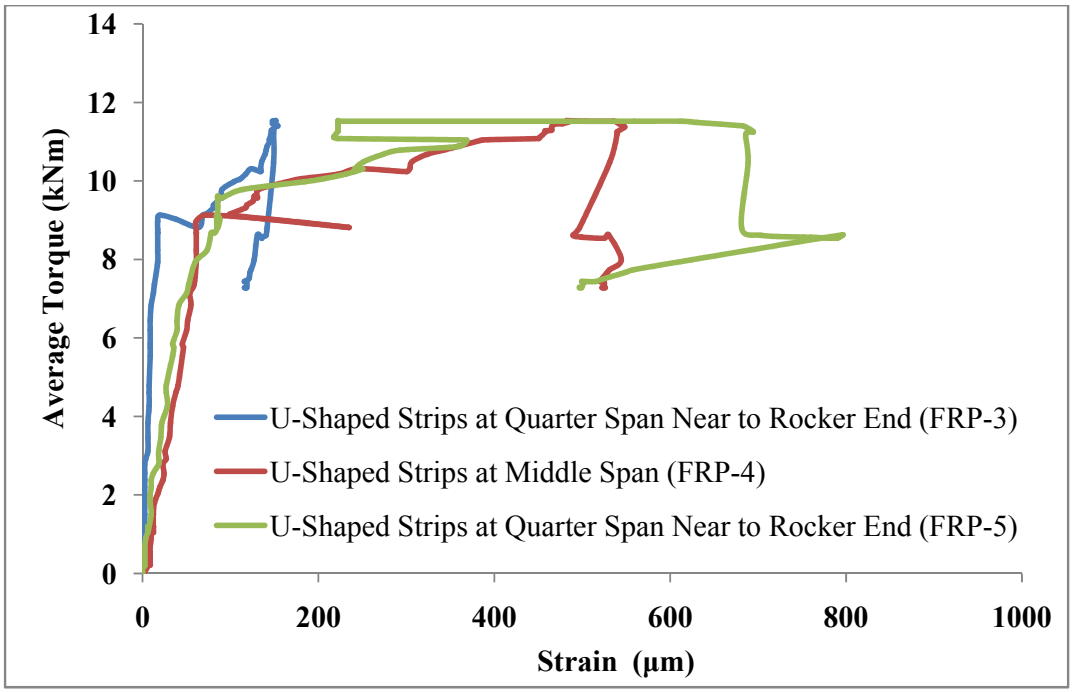

Fig. 96 Strain Vs Average Torque at U-Shaped CFRP Fabric Strips provided in Mid Span

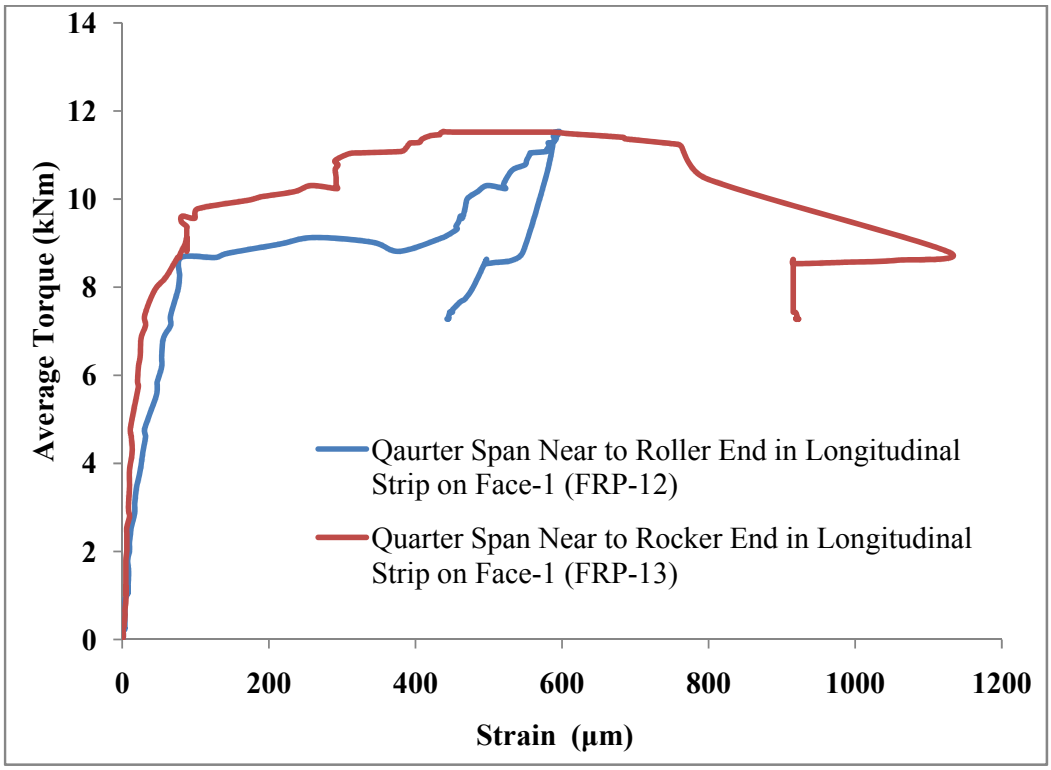

Fig. 97 Strain Vs Average Torque at Quarter Span in Longitudinal CFRP Fabric Strip on Face F-1

Maximum strain recorded in U-shaped CFRP Fabric Strips as well as Longitudinal CFRP Fabric Strips are presented in the following Table 18.

Table 18 Maximum Strain Recorded in U-Shaped and Longitudinal CFRP Fabric Strips

Position of Strain Gauge	Maximum Strain (μm)	Remarks
U-Shaped Strip near to Rocker End (FRP-1) on Face F-1	278	
U-Shaped Strip near to Rocker End (FRP-2) on Face F-1	55	
U-Shaped Strip near Quarter Span towards Rocker End (FRP-3)	154	
U-Shaped Strip in Middle Span (FRP-4)	548	
U-Shaped Strip near Quarter Span towards Roller End (FRP-5)	796	
U-Shaped Strip near to Roller End (FRP-6)	166	
U-Shaped Strip near to Roller End (FRP-7)	18	
U-Shaped Strip near to Rocker End (FRP-8) on Face F-3	43	
U-Shaped Strip near to Rocker End (FRP-9) on Face F-3	81	
U-Shaped Strip near to Roller End (FRP-10) on Face F-3	51	
U-Shaped Strip near to Roller End (FRP-11) on Face F-3	19	
Longitudinal Strip at Quarter Span near to Rocker End (FRP-12) on Face F-1	297	
Longitudinal Strip at Quarter Span near to Roller End (FRP-13) on Face F-1	1127	

CHAPTER – 9

DISCUSSIONS OF RESULTS

CHAPTER - 9

9.0 DISCUSSIONS OF RESULTS

Two specimens were tested, PTR-1(Reference Beam) and PTT-1 (Distress beam strengthened with U-shaped CFRP Fabric Strips and Longtudinal Strips. The reference beam shows three full spiral diagonal cracks and Torque Vs Twist Angle was good agreement with the past literature. The ultimate and cracking torque observed were more then 40% higher then the design by IS 456:200 and STAAD Pro V8i but 20% less then calculated from the Eq. (20) [Thomas T. C. Hsu (1968)] . The failure was crushing of concrete and yielding steel provided in tension at quarter span near to roller end. The strengthened beam PTT-1 was designed for the torque 7.42 kNm calculated from the Eq. (20) [Thomas T. C. Hsu (1968)]. Further the beam was strengthened with CFRP fabric Strips U-shaped 50 mm width spacing 125 mm c/c and 50 width two longitudinal Strips placed at centre of the Face-1 and Face-3.

The theoretical contribution of the CFRP was 11.86 kNm [A. Ghobarah et al (2002)-Eq. (47)] by assuming the design effective strain of the CFRP is 0.003 i.e. 20% of the ultimate strain . But from the recorded strain of CFRP contribution was 0.00114, hence it is effective strain recorded was 7% of the ultimate strain. Hence revised torque capacity by strengthened scheme was 4.31 kNm and Total capacity of the Strengthened Beam was 9.82 kNm. Experimental Torque was 10.44 kNm. It shows the good agreement between the theoretical and experimental results.

The failure was occurred due to anchorage, debonding of CFRP Fabric Strips and crushing of concrete as well as yielding of steel provided in compression zone. The contribution of CFRP strain was much below the expected due to anchorage and debonding failure.

Table 19 Comparison of Experimental and Theoretical Ultimate and Cracking Torque of Reference Beam PTR-1

	$T_{c,c}$	$T_{c,e}$	$T_{u,c}$	$T_{u,e}$	Remarks
Experimental Reference Beam (PTR-1)	-	9.78		14.14	
Elastic Theory (Timoshenko & Goodier 1969; Popov 1990	7.55	-	-	-	
TS 500 2000 (Turkish Standards Institutions)	7.81	-	-	-	
Thomas T. C. Hsu (1968)	-	-	-	17.21	

$T_{c,c}$ = Theoretical Cracking Torque

$T_{c,e}$ = Experimental Cracking Torque

$T_{u,c}$ = Theoretical Ultimate Torque

$T_{u,e}$ = Experimental Ultimate Torque

Theoretical and experimental ultimate torque of strengthened beam PTT-1 as presented in Table 20.

Table 20 Comparison of Experimental and Theoretical Ultimate Torque of Strengthened Beam PTT-1

$T_{u,RC,c}$ [Thomas T. C. Hsu (1968)] by using Eq. (20) (kNm)	7.42
$T_{u,FRP,c}$ [Ghobarah A et al (2002)] by using Eq. (47) (kNm) (assumed effective Strain 0.003 (20% of the ultimate Strain of FRP)	11.86
$T_{u,c}$ (kNm)	7.42+11.31 = 19.26
$T_{u,FRP,c}$ [Ghobarah A et al (2002)] by using Eq. (47) (kNm) (recorded effective Strain 0.00114 (7% of the ultimate Strain of FRP)	4.31
$T_{u,e}$ (kNm)	11.55
$T_{u,FRP,e}$ (kNm)	11.55-7.42 = 4.13

$T_{u,RC,c}$ = Theoretical Torque of RC Beam (Distressed Beam)

$T_{u,FRP,e}$ = $T_{u,e} - T_{u,RC,c}$ = Experimental Torque contributed from CFRP Fabric

$T_{u,FRP,c}$ = Theoretical Torque of Contributed from CFRP Fabric

$T_{u,c}$ = $T_{u,RC,c} + T_{u,FRP,c}$ = Theoretical Ultimate Torque

$T_{u,e}$ = Experimental Ultimate Torque

9.1 Applied Torque and Variation of Twist Angle

The Fig. 98 to 104 shows the relationship between the applied Torque at Rocker End, Roller End and Average of both Vs Recorded Twist angle in Degree per meter for both the test specimens (Reference Beam PTR-1 and Strengthened Beam PTT-1) and Fig. 105 shows the comparison of Average applied Torque Vs Recorded Strain of the both the specimens.

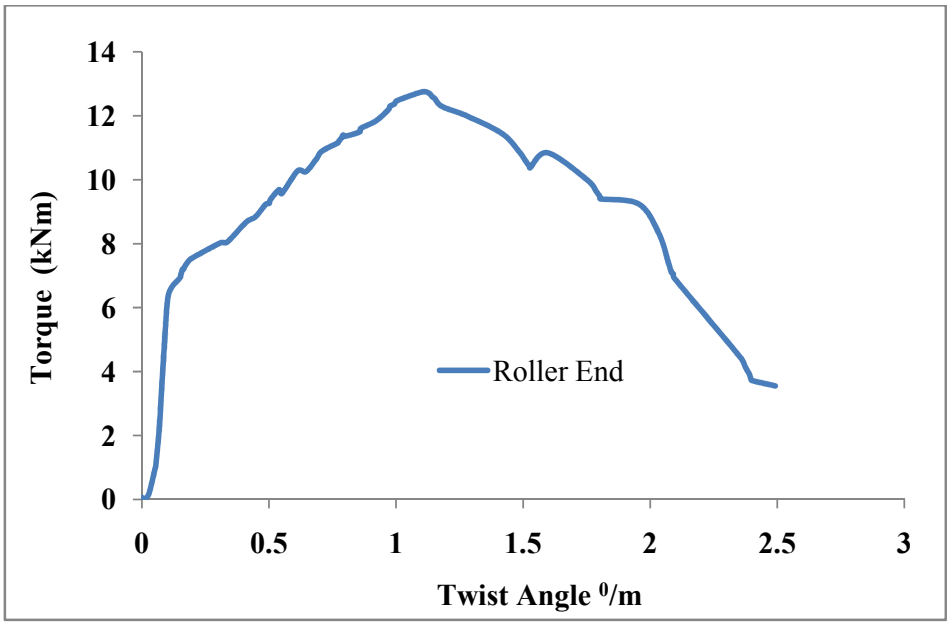

Fig. 98 Torque Vs Twist Angle in Degree at Roller End (Reference Beam PTR-1)

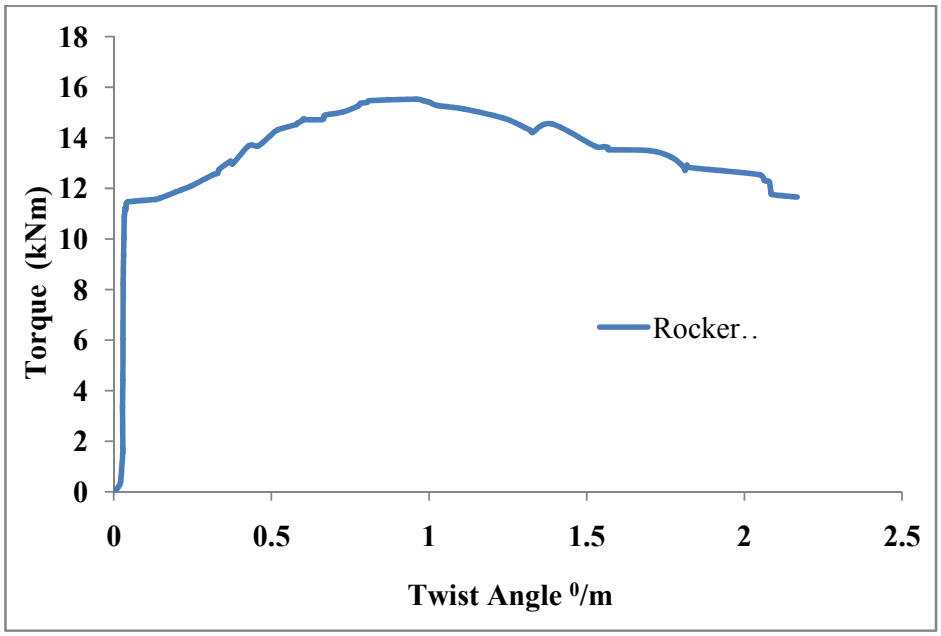

Fig. 99 Torque Vs Twist Angle in Degree at Rocker End (Reference Beam PTR-1)

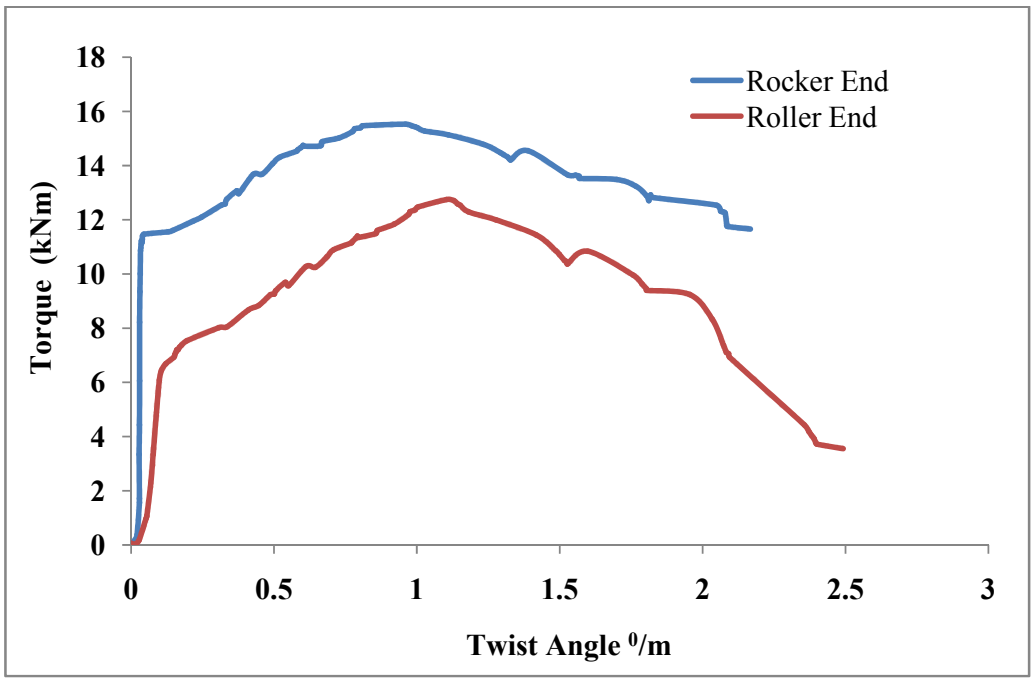

Fig. 100 Torque Vs Twist Angle in Degree at Both Ends (Reference Beam PTR-1)

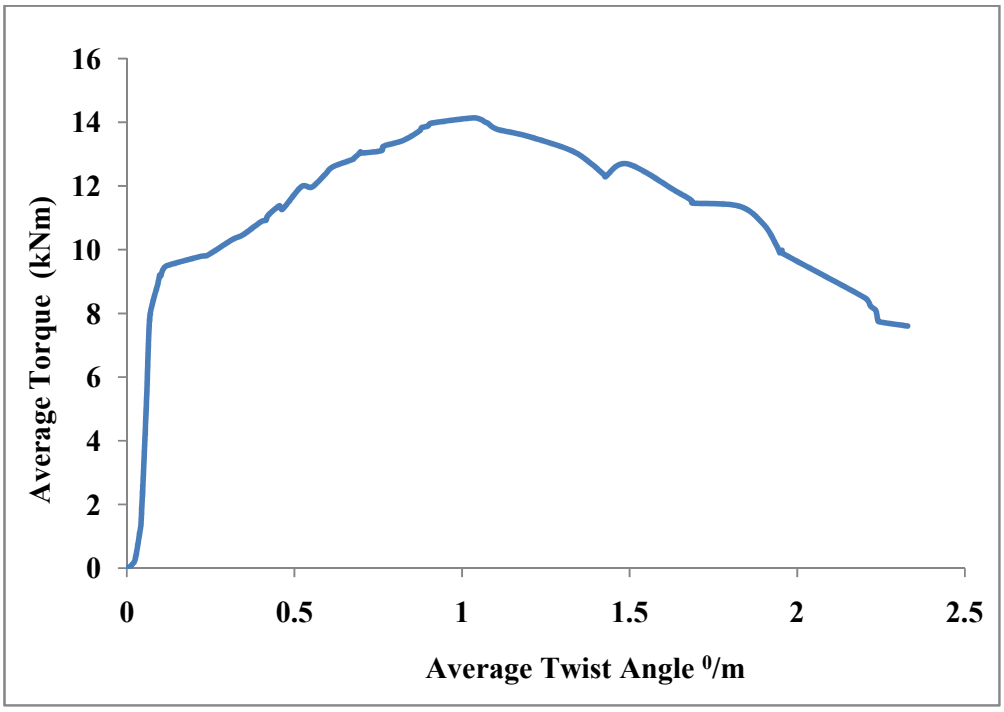

Fig. 101 Average Torque Vs Average Twist Angle in Degree (Reference Beam PTR-1)

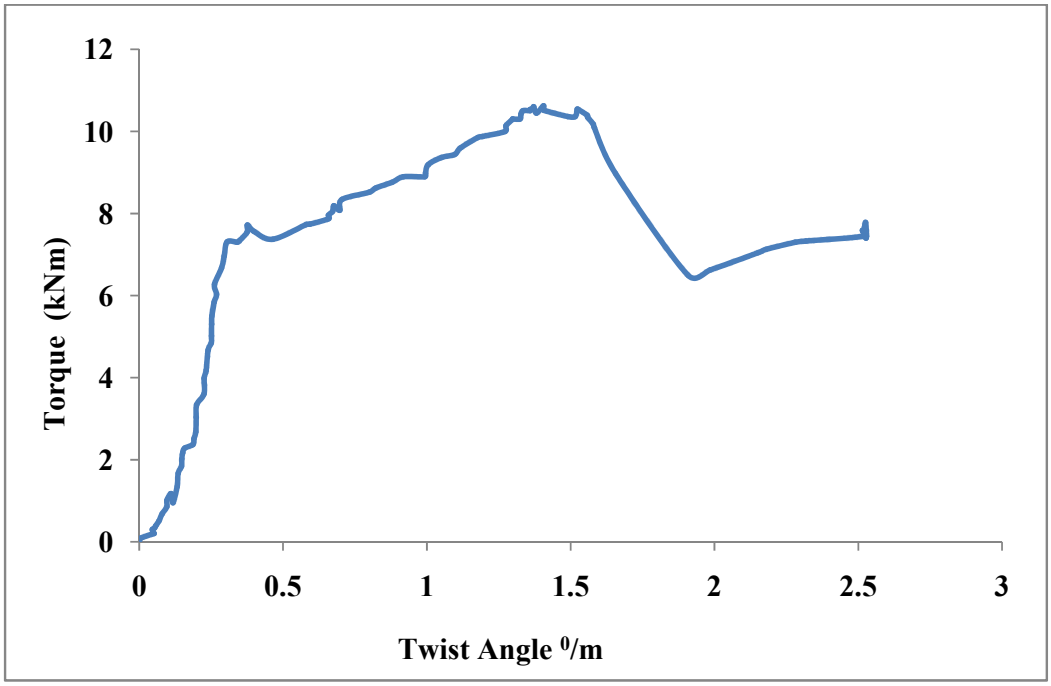

Fig. 102 Torque Vs Average Twist Angle in Degree at Rocker End (Beam PTT-1)

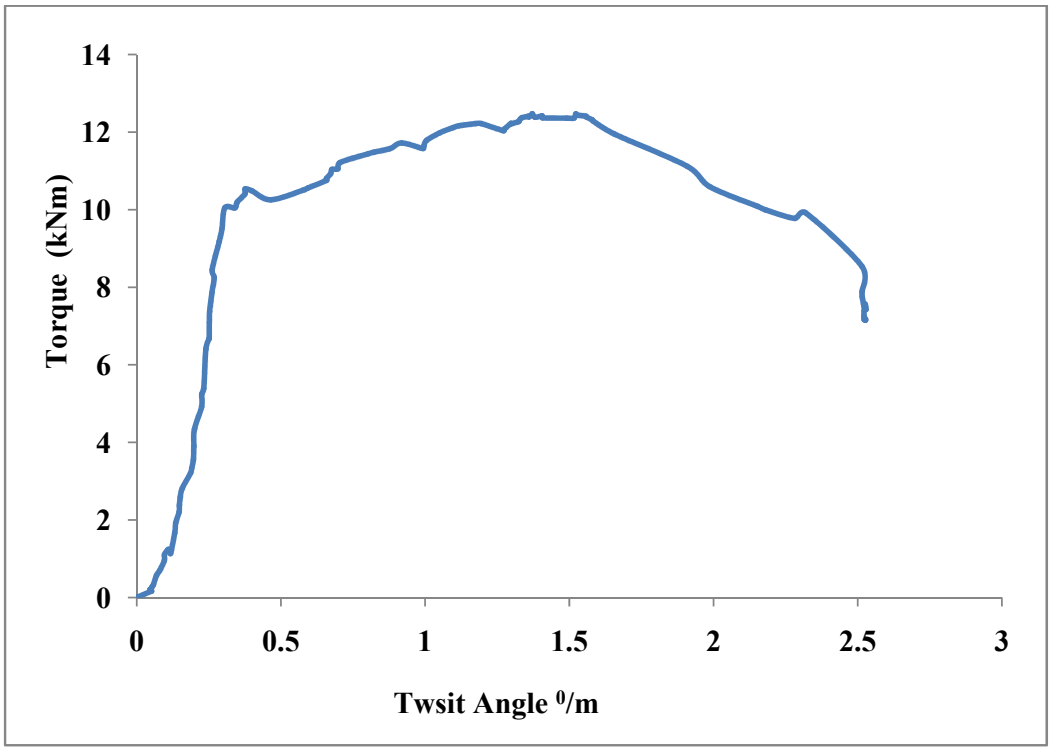

Fig. 103 Torque Vs Twist Angle in Degree at Roller End (Beam PTT-1)

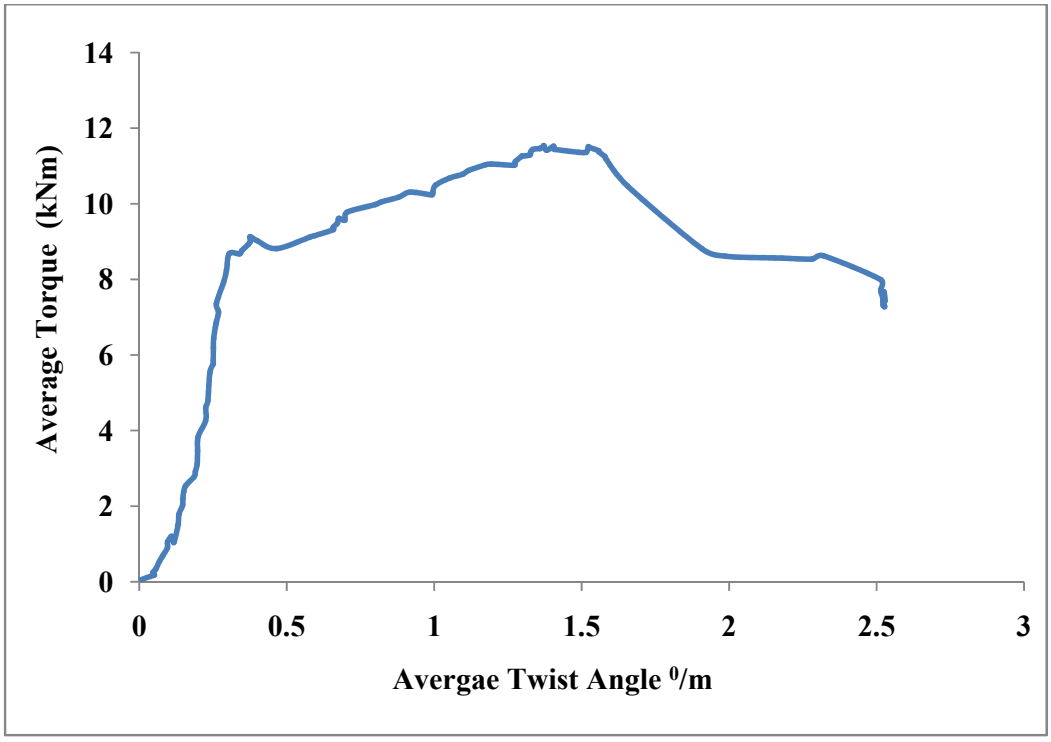

Fig. 104 Average Torque Vs Average Twist Angle in Degree (Beam PTT-1)

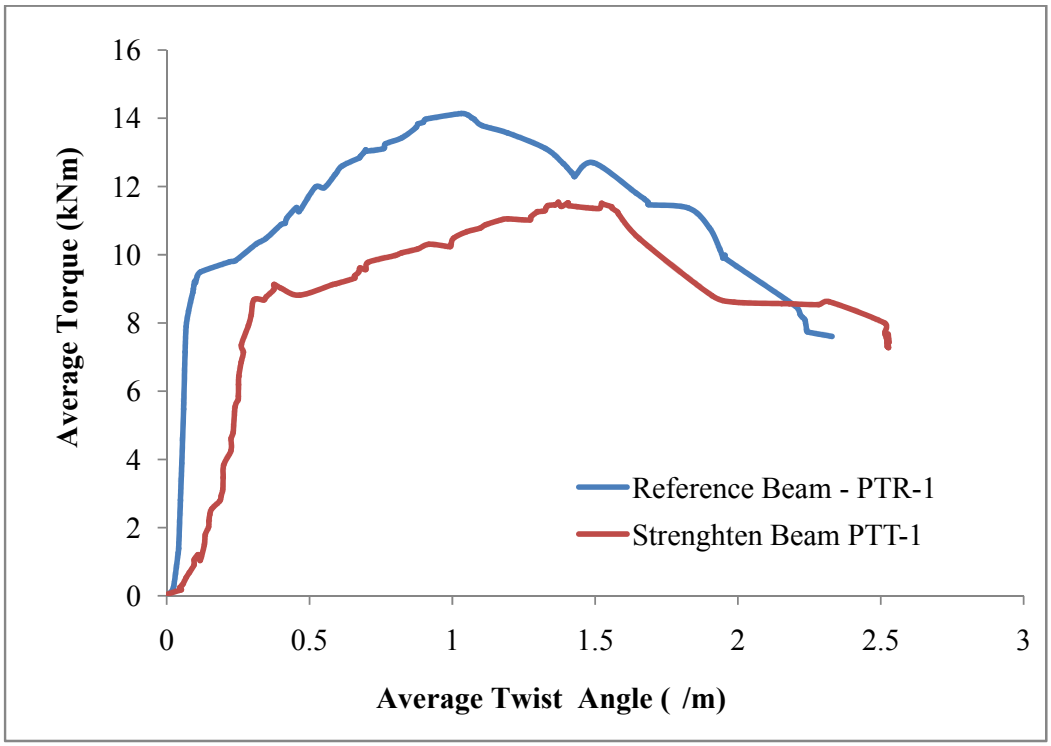

Fig. 105 Comparison of Average Torque Vs Average Twist Angle of Both the Specimens

9.2 Ductility

Experimental Twist Angle at Cracking and Ultimate Torque and Ductility Ratio [M.R. Mohammadizadeh and M.J. Fadaee (2009)] are presented in Table 21.

Table 21 Comparison of Ductility Ration of the Both the Specimens

Specimens	$\phi_{y,e}$ (Degree)	$\phi_{p,e}$ (Degree)	$\phi_{0.85p,e}$ (Degree)	$\mu_{\emptyset,e} = \frac{\emptyset_{p,e}}{\emptyset_{y,e}}$	$\mu_{0.85p,e} = \frac{\emptyset_{0.85p,e}}{\emptyset_{y,e}}$
Reference Beam PTR-1	0.120	1.032	2.234	8.6	18.62
Strengthened Beam PTT-1	0.305	1.49	1.780	4.89	5.84

$\phi_{y,e}$ = Experimental Twist Angle at Yielding

$\phi_{p,e}$ = Experimental Twist Angle at Ultimate Torque

$\phi_{0.85p,e}$ = Experimental Twist Angle at 85% Ultimate Torque beyond the peak

$\mu_{\emptyset,e}$ = Experimental Ductility Ratio

$\mu_{0.85\emptyset,e}$ = Experimental Ductility Ratio

$$\mu_{\emptyset,e} = \frac{\emptyset_{p,e}}{\emptyset_{y,e}}$$

9.3 Comparison of Applied Torque Vs Strain in Steel Reinforcement of Both the Specimens

Fig. 106 to 108 shows the relationship between the average applied Torque Vs Recorded Strain in quarter and mid span of the both the specimens.

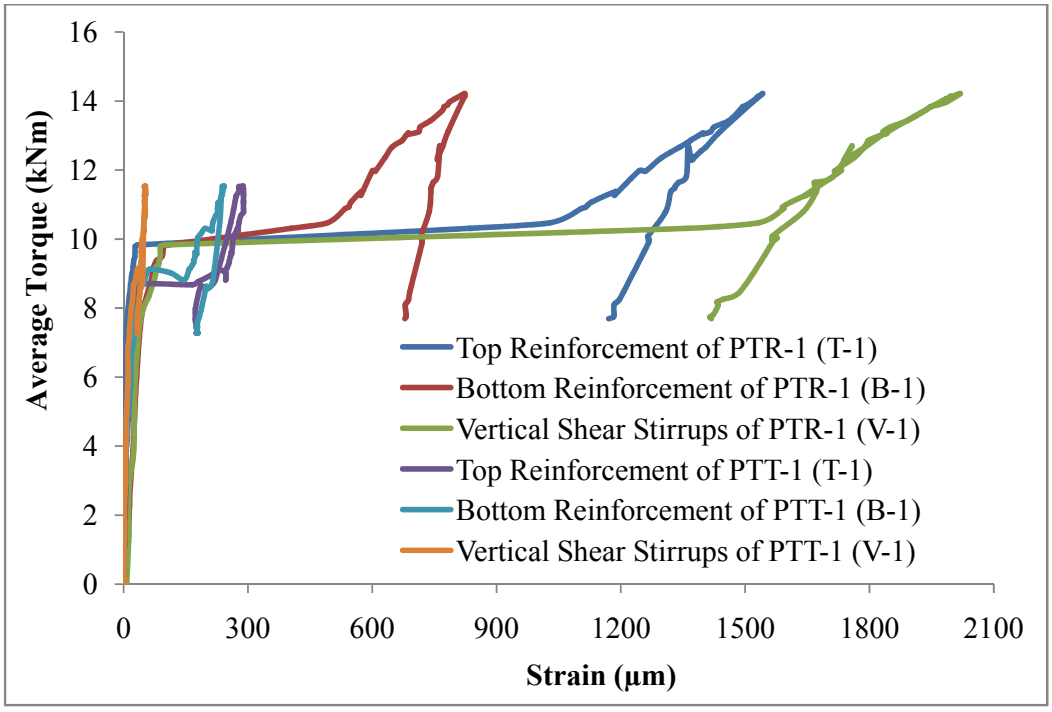

Fig. 106 Comparison of Average Torque Vs Recorded Strains at Quarter Span Towards Rocker End of Both the Specimens

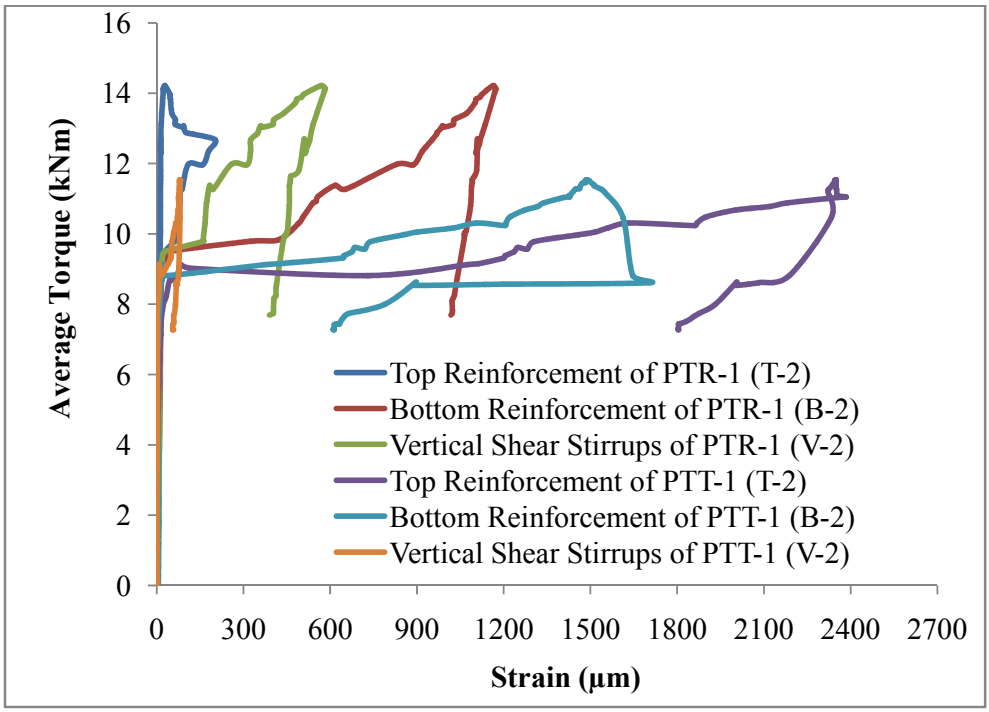

Fig. 107 Comparison of Average Torque Vs Recorded Strains at Middle Span Towards Rocker End of Both the Specimens

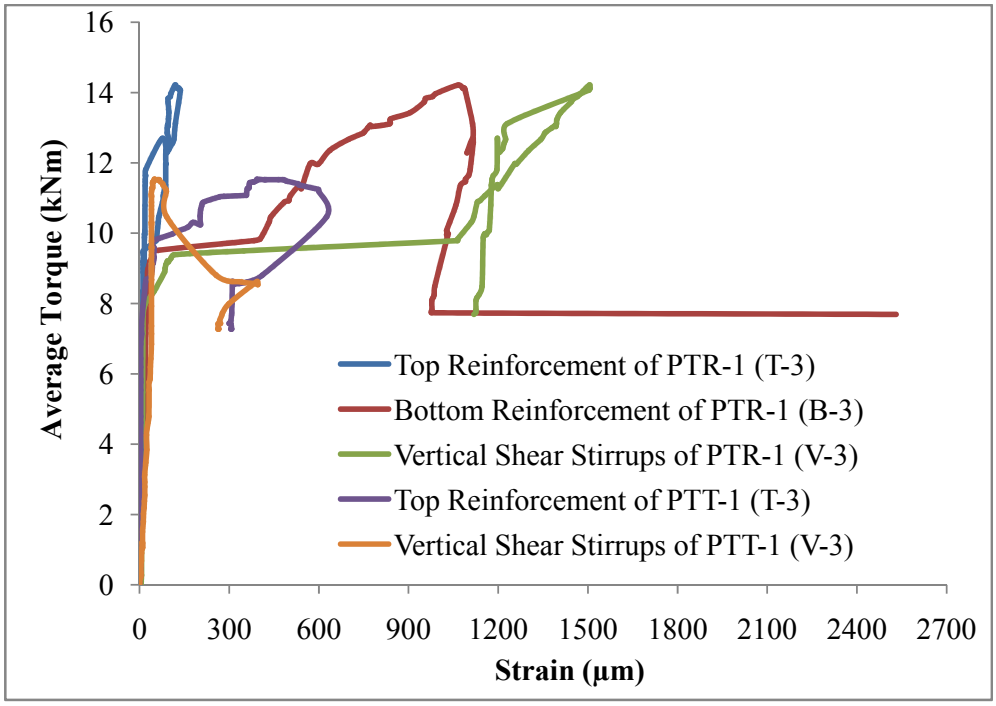

Fig. 108 Comparison of Average Torque Vs Recorded Strains at Quarter Span Towards Roller End of Both the Specimens

Table 22 presented the recorded strain in steel reinforcement of the both the specimens (PTR-1 and PTT-1)

Table 22 Maximum Strain Recorded in Tension, Compression Steel and Vertical Shear Stirrups of Both the Specimens

Position of Strain Gauge	Maximum Strain of PTR-1 (µm)	Maximum Strain of PTT-1 (µm)	Remarks
Steel in Compression at Quarter Span Towards Rocker End (T-1)	1541	289	
Steel in Compression at Mid Span (T-2)	202	2385	Yielded
Steel in Compression at Quarter span Toward Roller End (T-3)	137	626	
Steel in Tension at Quarter Span Towards Rocker End (B-1)	823	242	
Steel in Tension at Mid Span (B-2)	1173	1708	
Steel in Tension at Quarter span Toward Roller End (B-3)	2531	N.A.	Yielded
Vertical Shear Stirrups at Quarter Span Towards Rocker End (V-1)	2019	54	
Vertical Shear Stirrups at Mid Span (V-2)	583	82	
Vertical Shear Stirrups at Quarter Span Towards Roller End (V-3)	1506	396	

CHAPTER – 10

CONCLUSION

CHAPTER - 10

10.0 CONCLUSION

It is observed that the Beam PTT-1 that was deficient in torsion and has been strengthened using carbon FRP fabric strips has exhibited enhancement of torsional capacity by 58%. The torsional capacity of Strengthened Beam PTT-1 has achieved torsional capacity 81.69 % of the reference beam. The decrease in the torsion capacity is due to the discontinuity of the fabric strips that were used for the strengthening. This was created intentionally as in real life situation all the four faces of the beam could not be available. The relationship of Torque Vs Twist angle observed from the tests in reference beam is comparable to past literatures. The cracked as well as ultimate twist angle was increased in case of strengthened beam PTT-1. The failure mode in the strengthened beam was similar to the reference beam but the specimen PTT-1 has shown less ductility in comparison to the reference beam because percentage of increased cracked twist angle much more than that of ultimate twist angle. The carbon FRP Fabric strips did not rupture as the recorded strain was 7% (0.00114) of the ultimate strain 0.0155 due to anchorage failure and debonding of the carbon FRP fabric in strengthened beam PTT-I. The internal longitudinal steel observed to be yielded to both the cases. It can be concluded that the carbon FRP torsional wrapping may be used in the strengthening by taking proper care in the designing of the rehabilitation scheme.

10.1 Future Scope of Work

The effect in real life i.e. combined effect of flexural as well as torsion needs more investigations.

Study on the effect of fully wrapping, strips perpendicular to crack (45^0 to axis of the beam) by using strips of various types of FRP.

Further investigations are required to develop a comprehensive unified model to analyse both normal and strengthened RC beam.

Further investigations are required in the area of usage of prestressed FRP.

CHAPTER – 11

REFERENCE

REFERNCE

1. ACI 440.2R-08, (2008), "Guide for the design and construction of externally bonded FRP systems for strengthening concrete structures", Farmington Hills, Michigan: American Concrete Institute, 2008.
2. Ameli Mehran and Ronagh Hamid R.,(2007), "Analytical Method for Evaluating Ultimate Torque of FRP Strengthened Reinforced Concrete Beams", Journal of Composites for Construction © ASCE / July/August 2007, pp 384-390.
3. Ameli Mehran; Ronagh Hamid R.; and Dux Peter F., (2007), "Behavior of FRP Strengthened Reinforced Concrete Beams under Torsion", Journal of Composites for Construction © ASCE / March/April 2007, pp 192-200.
4. Boucif Guenaneche, Baghdad Krour, Abdeloauhed Tounsi, Abdelkader Fekrar, Samir Benyoucef, El Abbas Adda Bedia,(2010), "Elastic analysis of interfacial stresses for the design of a strengthened FRP plate bonded to an RC beam", International Journal of Adhesion & Adhesives (2010), Article in Press.
5. Concrete Society. Design guidance for strengthening concrete structures using fibre composite materials. Concrete Society Technical Report No. 55, 2000. 71p.
6. Constantin E. Chalioris, (2007), "Analytical Model for The Torsional Behaviour of Reinforced Concrete Beams Retrofitted With FRP Materials", Engineering Structures 29 (2007), pp 3263–3276
7. Constantin E. Chalioris, (2008), "Torsional strengthening of rectangular and flanged beams using carbon fibre-reinforced-polymers – Experimental study", Construction and Building Materials 22 (2008) pp 21–29
8. Deifalla A and Ghobarah A (2005), "Simplified Analysis for Torsionally Strengthened RC Beams Using FRP", Proceedings of the International Symposium on Bond Behaviour of FRP in Structures (BBFS 2005), Chen and Teng (eds) © 2005 International Institute for FRP in Construction, pp373-378
9. FIB, (2001), "Externally Bonded FRP Reinforcement for RC Structures", (CEB-FIB) Lausanne (Switzerland): The International Federation for Structural Concrete; 2001.Technical Report, 14, pp. 59-68.

10. Ghobarah A, Ghorbel MN, Chidiac SE., (2002), "Upgrading torsional resistance of reinforced concrete beams using fiber-reinforced polymer", J Comp Construct 2002;6(4):257–63.
11. Ghobarah A; Ghorbel M. N.; and. Chidiac S. E, (2002), "Upgrading Torsional Resistance of Reinforced Concrete Beams Using Fiber-Reinforced Polymer", JOURNAL OF COMPOSITES FOR CONSTRUCTION / NOVEMBER 2002, pp 257-263.
12. Gilbert Nkurunziza, Ahmed Debaiky, Patrice Cousin and Brahim Benmokrane, (2005), "Durability of GFRP bars: A critical review of the literature", Prog. Struct. Engineering Mater. 2005 @ John Wiley & Sons, Ltd; 7: pp 194–209.
13. Hii Adrian K.Y., Al-Mahaidi Riadh,(2006), "An experimental and numerical investigation on torsional strengthening of solid and box-section RC beams using CFRP laminates", Composite Structures 75 (2006), pp 213–221.
14. Hollaway L.C., (2010), "A review of the present and future utilisation of FRP composites in the civil infrastructure with reference to their important in-service properties", Construction and Building Materials (2010), Article in Press.
15. IS : 10262:2009 , "Concrete Mix Proportioning - Guidelines", Bureau of Indian Standards Manak Bhavan, New Delhi
16. IS : 1786:2008, "High Strength Deformed Steel Bars and Wires for Concrete Reinforcement-Specification", Bureau of Indian Standards Manak Bhavan, New Delhi
17. IS : 2386 (Part III)-1963 (Reaffirmed 2002) , "Methods of Test for Aggregates for Concrete- Specific Gravity, Density, Voids, Absorption and Bulking ", Bureau of Indian Standards Manak Bhavan, New Delhi
18. IS : 2386 (Part IV)-1963 (Reaffirmed 2007) , "Methods of Test for Aggregates for Concrete- Mechanical Properties", Bureau of Indian Standards Manak Bhavan, New Delhi
19. IS : 4031 (Part 4)-1988 (Reaffirmed 2005) , "Methods of Physical Test for Hydraulic Cement- Determination of Consistency of Standard Cement Paste", Bureau of Indian Standards Manak Bhavan, New Delhi

20. IS : 4031 (Part 5)-1988 (Reaffirmed 2005) , "Methods of Physical Test for Hydraulic Cement- Determination of Initial and Final Setting Times", Bureau of Indian Standards Manak Bhavan, New Delhi
21. IS : 4031 (Part 5)-1988 (Reaffirmed 2005) , "Methods of Physical Test for Hydraulic Cement- Determination of Compressive Strength of Hydraulic Cement other than Masonry Cement", Bureau of Indian Standards Manak Bhavan, New Delhi
22. IS : 456:2000 (Reaffirmed 2005) , "Plain and Reinforced Concrete -Code of Practice", Bureau of Indian Standards Manak Bhavan, New Delhi
23. IS : 516:1959 (Reaffirmed 2004) , "Methods of Tests for Strength of Concrete", Bureau of Indian Standards Manak Bhavan, New Delhi
24. IS: 383:1970 (Reaffirmed 2002) , "Specification for Coarse and Fine Aggregates from Natural Sources for Concrete", Bureau of Indian Standards Manak Bhavan, New Delhi.
25. Jing M, Raongjant W, Li ZX., (2007), "Torsional strengthening of reinforced concrete box beams using carbon fiber reinforced polymer", Compos Struct 2007;78(2):264–70.
26. Lau K.T., Zhou L.M and Wu J.-S. (2001), "Investigation on strengthening and strain sensing techniques for concrete structures using FRP composites and FBG sensors", Materials and Structures/Materiaux et Constructions, Vol. 34, January-February 2001, pp 42-50.
27. M.R. Mohammadizadeh and M.J. Fadaee, (2009)," Torsional Behaviour of High-Strength Concrete Beams Strengthened Using CFRP Sheets; an Experimental and Analytical Study", Transaction A: Civil Engineering Vol. 16, No. 4, pp. 321-330, © Sharif University of Technology, August 2009.
28. Metin Husem, Ertekin Oztekin and Selim Pul, (2010), "A calculation method of cracking moment for the high strength concrete beams under pure torsion", Sadhana Vol. 36, Part 1, February 2011, pp. 1–15 © Indian Academy of Sciences.
29. Ritchie, P.A., Thomas, D.A., Lu, L.W. and Connely, G.M., (1991), "External reinforcement of concrete beams using fiber reinforced plastics", ACI Structural Journal, 1991; 88(4):490-500.

30. Ronagh, H. R., and Dux, P. F. (2003). “Full-scale torsion testing of concrete beams strengthened with CFRP.” Proc., 1st Int. Conf. on the Performance of Construction Materials in the New Millennium, Cairo, 735–743.
31. Saadatmanesh, H., Ehsani, M.R., (1991), "RC beams strengthened with GFRP plates 1: Experimental study", Journal of Structural Engineering, 1991; 117(1):3417-33.
32. Saravanan Panchacharam (2002) “Torsional Behavior of Reinforced Concrete Beams Strengthened with FRP Composites” First FIB Congress, Osaka, Japan, October 13-19,2002, pp 1-11
33. Taheri F., Shahin K., Widiarsa I., (2002), “On the parameters influencing the performance of reinforced concrete beams strengthened with FRP plates”, Composite Structures 58 (2002), pp 217–226.
34. Thomas T. C. Hsu, (1968),” Torsion of Structural Concrete - A Summary of Pure Torsion”, American Concrete Institute Publication SP- 18, 165-178 (1968)
35. Triantafillou TC, Antonopoulos CP, (2000), “Design of concrete flexural members strengthened in shear with FRP”, Journal of Composites for Construction 2000; 4(4):198–205.
36. Vintzileou E, Panagiotidou E, (2007), “An empirical model for predicting the mechanical properties of FRP-confined concrete”, Construction & Building Materials 2007.
37. Wu Hwai-Chung, (2000), “Mechanical Interaction between Concrete and FRP Sheet”, Journal of Composites for Construction / May 2000, pp 96-98.